

MIXOTROPHIC AND EXTREMOPHILIC ALGAE FOR PHOTOSYNTHETIC  
BIOREFINERY

By

PIERRE WENSEL

A dissertation submitted in partial fulfillment of  
the requirements for the degree of

DOCTOR OF PHILOSOPHY

WASHINGTON STATE UNIVERSITY  
Department of Biological Systems Engineering

JULY 2013

To the Faculty of Washington State University:

The members of the Committee appointed to examine the dissertation of PIERRE WENSEL

find it satisfactory and recommend that it be accepted.

---

Shulin Chen, Ph.D., Chair

---

William C. Davis, Ph.D.

---

Pius M. Ndegwa, Ph.D.

---

Craig S. Frear, Ph.D.

## ACKNOWLEDGMENT

I express my sincere gratitude to my advisor, Dr. Shulin Chen, for the chance to pursue my PhD degree at the Department of Biological Systems Engineering at Washington State University. My committee members Dr. William C. Davis, Dr. Pius M. Ndegwa, and Dr. Craig S. Frear are also acknowledged for their valuable comments regarding dissertation and presentation, iterative revisions, and other suggestions. I thank Dr. Greg Helms and Dr. William Hiscox for assistance in  $^1\text{H}$  NMR analysis and manuscript suggestions, Dr. Helmut Kirchhoff for insights on light reactions and photosynthesis, Dr. Liang Yu for assistance with anaerobic digestion, Jesus Nunez-Garcia, Raul Peleaz-Samaniego, and Cynthia Alwine. I extend my thanks to Sensei Rob Bryner, Coaches Francois Wohlman and Tommie Smith of Santa Monica Track, Gabe Kubanda, George Fisher, Vinnie Richardson, and Keith Rideau of our band Love Electric, Dr. Gerwald Kohler, Dr. Gary Anderdon, Tristan Simon, UCHA, PIC Grey Army, Tom Shultz of Pan Am Flight 103, Nick, Tina, David Simpson, Chance DePriest of Lutz, FL. Sandalwood Apts., Mike, Pop, Yvette, Rodney of Tampa, FL. Rosewood Gardens Apts., George Lucas, Lewis Carol, Anne and Harold Shulteiss, S.F. Telegraph Hill, Black Rock City, Chess, Eric-Patrick-Merceric, Ferme, Hilary Matora, Memerochers of Asbestos, QC., Abi-Ghanem- Wensel-Oftedal family, Maria Mathilde von Glucksburg and all my loving relatives. Thank you to my incredible wife Rita for her endearing support. A splendid time is guaranteed for all.

MIXOTROPHIC AND EXTREMOPHILIC ALGAE FOR PHOTOSYNTHETIC  
BIOREFINERY

Abstract

by Pierre Wensel, Ph.D.  
Washington State University  
July 2013

Chair: Shulin Chen

Mass outdoor cultivation of microalgae faces challenges of low productivity, contamination, inefficient CO<sub>2</sub> supply, and difficulties in harvesting. A two-stage cultivation process was developed to address some of these challenges. This process involved culturing microalgae in a fermentor heterotrophically or photobioreactor mixotrophically as first-stage to rapidly obtain high cell densities for inoculating a phototrophic open-pond culture as second-stage. The pond system features high levels of NaHCO<sub>3</sub>, pH, and salinity. Two oleaginous, haloalkaline-tolerant, and dual-trophic green *Chlorella sp.* microalgae from soda lakes were isolated, identified, and compared using a multi-instrument approach as candidates for such a process. A model TAG was developed for rapid, non-destructive lipid quantitation using liquid-state <sup>1</sup>H NMR. The two-stage cultivation system and a high pH-mediated auto-flocculation method were tested on a selected strain with a 1 L fermentor and 40 L open-tank. The effects of carbon and nitrogen sources and levels, temperature, pH, diurnal light intensity, and HCl-mediated pH control were further determined. With increasing NaHCO<sub>3</sub> levels, cellular size and granularity increased,

carotenoid/chlorophyll ratio decreased, and chlorophyll-fluorescence parameters  $F_v/F_m$ ,  $\Psi_{II}$ , and NPQ remained relatively constant. Photosynthetic state transition occurred upon  $\text{NaHCO}_3$  addition.

To lay the groundwork for biorefinery simulation, an industrial-scale process to convert corn-stover into succinic acid and co-products was also developed. The finite volume method of Computational Fluid Dynamics (CFD) was coupled with kinetic, stoichiometric, mass, and energy balance equations using reported laboratory-scale experimental data to optimize the mixing process. This modeling approach can later be modified and used for other applications.

## TABLE OF CONTENTS

ACKNOWLEDGMENT .....	iii
LIST OF TABLES .....	viii
LIST OF FIGURES .....	ix
Chapter 1 : INTRODUCTION.....	1
1.1. Transition to Refining of Biomass .....	1
1.2. Advantages of Microalgal Biomass Feedstocks .....	3
1.3. Microalgal Biorefinery Cultivation and Harvesting Processes .....	9
1.4. Necessity for Technological Advancements and Process Simulation .....	24
1.5. References.....	28
Chapter 2 : MICROALGAE FOR TWO-STAGE CULTIVATION PART 1: BIO-PROSPECTING.....	41
2.1. Abstract .....	41
2.2. Introduction.....	42
2.3. Materials and Methods.....	45
2.4. Results and discussion .....	54
2.5. Conclusions.....	74
2.6. References.....	76
Chapter 3 : MICROALGAE FOR TWO-STAGE CULTIVATION PART II: OPTIMIZATION AND CHARACTERIZATION OF BIOMASS AND LIPID ACCUMULATION .....	81
3.1. Abstract .....	81
3.2. Introduction.....	83
3.3. Materials and Methods.....	84
3.4. Results and Discussion .....	91
3.5. Conclusions.....	125
3.6. References.....	128

Chapter 4 : SIMULATION WITH COMPUTATIONAL FLUID DYNAMICS OF SUCCINIC ACID AND CO-PRODUCT BIOREFINERY PROCESS .....	134
4.1. Abstract .....	134
4.2. Introduction.....	136
4.3. Materials and Methods.....	143
4.4. Results and Discussion .....	168
4.5. Conclusions.....	189
4.6. References.....	190
Chapter 5 : GENERAL CONCLUSIONS .....	199

## LIST OF TABLES

Table 1.1. Oil content for various microalgae [84] .....	24
Table 2.1. Final dry cell weights (DCW) of ALP2 and SLP2 microalgae cultivated for 10 days under different trophic modes on BG-11 medium supplemented with various carbon sources at 4.0 g C/L .....	62
Table 2.2. Final Fatty Acid Methyl Ester (FAME)-GC-based fatty acid profile of raw ALP2 open-tank PBR culture phototrophically grown on BG-11 <sub>0</sub> supplemented with 17.0 g/L NaHCO <sub>3</sub> and 0.133 g/L urea at HCl-adjusted pH 9 .....	73
Table 3.1. Anaerobically-digested food waste effluent properties.....	94
Table 3.2. Fatty-acid profile of ALP2 phototrophically grown on BG-11 <sub>0</sub> supplemented with 7.0 g/L NaHCO <sub>3</sub> and 22.0% (v/v) ADFW levels.....	99
Table 3.3. Performance of ALP2 phototrophically cultivated on BG-11 <sub>0</sub> supplemented with various NaHCO <sub>3</sub> levels, either 0.133 g/L or 0.529 g/L urea, and at HCl-mediated pH 9 .....	117
Table 4.1. Description of major process flow streams .....	145
Table 4.2. Yields, reaction rates, and titers for <i>C. glutamicum</i> , <i>A. succinogenes</i> , and <i>M. succiniciproducens</i> [3] .....	149
Table 4.3. Major processes and associated flow rates, temperatures, and pressures .....	170
Table 4.4. Dimensional Requirements of Units of Operation for Simulated Baseline Process..	172

## LIST OF FIGURES

Figure 1.1. Mass of Fuel vs. Volume of Fuel per Unit Energy [8].....	3
Figure 1.2. Schematic depicting the microalgal intracellular photosynthetic production of lipids, starches, and other products [9] .....	5
Figure 1.3. Value Pyramid of Multiple Products from Microalgal Biomass [2].....	8
Figure 1.4. Schematic depicting microalgal cultivation, harvesting, and downstream biomass conversion processes [26] .....	9
Figure 1.5. Schematic of Microalgal-Based Biorefinery Processes for Biodiesel and Aviation Fuel [27].....	11
Figure 1.6. Schematic of Microalgal-Based Biorefinery for Biodiesel Fuel and Other Co-Products [2].....	11
Figure 1.7. TAG transesterification process for biodiesel [8].....	12
Figure 1.8. Flotation-assisted membrane/orifice sparged PBR built by Pierre Wensel .....	15
Figure 2.1. Plot depicting (Left) forward-scatter vs. side-scatter and (Right) fluorescent PE-Cy5.5 channel vs. side-scatter during Flow Assisted Cell Sorting (FACS) of ALP2 microalgae .....	56
Figure 2.2. Laser-confocal image of ALP2 cells stained with Nile-Red for TAG-lipid fluorescence .....	57
Figure 2.3. UV-Vis multi-wavelength absorbance spectra of ALP2 methanol extracts .....	58
Figure 2.4. UV-irradiated agarose gel depicting electrophoretically migrated PCR amplicons for	

ALP2 (lane 2), SLP2 (lane 3) run alongside a 2-log DNA ladder (lane 1)..... 59

Figure 2.5. Static liquid-state  $^1\text{H}$  NMR spectra of isolated and pooled neutral lipid fractions in  $\text{CDCl}_3$  for ALP2 cells grown in BG-11<sub>0</sub> medium supplemented with 10 g/L  $\text{NaHCO}_3$  and 0.133 g/L urea at HCl-adjusted pH 9. Integral values shown in red above respective peaks including glycerol protons were used to determine the ratio of poly-unsaturated to mono-unsaturated to saturated fatty acids for the isolated TAGs ..... 65

Figure 2.6. Liquid-state  $^1\text{H}$  NMR spectra of ALP2 1<sup>st</sup>-stage flask culture (Red Line) heterotrophically cultivated in BG-11<sub>0</sub> medium supplemented with 10 g/L glucose and 0.529 g/L urea immediately prior to inoculation of second-stage flask culture (Black Line) phototrophically cultivated in BG-11<sub>0</sub> medium supplemented with 10 g/L  $\text{NaHCO}_3$  and 0.032 g/L urea, pH 9.... 67

Figure 2.7. (A) Stacked plot of continuous flow-cell liquid-state  $^1\text{H}$  NMR spectra of ALP2 second-stage flask culture phototrophically cultivated in flask containing BG-11<sub>0</sub> supplemented with 10 g/L  $\text{NaHCO}_3$  and 0.032 g/L urea, pH 9 during initial 92 hour period. Initial sharp peaks at early time points are primarily due to small molecule contaminants in the culture medium. (B) Stacked plot of spectra taken during lipid accumulation stage from 120 hours to 162 hours. Spectra were taken hourly. (C) Static  $^1\text{H}$  NMR spectrum of a sample of culture taken at 92 hours. (D) Static  $^1\text{H}$  NMR spectrum of a sample of culture taken at 162 hours ..... 69

Figure 2.8. Flow cytometric plots for ALP2 (red population) and contaminating cyanobacteria (blue population) phototrophically grown on BG-11<sub>0</sub> medium supplemented with 10.0 g/L

NaHCO<sub>3</sub> and 0.032 g/L urea with HCl-adjusted pH 9 during second-stage of small-scale flask two-stage process. Forward (FSC-H) and side (SSC-H) scatter for cultures at (Top Left) time = 0 days and (Top Right) time = 7 days are depicted. FL3 (FL3-H) and FL4 (FL4-H) fluorescence for cultures at (Bottom Left) time = 0 days (Bottom Right) time = 7 days are depicted ..... 71

Figure 2.9. OD<sub>680</sub> as function of time for ALP2 cultivated in first-stage 1 L fermentor followed by second-stage indoor 40-L open-tank PBR. Arrows designate addition of H<sub>2</sub>O to compensate for evaporative losses ..... 72

Figure 3.1. OD<sub>680</sub> as function of time for ALP2 heterotrophically grown on BG-11 medium supplemented with 0, 1, 5, 10, and 20 g/L glucose at 21°C ..... 92

Figure 3.2. OD<sub>680</sub> as function of time for ALP2 heterotrophically grown on BG-11<sub>0</sub> medium supplemented with 10 g/L glucose and various nitrogen sources at different temperatures. .... 93

Figure 3.3. OD<sub>680</sub> as function of time for ALP2 phototrophically grown on BG-11 medium supplemented with 1.4, 7.0, 14.0, and 28.0 g/L NaHCO<sub>3</sub> levels with pH initially adjusted to 7 but subsequently left unadjusted ..... 96

Figure 3.4. High-resolution magic angle-spinning (HR-MAS) <sup>1</sup>H NMR spectra of raw ALP2 culture phototrophically grown on BG-11<sub>0</sub> supplemented with 3.5 g/L NaHCO<sub>3</sub> and 0.133 g/L urea at HCl-adjusted pH 9. Red integral values shown over respective peaks ..... 100

Figure 3.5. (A) OD<sub>680</sub>, (B) cell density, (C) pH, (D) total nitrogen remaining in medium, (E) total inorganic carbon remaining in medium, and (F) net <sup>1</sup>H NMR-based neutral lipid concentration as

function of time for ALP2 cultures phototrophically grown in a diurnal light cycle on BG-11 <sub>0</sub> supplemented with 0.133 g/L urea and either 1.4 or 17.0 g/L NaHCO <sub>3</sub> , with pH either left unadjusted or adjusted to 9 .....	108
Figure 3.6. ALP2 net photosynthesis as function of pH and NaHCO <sub>3</sub> level.....	114
Figure 3.7. Normalized 77K-435 nm excitation wavelength as function of emittance for ALP2 transitioned from 0.84 to 33.64 g/L NaHCO <sub>3</sub> .....	115
Figure 3.8. Liquid-state static <sup>1</sup> H NMR spectra of raw ALP2 culture phototrophically grown on BG-11 <sub>0</sub> supplemented with 10.0 g/L NaHCO <sub>3</sub> and 0.133 g/L urea at HCl-adjusted pH 9. Blue integral values shown below respective peaks.....	118
Figure 3.9. Three-Dimensional flow-cytometric plots depicting histogram (vertical axis), cellular size (FSC axis), and granularity (SSC axis) for ALP2 phototrophically grown on BG-11 <sub>0</sub> medium supplemented with 0.133 g/L urea and either (Left) 1.4 g/L or (Right)17.0 g/L NaHCO <sub>3</sub> levels at HCl-adjusted pH 9 .....	119
Figure 3.10. Chlorophyll fluorescence-based photosynthetic parameters of phototrophically grown ALP2 as function of NaHCO <sub>3</sub> levels initially supplemented to BG-11 <sub>0</sub> medium, along with 0.529 g/L urea, at HCl-adjusted pH 9 .....	121
Figure 3.11. Total ALP2 chlorophyll and carotenoid content in methanol extracts from phototrophically grown ALP2 as function of NaHCO <sub>3</sub> and urea levels at HCl-adjusted pH 9..	122
Figure 4.1. General flow diagram for succinic acid biorefinery.....	144

Figure 4.2. Algorithm of coupled CFD fermentor simulation .....	150
Figure 4.3. Changes in major stream flow rates throughout process.....	169
Figure 4.4. Lignin microfiltration membrane area and power consumption vs. recirculation rate .....	173
Figure 4.5. Graphical estimation of optimal steady-states and dilution rate for <i>M. succinoproducens</i> fermentor .....	174
Figure 4.6. CFD Simulation of Cooling Heat Transfer Area vs. Impeller Speed for 178 m <sup>3</sup> fermentor.....	175
Figure 4.7. CFD average liquid velocity flow fields at 10, 100, and 200 rpm in 178 m <sup>3</sup> fermentor .....	176
Figure 4.8. Cooling heat transfer area requirement vs. impeller diameter for 178 m <sup>3</sup> fermentor.....	177
Figure 4.9. CFD Liquid velocity flow patterns at 78 m <sup>3</sup> and 178 m <sup>3</sup> fermentor volumes .....	177
Figure 4.10. CFD Liquid velocity flow patterns at alternating (left) and fixed axial impeller spacing (right) for 78 m <sup>3</sup> fermentor .....	179
Figure 4.11. Adsorption equilibrium curve and operating line for glucose removal .....	182
Figure 4.12. Estimation of gel polarization concentration for nanofiltration .....	184
Figure 4.13. Periods of return of investment for succinic acid selling price of \$1 U.S./kg.....	189

## CHAPTER 1 : INTRODUCTION

### 1.1. Transition to Refining of Biomass

The continued consumption of chemicals and aviation and diesel fuels derived from the traditional refining of fossil-based, petroleum feedstocks is now widely considered unsustainable because of concerns over national security, rising prices in crude oil, climate changes, and the need for rural development. Biomass is currently viewed as the only long-term, CO<sub>2</sub>-neutral, renewable carbon source that can be directly used to produce chemicals like succinic acid and drop-in, high-energy density liquid “biofuels” to eventually totally displace petroleum-derived transport fuels [1-4]. Biomass can include various types of biowaste (i.e. food wastes, municipal wastes, agricultural wastes), energy crops (i.e. edible and non-edible oilseeds), and aquatic plants [3]. The DOE and USDA estimate that at least 1.3 billion sustainable dry tons are available annually from forestry and agricultural lands in the U.S. to displace petroleum-based fuels and products. The biorefinery is the most promising way to create a new, domestic, biomass-based industry [2, 5]. A biorefinery is essentially a facility that integrates processes, technologies, and equipment to transform and convert the different primary components of raw, renewable biomass feedstocks (i.e. carbohydrates, protein, lipids) and their intermediates into transportation fuel, power, and multiple value-added chemicals and advanced materials within the framework of minimum waste and emissions and fossil inputs [2, 3, 5].

Examples of biofuels include biodiesel and renewable jet fuel. Beside sustainability, biodiesel

and renewable jet fuel offers other significant advantages over petrodiesel and conventional jet fuel, respectively. The synthetic paraffin kerosenes (SPK) that comprise renewable jet fuel are devoid of sulfur and aromatics for a cleaner burn [6]. Although its 37.27 MJ/kg energy density is 9% lower than that of #2 low-sulfur petrodiesel, biodiesel also has no sulfur and much higher cetane rating, oxygenation, and hydrogenation for more complete combustion and fewer emissions [7]. Biodiesel is also safer to handle and transport because it has a higher flash point of 148°C compared to 52°C for petrodiesel [7]. Biodiesel can also be conveniently “dropped-in” without vehicular modification [3] and used in pure form (B100) or blended with other petroleum fuels like #2 low sulfur diesel, #1 diesel/kerosene, and heating oil at a wide range of concentrations [7]. Also, the higher solvating and lubricative properties of biodiesel can in low altitudes and high pressure systems actually break down deposits, reduce the wear, and increase the life of fuel pump injection equipment relying on fuel-based lubrication. Most natural rubber gaskets and hoses of vehicles manufactured after 1992 were replaced with FKM, which is nonreactive to biodiesel, and additives to significantly lower the pour point and cold filter plugging point of pure biodiesel are now commercially available [7]. Properties of various fuels are presented (Figure 1.1)

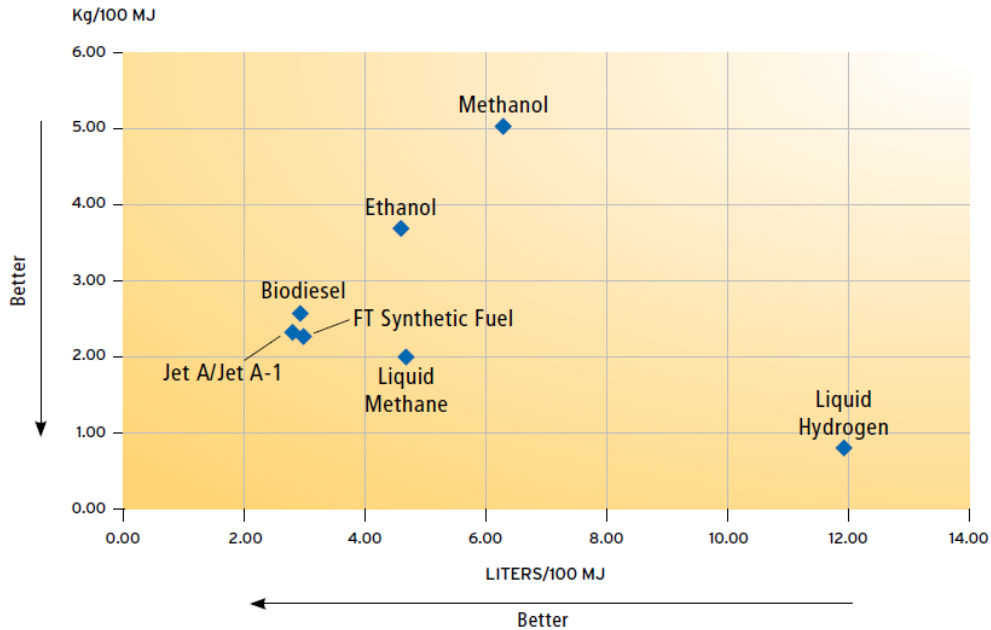


Figure 1.1. Mass of Fuel vs. Volume of Fuel per Unit Energy [8]

## 1.2. Advantages of Microalgal Biomass Feedstocks

Third-generation advanced biofuels are derived from microorganisms like yeast and microalgae [2, 9, 10]. Following the extensive research conducted during the National Renewable Energy Laboratory's (NREL) Aquatic Species Program of the 1970s-1990s, microalgae have been identified as a promising and viable biomass feedstock for the production of these [1, 2, 9-11] and valuable co-products [9, 10]. Algae are a large and heterogeneous collection of simple, typically autotrophic, eukaryotic, and aquatic organisms from diverse environments [3]. They can photosynthetically convert inexpensive and abundant sunlight energy, CO<sub>2</sub>, and water into chemical energy and biomass in the form of carbohydrates, lipids, proteins, and other metabolites [9]. Algae can be generally grouped as either multicellular macroalgae (a.k.a. seaweed) that

include brown algal kelps, or unicellular and microscopic microalgae [3]. Microalgae possess photosynthetic chloroplast organelles and primarily synthesize and accumulate energy-rich storage compounds like starches and the neutral lipid triacylglycerides (TAG) [4] (Figure 1.2). These lipids are used to later produce SPK for aviation [1] and biodiesel for electrical power generation [2] and ground transportation [3]. Over 30,000 diverse microalgal species in the world have been described [10], but the most commercially important belong to the diatoms and the green algae genus *Chlorella*, *Dunaliella*, and *Haematococcus*[3].

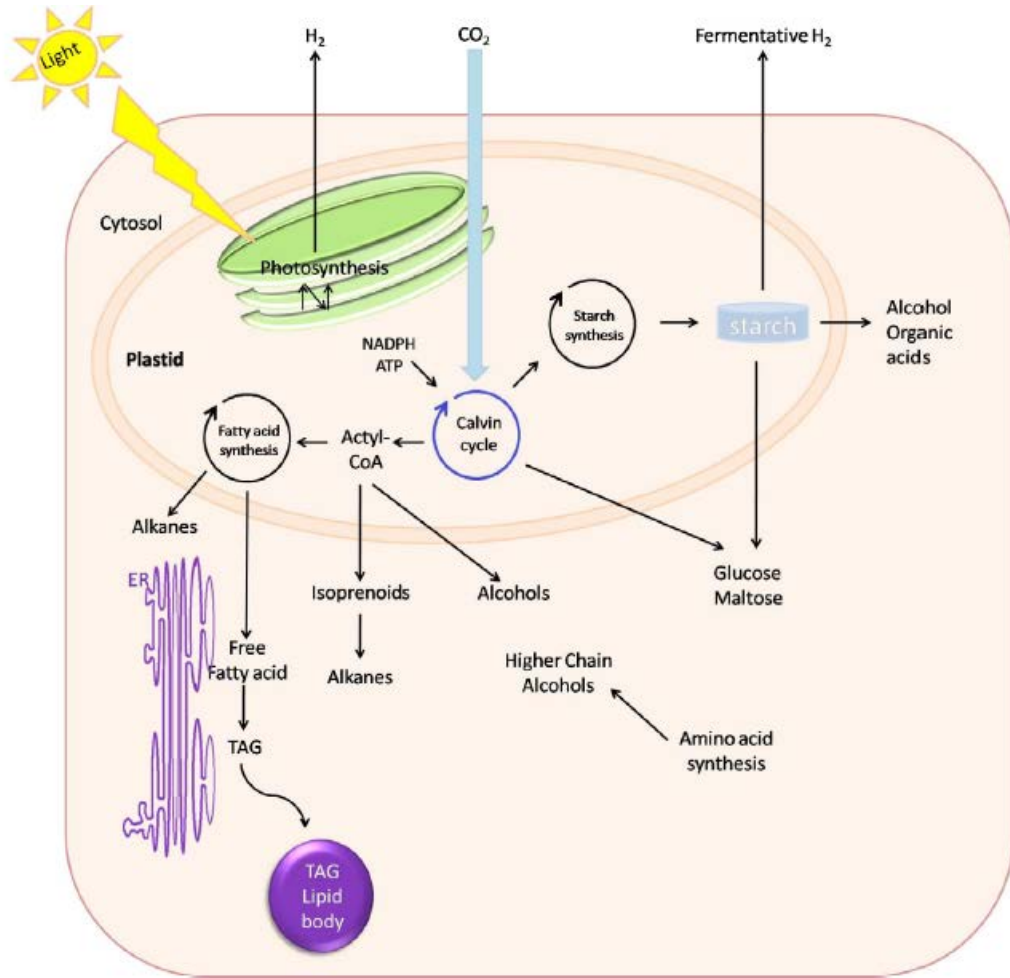


Figure 1.2. Schematic depicting the microalgal intracellular photosynthetic production of lipids, starches, and other products [9]

There are various advantages of microalgae over any other biomass feedstock as a source of biofuels and co-products:

1. Microalgae synthesize and accumulate larger intra-cellular quantities of lipids for biodiesel and aviation fuel than first-generation biomass feedstocks like terrestrial vegetable oil-seed crops. Depending on microalgal species, oil contents range 16–77% dry cell weight of biomass, with 30%

common [2, 9]. Microalgae also have exponential growth proliferation rates 20-30 times higher than those of terrestrial plants and can double their biomass in periods as short as 3.5 hrs [10]. Such higher biomass productivity is attributable to their simpler, non-vascular structure that is devoid of functional parts like roots, leaves, and lignin. This can also be attributed to their more efficient photosynthesis compared to agricultural and large terrestrial C4 plants that form four-carbon stable intermediates and have lower photo conversion efficiencies. Microalgae can also grow in suitable culture vessels in every season throughout the year in warm, tropical, and subtropical climates [5]. For these reasons, microalgal annual oil yields on an area basis exceed those of the best producing oil crops [2, 3, 9].

2. Unlike the animals and crops from which fats and seed oils are derived, microalgae can tolerate and be cultivated on marginal lands (e.g. non-arable, infertile, desert, arid and semi-arid lands)[1-3, 9, 12]. Thus, they do not directly compete for the farm land needed for conventional human agriculture production of food crops and livestock fodder [3, 12].

3. Microalgae can also tolerate and be cultivated in saline, hypersaline, fresh, brackish wastewaters in lakes, rivers, and oceanic coastal areas and thus do not compete for water resources with conventional agriculture [2, 3, 5, 12-14].

4. Microalgae can use nitrogen and phosphorus and remove some heavy metals from diverse wastewater sources (e.g. agricultural-food processing runoff, organic effluent from concentrated animal feed operations, and industrial and municipal wastewaters) during growth. This provides

the additional economic benefit of sustainable wastewater bioremediation [2, 3, 5, 12-14].

Microalgal cultivation also does not require or compete for the herbicides or pesticides application used in agriculture [3, 5].

5. Most microalgae can fix or reduce CO<sub>2</sub> as primary carbon source into biomass and other metabolic organic products via photosynthesis at rates that are 10–50 times higher than those of terrestrial plants [9]. Algae typically consume 1.83 g CO<sub>2</sub> to produce 1 g of biomass [1, 3]. Thus, microalgal cultivation potentially represents a way to sequester naturally-occurring and anthropogenic waste greenhouse gas CO<sub>2</sub> from the atmosphere, flue emissions from fossil fuel-fired power plants, and other sources, into a carbon cycle in which no additional CO<sub>2</sub> is emitted [1-3].

6. Microalgal-derived biofuels are free of sulfur and non-toxic [3, 9].

7. Microalgae can tolerate, adapt to, and be cultivated in extreme environmental conditions like those involving low sunlight, minimal CO<sub>2</sub>, high alkalinity, and salinity [1, 15, 16].

8. Some microalgae species offer the additional flexibility to grow heterotrophically [17-20] and mixotrophically [21-23] on organic carbon in fermenters and photobioreactors when outdoor temperatures are too low.

9. A wide array of products for a multitude of applications have great potential to be manufactured from a microalgal biomass feedstock (Figure 1.3)[2].

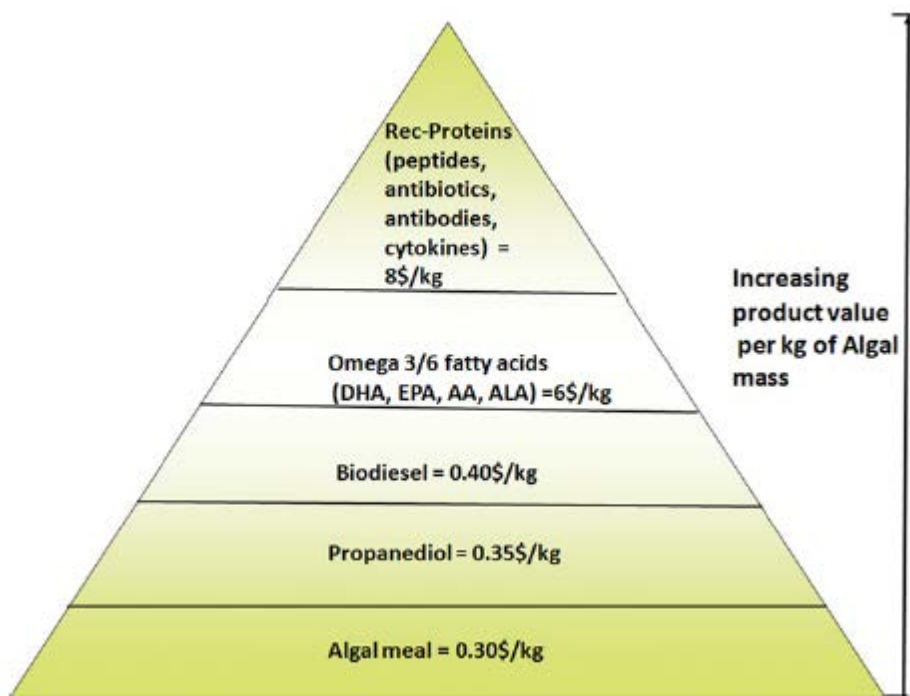


Figure 1.3. Value Pyramid of Multiple Products from Microalgal Biomass [2]

These include energy products (e.g. aviation biofuel[2], biodiesel[9], bioethanol[2, 9], biomethane[2, 3], biohydrogen[2, 3]) and other beneficial, value-added chemical co-products or byproducts (e.g. fertilizer[2, 3, 12], glycerine, toxins[5], sterols[5], detergents, medically-important biopolymers or plastics [2], polysaccharides[5, 24], enzymes and recombinant proteins[2, 12], peptides, cosmetics, pigments[2], feed for aquaculture and livestock [2, 3, 12], pharmaceuticals, fine human food supplements [25] and nutraceuticals like carotenoids, antioxidants, and long-chain polyunsaturated  $\omega$ -3 fatty acids, vitamins, anti-fungal microbial, anti-viral toxins [3, 5, 9].

### 1.3. Microalgal Biorefinery Cultivation and Harvesting Processes

A microalgal-based biorefinery aiming to obtain such a wide range of products can include steps involving upstream microalgal cultivation and harvesting, as well as downstream biomass isolation and conversion processes for lipid, protein, and carbohydrate fractions (Figures 1.4, 1.5, 1.6).

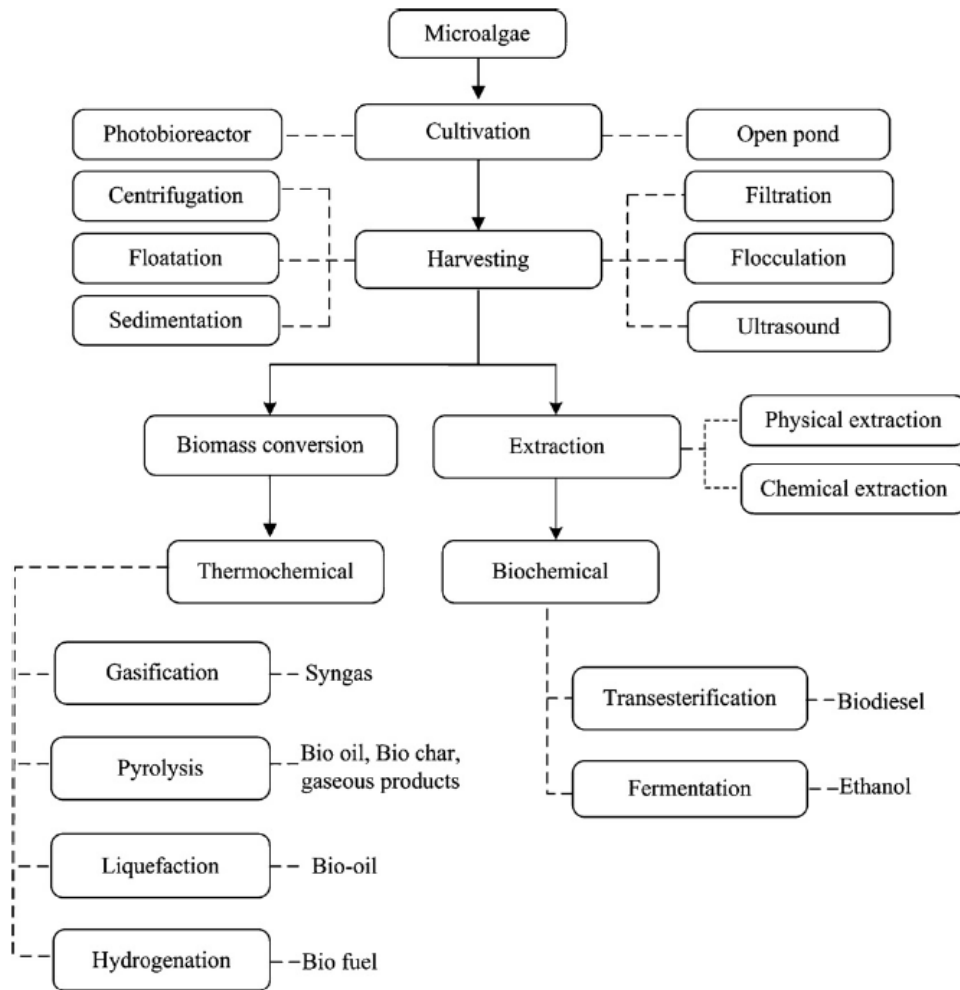


Figure 1.4. Schematic depicting microalgal cultivation, harvesting, and downstream biomass conversion processes [26]

The main lipid components of the microalgal biomass are triacylglycerides (TAG), free fatty acids, waxes, sterols, hydrocarbons, glycolipids, and phospholipids [10]. These can be generally classified as storage or membrane lipids [5] or also as polar (i.e. phospholipids, glycolipids) or neutral (i.e. TAGs and waxes)[11]. Storage lipids are mainly neutral lipids like TAGs constituting 20-40% of the total lipids, with fatty acids containing 14-20 carbons with lower degree of unsaturation useful for biodiesel manufacture [9]. TAGs are three chains of fatty-acids joined by a glycerin molecule whose synthesis pathway involves the three main steps: (1) the conversion of acetyl-Co A to malonyl-CoA, catalyzed by acetyl-Co A carboxylase (ACCase); (2) the elongation of the carbon chain of fatty acids; and (3) TAG formation [9, 11].

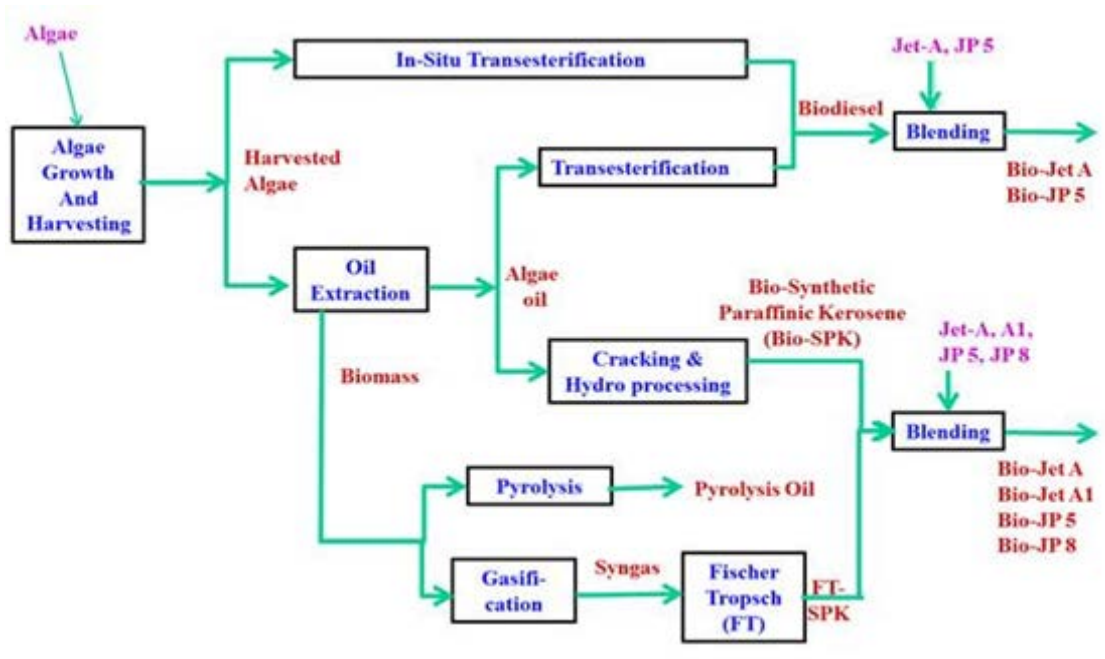


Figure 1.5. Schematic of Microalgal-Based Biorefinery Processes for Biodiesel and Aviation

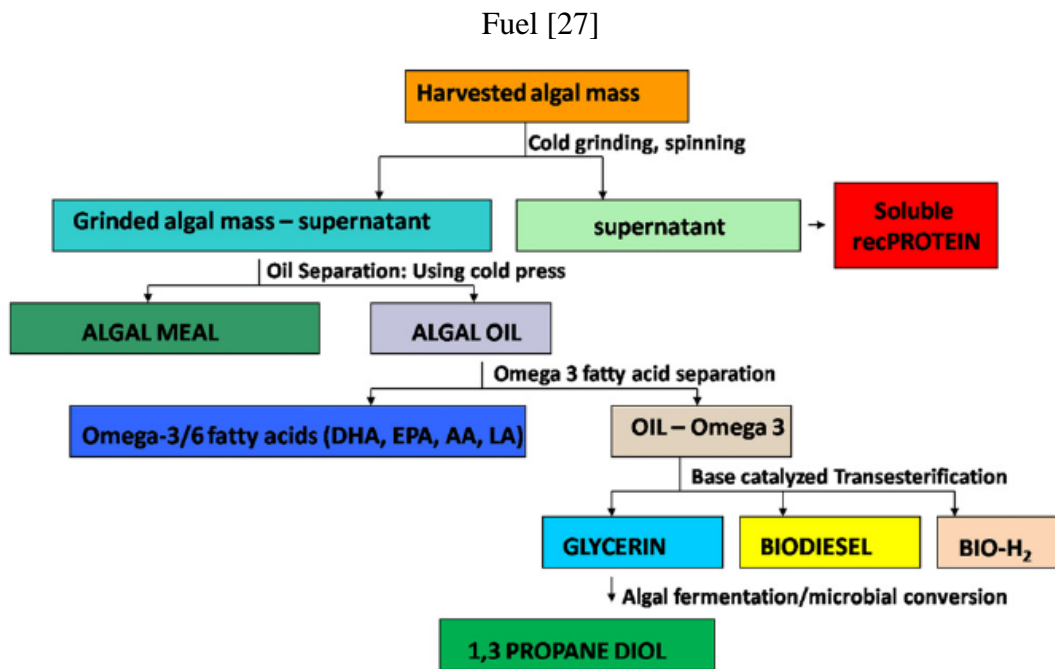


Figure 1.6. Schematic of Microalgal-Based Biorefinery for Biodiesel Fuel and Other

Co-Products [2]

Once cultivated microalgae are harvested, TAGs and free fatty acids are typically extracted from dewatered and dried biomass with organic solvent (i.e. hexane) or mechanical means, leaving residual biomass or meal. During subsequent conventional transesterification reactions on the separated oils, triglycerides (TAGs) are converted to diglycerides (DAGs), then diglycerides are converted to monoglycerides (MAGs), and then monoglycerides are converted to Fatty Acid Alkyl Esters (i.e. FAME or FAEE) as biodiesel) and glycerol as by-product [10, 12] when the glycerin of the TAG/DAG/MAGs are replaced with methanol (or ethanol) using a catalyst that is either alkali, acid, or lipase[3] (Figure 1.7).

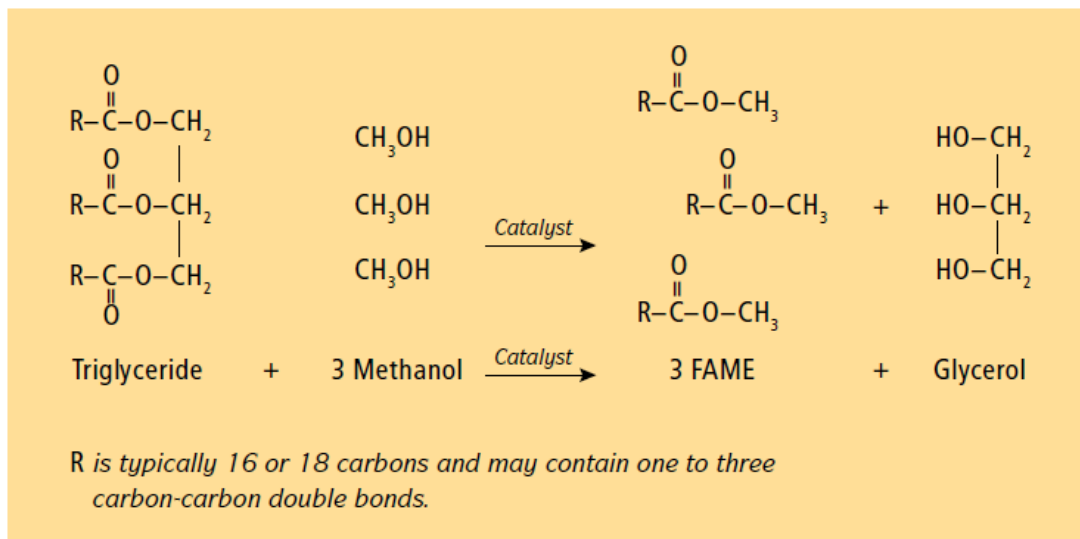


Figure 1.7. TAG transesterification process for biodiesel [8]

The separated oils can also undergo hydrotreatment and catalytic cracking to yield synthetic paraffin kerosene (Bio-SPK) which can be blended to yield aviation fuel [6, 27]. The residual algal meal is a rich source of high-quality protein, carbohydrates[2], residual lipids, vitamins, micronutrients and trace elements, and pigments (i.e. chlorophyll and carotenoids) that can be used as feed for livestock or aquaculture[2, 3, 12], anaerobically digested to biomethane [3, 12] and applied as fertilizer[2, 3, 12], or fermented for bioethanol[2, 9]. The dry residual microalgal biomass can also instead undergo a thermochemical gasification process to produce syn-gas (CO, H<sub>2</sub>) that then undergoes a Fisher-Tropsch (FT) synthesis process to yield SPK for aviation fuels[2, 4, 6, 28, 29]. Alternatively, the whole wet microalgae can be hydrothermally liquefied [4], and the whole dried microalgae can be pyrolyzed to a bio-oil that is then refined to other fuel and chemical products [3, 10].

Microalgae are capable of phototrophic, and in some cases, heterotrophic and/or mixotrophic cultivation [17, 18, 30, 31]. Microalgal phototrophic growth is based on using light and CO<sub>2</sub> to produce chemical energy during photosynthesis. This offers the advantage of CO<sub>2</sub> sequestration [3, 32] and lower contamination risk [2], but the disadvantage of poor light penetration in dense cultures due to mutual shading [1]. Heterotrophic growth involves growing in the dark on organic carbon (i.e. glucose, acetate, glycerol, fructose, sucrose, lactose, galactose, and mannose) as a carbon source [2, 33]. This offers the advantage of higher efficiency, biomass productivity, oil yields, and no light requirement [18] but the disadvantage of higher contamination risk.

Mixotrophic growth is a combination of phototrophic and heterotrophic growth [33]. Mixotrophic growth involves using organic carbon via oxidative phosphorylation, as well as inorganic carbon and light via photosynthesis [22, 34]. Mixotrophic growth has reportedly resulted in the highest oil and biomass productivities for all growth modes for *Chlorella sp.*[33, 35]. Mixotrophic operation costs are high because of special precautions to reduce the risk of contamination and satisfy light requirements for enclosed photobioreactors during scaling-up.

The two common microalgal culturing systems are artificial open-ponds and engineered closed photobioreactors (PBRs) [36, 37] (Figure 1.8). Open-ponds involve phototrophic cultivation using free sunlight that depends on daily and seasonal variations in light intensity. Open ponds have a variety of shapes and sizes, but the most commonly used pond design is a closed-loop rectangular raceway pond. These are constructed from two trenches dug in the ground with a separating barrier that enables water to flow in a circular motion around the pond like a racetrack with recirculation channels [1, 5]. The bottom of the pond is compacted and lined with polyvinylchloride (PVC) to prevent the loss of media and nutrients [1]. The pond usually operates at between 0.1-0.3 m liquid depth to maximize sunlight penetration [1]. Appropriate pH can be adjusted by ventilation or gassing with CO<sub>2</sub> or air/CO<sub>2</sub> mixture. A paddle wheel mixes and circulates microalgal biomass to prevent the settling and clumping [1]. Mixing also ensures dispersal of sparged CO<sub>2</sub> bubbles for high gas-liquid mass transfer, uniform light exposure, uniform nutrient concentration, and removal of dissolved oxygen [5] which can cause

photo-oxidative damage to the photosynthetic apparatus at saturation light intensity. Flow is guided around bends by baffles positioned in the flow.

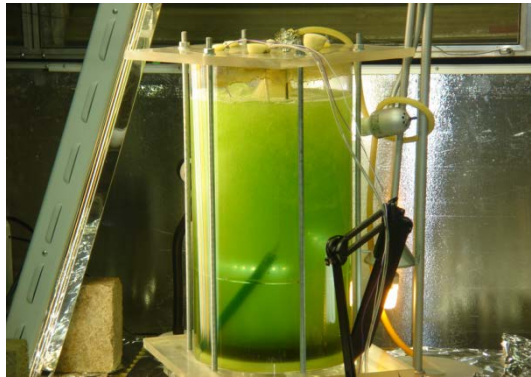


Figure 1.8. Flotation-assisted membrane/orifice sparged PBR built by Pierre Wensel

Continuous daily harvesting of open-pond cultures, behind the paddle wheel usually, promotes high growth rates by preventing nutrient depletion and mutual shading caused by high cell densities [1]. Equal and constant feed and harvest rates for new culture medium and microalgal broth make the process continuous[1, 5]. Flocculation-mediated harvesting generally works on the premise that the usually repulsive negative-charge on microalgae can be shielded by added flocculants (i.e.  $\text{Al}_2(\text{SO}_4)_3$ ,  $\text{FeCl}_3$ ,  $\text{Fe}_2(\text{SO}_4)_3$ ) to allow attraction and microalgal coagulation[1]. Microalgal surface charge at physiological conditions is typically negative, with zeta potential ranging from 25 to 240 mV [11].

Open-pond systems feature low capital/construction costs [1, 3], ease of scale-up, large production capacity, simple operation with few variables to control ( $\text{CO}_2$  and nutrient concentration). Raceway pond operational costs include maintenance, harvesting and de-watering,

microalgal nutrients, electricity and supplementary heating costs for pumps, blowers, and paddle-wheel motors [1, 3].

However, large-scale, outdoor cultivation and harvesting in open-ponds of a photosynthetic biorefinery are still constrained in part by low revenues associated with low biomass and oil volumetric productivity (i.e. biomass concentrations of 0.5-1.5 g dry weight L<sup>-1</sup> and biomass productivities of 0.05-0.2 g L<sup>-1</sup> day<sup>-1</sup>) [5, 38], lack of year-round operations due to cold and dark nights and winters, variable diurnal sunlight, and inadequate temperature controls [1, 39], and contamination by airborne invasive species [40, 41], as well as high costs associated with unsustainable supplies of nutrients (e.g.; nitrogen [2, 42-44] and phosphorous[2, 3, 11]) and inorganic carbon [45], surface land acreage for inoculum and primary cultures [39, 41], high freshwater usage and evaporation rates due to high surface areas[1, 41] and inefficient harvesting [3, 46, 47]. Appropriate microalgal strain selection [9], identifying preferable operating culture conditions[9], medium composition, and environmental factors via greater understanding of microalgal photosynthetic metabolism and physiology[9, 11], proper siting of algal biorefinery [1], and design of efficient and economically feasible microalgae cultivation systems [9] are critical to overcome these challenges for improved and optimal production of biomass and target-products (i.e. lipids, carbohydrates, proteins and pigments) in an algal biorefinery[9, 48].

Major physical stimuli for lipid productivity are temperature and light (i.e. wavelength and intensity), and major chemical stimuli are pH, salinity, mineral salts, carbon source and

concentration, and nitrogen source and concentration [9]. To maximize productivity, saturation light intensity should be distributed throughout the open-pond. Light attenuation caused by shading effects [1], increasing cell density and secreted product concentrations, sparged air bubbles, or biofilms on transparent wall surfaces, can all be minimized by sufficient mixing strategies and daily harvesting [9]. High light intensity can lower total polar lipid content and increase total neutral storage lipids (TAGs) [9]. Microalgal TAG lipid accumulation is enhanced and can sometimes double at the expense of slower cell growth via several specific cultivation conditions or other environmental/nutritional factors like high C/N medium [1, 9], high pH, cultivation phase, or sulfur or phosphate nutritional depletion stress conditions. Both the lipid content and biomass production rate should therefore be considered simultaneously to ensure efficient microalgal lipid production[9]. Nitrogen limitation is the most widely used and reliable strategy to increase microalgal lipid content[9].

Challenges associated with long residence times and contamination of outdoor open-pond cultures [36] could be overcome by selecting and using a multi-trophic microalgae that can be efficiently cultured under heterotrophic or mixotrophic conditions as well as phototrophic conditions [45]. A two-stage cultivation strategy was previously devised around this concept[39]. Heterotrophic *Chlorella sp.* culture conditions in a closed fermentor (first-stage) enabled the use of glucose organic carbon substrate [39] to rapidly achieve high densities as inoculum for an outdoor phototrophic open-pond culture (second-stage). At this second-stage open-pond culture, residence

time was minimized, and a dominant monoculture of desired *Chlorella sp.* microalgae was established by allowing it to outcompete or withstand undesirable environmental contaminants like bacteria, viruses, fungi, zooplankton, insects, leaves, and other airborne debris[39, 45]. Commercially feasible, low-maintenance, low surface area-volume ratio fermentors currently used for industrial production of medicines, beverages, food additives, and energy [17, 49] could be used for such first-stage heterotrophic cultivation without light-limitation[17, 49].

Additionally, the organic carbon for such first-stage heterotrophic cultivation in an integrated photosynthetic algal biorefinery could be alternately derived from cheap ligno-cellulosic waste biomass feedstocks and other sources. These include acetic acid from pyrolyzed forestry residues[50], glucose from pre-treated and enzymatically hydrolyzed agricultural crop residues like rice straw[51], and waste crude glycerol from the biodiesel trans-esterification processes after distillation removal of residual inhibitory methanol[52]. The high logistical feedstock costs associated with transporting, storing, and grinding such ligno-cellulosic biomass like wheat-straw to uniform particle size prior to pyrolysis, gasification, or combustion at a biorefinery have previously been addressed via a torrefaction pre-treatment[53]. Torrefaction is a low-temperature (250-300°C) and self-sustaining thermochemical pre-treatment occurring in an inert, O<sub>2</sub>-less atmosphere [53]. It results not only in a drier, more brittle, and hydrophobic solid biomass but also in combustible high-heating value gases (CO, CH<sub>4</sub>), and a liquid condensate containing potentially useful carboxylic acids (i.e. acetic, formic, and butyric acids) arising mostly from the

thermal-degradation of hemicellulose [53].

As well-adapted oxygenic photosynthetic organisms, microalgae at first glance appear to be ideal candidates to remove the ambient (i.e. 385 ppm [1]) greenhouse gas CO<sub>2</sub> outdoors in outdoor large-scale open ponds and sequester it in the form of biomass. However, under these conditions microalgae growing in full sunlight become carbon-limited where the rate of carbon uptake and use in the culture exceeds the diffusive mass transfer of CO<sub>2</sub> from atmospheric gas into the medium. To compensate for this, microalgae have evolved energy-intensive Carbon Concentrating Mechanisms (CCM) [54, 55] to import and concentrate CO<sub>2</sub> around the enzyme RuBisCo, potentially at the expense of downstream metabolic processes like those involving TAG neutral lipid accumulation.

The previously proposed alternative of directly compressing and sparging a concentrated CO<sub>2</sub>-containing waste exhaust from fermentor or flue gas (~11% (v/v)) from lignin-fired boilers of an integrated corn-ethanol biorefinery into outdoor microalgal cultures is also troublesome [45, 56]. For instance, GreenFuel Technologies had tried to adapt microalgae to grow in closed PBRs aerated with unfiltered flue gas [1]. Operations were discontinued due to inconsistencies and unexpected consequences of large-scale growth in closed systems during pilot plant demonstrations [1].

Sparging large quantities of waste CO<sub>2</sub> into the open-pond would acidify the culture medium, increase the risk of contamination, and potentially affect adversely the microalgal physiology. A

microalgal species able to withstand pH shifts (and high  $\text{SO}_x/\text{NO}_x$  concentrations if flue gas was used as  $\text{CO}_2$  source) would also need to be selected. Other limiting factors include the relatively large land area required. For instance, it was previously suggested that a 1MW plant facility producing 8,323 metric tons of  $\text{CO}_2$  would require between a 16 hectare algal bioreactor facility yielding  $80 \text{ g dry weight m}^{-2} \text{ day}^{-1}$  or a 64 hectare algal facility yielding  $20 \text{ g dry weight m}^{-2} \text{ day}^{-1}$  [57]. Other drawbacks include the inability to capture more than 25-30% of  $\text{CO}_2$  in one pass from a flue stream and prevent medium acidification and the undeveloped state of this technology [57]. Storability of  $\text{CO}_2$  during nights and winters when it is least needed, and its retention during hot days, are also low due to low solubility and high surface area-induced out-gassing [45]. These in turn result in high capital and operating costs of compressors and sparging of flue gas. However, using  $\text{NaHCO}_3$  instead of  $\text{CO}_2$  as inorganic carbon supply offers multiple advantages:

First, bicarbonate is more soluble, transportable, and storable at night when least needed compared to  $\text{CO}_2$  gas, representing savings by reduced pressurization requirements and outgassing losses in highly evaporative, high surface-area open-ponds [45]. There is a complex relationship between  $\text{CO}_2$  concentration and pH in microalgal bioreactor systems, owing to the underlying chemical equilibrium among such chemical species as  $\text{CO}_2$ ,  $\text{H}_2\text{CO}_3$ ,  $\text{HCO}_3^-$ , and  $\text{CO}_3^{2-}$ . A closed-loop integrated system was previously described whereby carbonate-enriched spent alkaline media from phototrophic open-ponds used to cultivate halo-alkaline tolerant microalgae is recycled to reactors that capture and convert the  $\text{CO}_2$  from scrubbed and cooled waste flue-gas

emissions, etc. to produce bicarbonate-enriched supplement media for the open-ponds [45, 58]. Previous research has described reactors [59, 60] that could potentially feature highly loaded, active, stable[61], thermohaloalkaline-tolerant [62-68] $\alpha$ -carbonic anhydrase enzyme that is covalently attached and immobilized in protective and aqueous hydrogel surrounded by countercurrent hollow fibers[69-73]. The drawbacks of this technology would be the high cost of cultivating *E.coli* on organic carbon to express a recombinant carbonic anhydrase enzyme that then requires expensive chromatographic purification [74] and destabilizing solvent-mediated immobilization. Both proximity of such CO<sub>2</sub> capture/conversion reactors to open-pond PBRs as well as microalgal tolerance to extreme bicarbonate levels maximize the efficiency of recycling evaporative water and alkaline buffer capacity of spent growth media [45]. This is because costs associated with the compression, piping, and transportation of flue gas and recycled spent media increase with distance and bicarbonate dilution [45, 75].

Second, bicarbonate is more useful than acidifying CO<sub>2</sub> to reduce contamination risks in outdoor open-ponds. For instance, high bicarbonate content and low concentrations of gaseous CO<sub>2</sub> were identified as the major factors that prevented the contamination of halo-alkaline tolerant *Spirulina sp.* cultures by *Chlorella sp.* [1, 11, 76]. In addition to high inoculation cell densities obtained from heterotrophic first stages, commercial cultivation of halo-alkaliphiles or halo-alkaline tolerant phototrophs that can uniquely withstand and even thrive on the high salinity and the high external pH, OH<sup>-</sup>, and carbonate (Na<sub>2</sub>CO<sub>3</sub>) levels from the photosynthetic

consumption of high bicarbonate levels represents a way to limit outdoor contamination by intolerant invasive species. For instance, a controlled pH 10 and 0.2 M (16.8 g/L)  $\text{NaHCO}_3$  were used to limit outdoor contamination in large-scale open-pond *Spirulina platensis* cyanobacteria cultures [1, 76]. Bicarbonate is also lower in cost and contamination risk compared to glucose and other organic carbon sources when cultivating in cheaper and scalable outdoor open-pond PBRs.

Third, bicarbonate is potentially preferred by microalgae for both growth and lipid accumulation [77, 78]. Phototrophs have already developed efficient carbonic anhydrase-mediated enzymatic conversion and active/passive transporter systems for the uptake of  $\text{HCO}_3^-$  and its conversion to  $\text{CO}_2$  for photosynthesis [54]. Carbon-limited *Syecococcus lkopoliensis* grown in chemostats exhibited a very high photosynthetic affinity for and used  $\text{HCO}_3^-$  rather than  $\text{CO}_2$  for growth [79]. Furthermore, supplementation of  $\text{HCO}_3^-$  to nitrogen-starved,  $\text{CO}_2$ -sparged *Chlamydomonas reinhardtii* microalgal cultures reportedly triggered a photosynthetic increase in both pH and their neutral TAG-lipid accumulation [77]. Fourth, the alkalinity supplied by high  $\text{NaHCO}_3$  levels and the resulting high pH resulting from its photosynthetic consumption can potentially enable  $\text{Mg}(\text{OH})_2$ -mediated auto-flocculation to cost-effectively harvest and de-water microalgae [46, 80, 81]. Challenges associated with outdoor contamination [76], low volumetric lipid productivity [5, 77], harvesting [3, 46, 80], and supply of inorganic carbon to 2nd-stage open-pond phototrophic cultures [45] could therefore be overcome by using high levels of bicarbonate salts that maintain a moderately high pH via bicarbonate

buffering.

With all things considered, selection of a microalgal species for growing biomass and manufacturing targeted products should therefore be based on at least the following criteria: (1) ability to grow in extreme medium conditions (i.e. high pH, salinity, alkalinity, high levels of NO<sub>x</sub>/SO<sub>x</sub> from flue gas if such process was implemented[1]); (2) high specific growth rates[1]; (3) cell characteristics to reduce harvesting costs (i.e. filamentous *Spirulina* sp. cyanobacteria[1, 3, 11]); (4) tolerance to temperature [1, 9] and diurnal and cloud/weather-related light intensity variations[1]; (5) ability to outcompete invasive species and establish mono-culture[1], (6) ability to also grow quickly heterotrophically or mixotrophically on a wide range of organic carbon substrates [82, 83], and (7) high intra-cellular lipid content within cells[1, 9]. There is considerable variation in the fatty acid profile, utility, and % content of TAG pre-cursor to biodiesel among the different microalgae species [84](Table 1.1). Genetic manipulation is another way to generate a high-performance microalgal strain [1]. Among such efforts are the increase of areal productivity by altering photosynthetic antenna size and the augmentation of lipid content via metabolic engineering [1, 3, 85, 86].

Table 1.1. Oil content for various microalgae [84]

<b>Microalgae</b>	<b>Oil content (dry weight %)</b>
<i>Boytyococcus braunii</i>	25-75
<i>Chlorella protothecoides</i>	14-57
<i>Cryptocodinium cohnii</i>	20-51
<i>Dunaliella teriolecta</i>	16-71
<i>Nannochloris sp.</i>	20-56
<i>Neochloris oleoabundans</i>	29-65
<i>Phaeodactylum tricornutum</i>	18-57
<i>Schizochytrium sp.</i>	50-77
<i>Skeletonema coastatum</i>	13-51

#### 1.4. Necessity for Technological Advancements and Process Simulation

Life cycle analysis, mass and energy balances, and cost assessment must be performed to justify to funding investors (i.e. debt and equity financiers) and other stakeholders the economic feasibility and environmental impacts of any future capital-intensive algal biorefinery projects [2, 3, 9, 87]. Chapter 2 of this work therefore describes a novel two-stage cultivation and harvesting technological strategy that was proposed and demonstrated to address these biorefinery challenges by isolating unique, multi-trophic, oleaginous, haloalkaline-tolerant microalgae that were likely compatible with the process. Two-stage cultivation and harvesting in this case involves cultivating microalgae in a heterotrophic fermentor or mixotrophic PBR (1st-stage) to rapidly obtain high cell densities and inoculate a phototrophic open-pond culture (2nd-stage) featuring high levels of

NaHCO<sub>3</sub>, pH, and salinity. Chapter 3 of this work describes optimization of first and second-stage cultivation conditions and additional insight obtained from the characterization of the photosynthetic and physiological response, as well as growth and lipid accumulation characteristics, of such microalgae when cultivated in extreme conditions involving high pH and alkalinity. Additionally, ammonia-containing anaerobically-digested food waste effluent was explored as an alternative and more cost-effective source of nitrogen and phosphorous for microalgal open-pond cultivation than NaNO<sub>3</sub> [2, 3, 11, 12].

Life cycle analysis and cost assessment for the various processes of a proposed microalgal biorefinery could also be greatly improved if they were based on the outputs of highly predictive, robust, coupled mathematical models that are calibrated against laboratory-scale experimental data to simulate multiple, linked, continuous (non-batch), industrial-scale units of operation. In particular, the open-pond or PBRs used to inoculate it are units of operation whose proper simulation under various configurations and conditions offers many valuable cost-saving and revenue-enhancing opportunities for commercial design, scale-up, and optimization of the microalgal cultivation process [11]. PBR models in literature are typically deterministic ordinary differential equation structures with simplified Droop or Monod-type kinetics assumed [11].

However, models that couple mass and energy balances, heat and mass transfer correlations, and experimentally derived microalgal kinetics to the finite volume method of Computational Fluid Dynamics (CFD) should better and more quickly account for the non-idealities of a

large-scale reactor in terms of gradients in nutrient concentration, cell density, light intensity, and temperature. For instance, the extent that a plug-flow model is applicable to an elongated, unevenly mixed raceway open-pond with axial and radial dispersion can be further evaluated by such model.

CFD involves numerical solution of conservation equations for mass, momentum and energy in a flow geometry of interest, together with additional subsidiary sets of equations reflecting the considered problem. Flow optimization via this tool represents significant savings in time and resources and increased profitability for biorefinery processes by quickly providing more data for multiple scenarios or conditions than physical trials and reducing the need for numerous, expensive experiments involving prototype PBRs, open-ponds, and measurement probes[11]. Compared to laboratory experimentation, the combined effect that changing input parameters like CO<sub>2</sub>-sparging flow rate, paddle-wheel diameter, incident light intensity and light source positioning, dilution rates, nutrient feed concentration, and reactor dimensions simultaneously have on microalgal volumetric lipid productivity can be more quickly ascertained by a CFD model where expressions describing hydrodynamics and intra-microalgal physiological changes (e.g. stoichiometry and kinetics of lipid synthesis) are intricately linked [11].

PBRs or open-ponds with quickly alternating light/dark regimes (flashing-light effect) especially require such rigorously coupled models. This is because the light intensity gradient is affected by (1) microalgal cell density and cell size that iteratively depend on an incident

light-dependent growth rate[88], (2) dynamic microalgal optical properties (chlorophyll absorption and scattering coefficients) that iteratively depend on incident light-dependent metabolic biochemical reactions[89], and (3) dynamic CO<sub>2</sub> bubble optical properties (scattering coefficient) that depend on hydrodynamically-influenced gas-liquid mass transfer [90]. Microalgal incident light intensity and exposure time itself is governed by its hydrodynamically-determined 3-dimensional location within the reactor.

Chapter 4 describes the development of a rudimentary process model that couples CFD hydrodynamics with microbial kinetics, energy and mass conservation, and heat and mass transfer. This model was applied to simulate a continuous, industrial-scale fermentor for the production of high-value succinic acid and co-products by the *M. succiniciproducens* within a novel, commercial-scale, integrated biorefinery process that used corn-stover biomass feedstock. Any future microalgal biorefinery will also involve multiple downstream units of operation for the isolation and purification of valuable products. Therefore, the aforementioned coupled CFD model was part of a larger linked framework of equations to design and simulate under various input parameters such potential downstream units of operation. The experience from these efforts can then be applied to simulation of an algal photosynthetic biorefinery.

## 1.5. References

- [1] J.N. Rosenberg, A. Mathias, K. Korth, M.J. Betenbaugh, G.A. Oyler. Microalgal biomass production and carbon dioxide sequestration from an integrated ethanol biorefinery in Iowa: A technical appraisal and economic feasibility evaluation. *Biomass & Bioenergy* 35 (2011) 3865-76.
- [2] B.G. Subhadra. Sustainability of algal biofuel production using integrated renewable energy park (IREP) and algal biorefinery approach. *Energy Policy* 38 (2010) 5892-901.
- [3] J. Singh, S. Cu. Commercialization potential of microalgae for biofuels production. *Renewable & Sustainable Energy Reviews* 14 (2010) 2596-610.
- [4] L.G. Alba, C. Torri, C. Samori, J. van der Spek, D. Fabbri, S.R.A. Kersten, et al. Hydrothermal Treatment (HIT) of Microalgae: Evaluation of the Process As Conversion Method in an Algae Biorefinery Concept. *Energy & Fuels* 26 (2012) 642-57.
- [5] S.A. Khan, Rashmi, M.Z. Hussain, S. Prasad, U.C. Banerjee. Prospects of biodiesel production from microalgae in India. *Renewable & Sustainable Energy Reviews* 13 (2009) 2361-72.
- [6] J.D. Kinder, T. Rahmes. Evaluation of Bio-Derived Synthetic Paraffinic Kerosenes (Bio-SPK). Sustainable Biofuels Research & Technology Program. The Boeing Company, 2009. p. 1-12.
- [7] E.W. Thomas, R.E. Fuller, K. Terauchi. <http://en.wikipedia.org/wiki/Biodiesel>. 2013.
- [8] G. Hemighaus, T. Boval, J. Bacha, F. Barnes, M. Franklin, L. Gibbs, et al. Aviation Fuels Technical Review. G. Hemighaus, (Ed.). Chevron Corporation, Houston, 2006. p. 1-96.

- [9] H.W. Yen, I.C. Hu, C.Y. Chen, S.H. Ho, D.J. Lee, J.S. Chang. Microalgae-based biorefinery: From biofuels to natural products. *Bioresource Technology* 135 (2012) 166-74.
- [10] A.D. Gonzalez-Delgado, V. Kafarov. Microalgae based biorefinery: Issues to Consider. *Ciencia Tecnologia Y Futuro* 4 (2011) 5-21.
- [11] H.C. Greenwell, L.M.L. Laurens, R.J. Shields, R.W. Lovitt, K.J. Flynn. Placing microalgae on the biofuels priority list: a review of the technological challenges. *Journal of the Royal Society Interface* 7 (2010) 703-26.
- [12] B. Subhadra, G. Grinson. Algal biorefinery-based industry: an approach to address fuel and food insecurity for a carbon-smart world. *Journal of the Science of Food and Agriculture* 91 (2010) 2-13.
- [13] A. Bhatnagar, M. Bhatnagar, S. Chinnasamy, K.C. Das. *Chlorella minutissima*-A Promising Fuel Alga for Cultivation in Municipal Wastewaters. *Applied Biochemistry and Biotechnology* 161 (2010) 523-36.
- [14] Y.C. Li, W.G. Zhou, B. Hu, M. Min, P. Chen, R.R. Ruan. Integration of algae cultivation as biodiesel production feedstock with municipal wastewater treatment: Strains screening and significance evaluation of environmental factors. *Bioresource Technology* 102 (2011) 10861-7.
- [15] A.M. Santos, M. Janssen, P.P. Lamers, W.A.C. Evers, R.H. Wijffels. Growth of oil accumulating microalga *Neochloris oleoabundans* under alkaline-saline conditions. *Bioresource Technology* 104 (2012) 593-9.

- [16] L.M. Gerasimenko, A.V. Dubinin, L.L. Mityushina, G.A. Zavarzin. A microscopic green alga from soda lakes. *Microbiology* 68 (1999) 610-4.
- [17] O. Perez-Garcia, F.M.E. Escalante, L.E. de-Bashan, Y. Bashan. Heterotrophic cultures of microalgae: Metabolism and potential products. *Water Research* 45 (2011) 11-36.
- [18] H. Xu, X.L. Miao, Q.Y. Wu. High quality biodiesel production from a microalga *Chlorella protothecoides* by heterotrophic growth in fermenters. *Journal of Biotechnology* 126 (2006) 499-507.
- [19] J.G. Day, A.J. Tsavalos. An investigation of the heterotrophic culture of the green alga *Tetraselmis*. *Journal of Applied Phycology* 8 (1996) 73-7.
- [20] T. Heredia-Arroyo, W. Wei, B. Hu. Oil Accumulation via Heterotrophic/Mixotrophic *Chlorella protothecoides*. *Applied Biochemistry and Biotechnology* 162 (2010) 1978-95.
- [21] Y.C. Li, W.G. Zhou, B. Hu, M. Min, P. Chen, R.R. Ruan. Effect of light intensity on algal biomass accumulation and biodiesel production for mixotrophic strains *Chlorella kessleri* and *Chlorella protothecoide* cultivated in highly concentrated municipal wastewater. *Biotechnology and Bioengineering* 109 (2012) 2222-9.
- [22] M.X. Wan, P. Liu, J.L. Xia, J.N. Rosenberg, G.A. Oyler, M.J. Betenbaugh, et al. The effect of mixotrophy on microalgal growth, lipid content, and expression levels of three pathway genes in *Chlorella sorokiniana*. *Applied Microbiology and Biotechnology* 91 (2011) 835-44.
- [23] A. Bhatnagar, S. Chinnasamy, M. Singh, K.C. Das. Renewable biomass production by

mixotrophic algae in the presence of various carbon sources and wastewaters. *Applied Energy* 88 (2011) 3425-31.

[24] S. Singh, S. Arad, A. Richmond. Extracellular polysaccharide production in outdoor mass cultures of *Porphyridium sp* in flat plate glass reactors. *Journal of Applied Phycology* 12 (2000) 269-75.

[25] M. Gors, R. Schumann, D. Hepperle, U. Karsten. Quality analysis of commercial *Chlorella* products used as dietary supplement in human nutrition. *Journal of Applied Phycology* 22 (2010) 265-76.

[26] E. Suali, R. Sarbatly. Conversion of microalgae to biofuel. *Renewable and Sustainable Energy Reviews* 16 (2012) 4316-42.

[27] M. Elmoraghy, I.H. Farag. Green Approach to Produce Bio-jet Fuel from Microalgae. AIChE 2012 Annual Meeting American Institute of Chemical Engineers 2012.

[28] P. Novelli. Sustainable Way for Alternative Fuels and Energy for Aviation (SWAFEA) Final Report. European Commission's Directorate General for Transport and Energy 2011. p. 1-111.

[29] G. Hemighaus, T. Boval, C. Bosley, R. Organ, J. Lind, R. Brouette, et al. Alternative Jet Fuels-A supplement to Chevron's Aviation Fuels Technical Review. In: G. Hemighaus, (Ed.). Chevron Corporation, Houston, 2006. p. 1-14.

[30] Z.Y. Wu, C.B. Qu, X.M. Shi. Biochemical System Analysis of Lutein Production by Heterotrophic *Chlorella pyrenoidosa* in a Fermentor. *Food Technology and Biotechnology* 47

(2009) 450-5.

[31] D. Mitra, J.H.v. Leeuwen, B. Lamsal. Heterotrophic/mixotrophic cultivation of oleaginous *Chlorella vulgaris* on industrial co-products. *Algal Research* 1 (2012) 40-8.

[32] S. Velea, N. Dragos, S. Serban, L. Ilie, D. Stalpeanu, A. Nicoara, et al. Biological Sequestration of Carbon Dioxide from Thermal Power Plant Emissions, by Absorbtion in Microalgal Culture Media. *Romanian Biotechnological Letters* 14 (2009) 4485-500.

[33] Y.N. Liang, N. Sarkany, Y. Cui. Biomass and lipid productivities of *Chlorella vulgaris* under autotrophic, heterotrophic and mixotrophic growth conditions. *Biotechnology Letters* 31 (2009) 1043-9.

[34] C. Yang, Q. Hua, K. Shimizu. Energetics and carbon metabolism during growth of microalgal cells under photoautotrophic, mixotrophic and cyclic light-autotrophic/dark-heterotrophic conditions. *Biochemical Engineering Journal* 6 (2000) 87-102.

[35] W.B. Kong, H. Song, Y.T. Cao, H. Yang, S.F. Hua, C.G. Xia. The characteristics of biomass production, lipid accumulation and chlorophyll biosynthesis of *Chlorella vulgaris* under mixotrophic cultivation. *African Journal of Biotechnology* 10 (2011)11620-30.

[36] C.U. Ugwu, H. Aoyagi, H. Uchiyama. Photobioreactors for mass cultivation of algae. *Bioresource Technology* 99 (2008) 4021-8.

[37] Y. Chisti. Biodiesel from microalgae. *Biotechnology Advances* 25 (2007) 294-306.

[38] K.K. Sharma, H. Schuhmann, P.M. Schenk. High Lipid Induction in Microalgae for Biodiesel

Production. *Energies* 5 (2012) 1532-53.

[39] Y.B. Zheng, Z.Y. Chi, B. Lucker, S.L. Chen. Two-stage heterotrophic and phototrophic culture strategy for algal biomass and lipid production. *Bioresource Technology* 103 (2012) 484-8.

[40] N.R. Moheimani, M.A. Borowitzka. The long-term culture of the coccolithophore *Pleurochrysis carterae* (Haptophyta) in outdoor raceway ponds. *Journal of Applied Phycology* 18 (2006) 703-12.

[41] V. Patil, K.Q. Tran, H.R. Giselrod. Towards sustainable production of biofuels from microalgae. *International Journal of Molecular Sciences* 9 (2008) 1188-95.

[42] E.D.G. Danesi, C.D.O. Rangel-Yagui, J.C.M. de Carvalho, S. Sato. An investigation of effect of replacing nitrate by urea in the growth and production of chlorophyll by *Spirulina platensis*. *Biomass & Bioenergy* 23 (2002) 261-9.

[43] D. Soletto, L. Binaghi, A. Lodi, J.C.M. Carvalho, A. Converti. Batch and fed-batch cultivations of *Spirulina platensis* using ammonium sulphate and urea as nitrogen sources. *Aquaculture* 243 (2005) 217-24.

[44] A. Converti, S. Scapazzoni, A. Lodi, J.C.M. Carvalho. Ammonium and urea removal by *Spirulina platensis*. *Journal of Industrial Microbiology & Biotechnology* 33 (2006) 8-16.

[45] Z.Y. Chi, J.V. O'Fallon, S.L. Chen. Bicarbonate produced from carbon capture for algae culture. *Trends in Biotechnology* 29 (2011) 537-41.

[46] D. Vandamme, I. Foubert, I. Fraeye, B. Meesschaert, K. Muylaert. Flocculation of *Chlorella*

*vulgaris* induced by high pH: Role of magnesium and calcium and practical implications. *Bioresource Technology* 105 (2012) 114-9.

[47] S.A. Scott, M.P. Davey, J.S. Dennis, I. Horst, C.J. Howe, D.J. Lea-Smith, et al. Biodiesel from algae: challenges and prospects. *Current Opinion in Biotechnology* 21 (2010) 277-86.

[48] K. Raetz. Challenges and Advances in Making Microalgae Biomass a Cost Efficient Source of Biodiesel. *Basic Biotechnology* 5 (2009) 37-43.

[49] F. Bumbak, S. Cook, V. Zachleder, S. Hauser, K. Kovar. Best practices in heterotrophic high-cell-density microalgal processes: achievements, potential and possible limitations. *Applied Microbiology and Biotechnology* 91 (2011) 31-46.

[50] Y. Liang, X. Zhao, Z. Chi, M. Rover, P. Johnston, R. Brown, et al. Utilization of acetic acid-rich pyrolytic bio-oil by microalga *Chlamydomonas reinhardtii*: Reducing bio-oil toxicity and enhancing algal toxicity tolerance. *Bioresource Technology* 133 (2013) 500-6.

[51] P.L. Li, X.L. Miao, R.X. Li, J.J. Zhong. In Situ Biodiesel Production from Fast-Growing and High Oil Content *Chlorella pyrenoidosa* in Rice Straw Hydrolysate. *Journal of Biomedicine and Biotechnology* (2011) 1-8.

[52] J. O'Grady, J.A. Morgan. Heterotrophic growth and lipid production of *Chlorella protothecoides* on glycerol. *Bioprocess and Biosystems Engineering* 34 (2011) 121-5.

[53] J.S. Tumuluru, C.T. Wright, J.R. Hess, K.L. Kenney. A review of biomass densification systems to develop uniform feedstock commodities for bioenergy application. *Biofuels*

Bioproducts & Biorefining-Biofpr 5 (2011) 683-707.

[54] M. Giordano, J. Beardall, J.A. Raven. CO<sub>2</sub> concentrating mechanisms in algae: Mechanisms, environmental modulation, and evolution. *Annual Review of Plant Biology* 56 (2005) 99-131.

[55] M.R. Badger, G.D. Price. CO<sub>2</sub> concentrating mechanisms in cyanobacteria: molecular components, their diversity and evolution. *Journal of Experimental Botany* 54 (2003) 609-22.

[56] L. Xu, P.J. Weathers, X.R. Xiong, C.Z. Liu. Microalgal bioreactors: Challenges and opportunities. *Engineering and Life Sciences* 9 (2009) 178-89.

[57] J.L. Milne, Jeffrey C. Cameron, Lawrence E. Page, Sally M. Benson, Himadri B. Pakrasi. Algal Technologies for Biological Capture and Utilization of CO<sub>2</sub> Require Breakthroughs in Basic Research. *Perspectives on Biofuels: Potential Benefits and Possible Pitfalls*. American Chemical Society 1116 (2012) 107-41.

[58] Z. Chi, Y. Xie, F. Elloy, Y. Zheng, Y. Hu, S. Chen. Bicarbonate-based Integrated Carbon Capture and Algae Production System with alkalihalophilic cyanobacterium. *Bioresource Technology* 133 (2013) 513-21.

[59] R.M. Cowan, J.J. Ge, Y.J. Qin, M.L. McGregor, M.C. Trachtenberg. CO<sub>2</sub> capture by means of an enzyme-based reactor. *Advanced Membrane Technology* 984 (2003) 453-69.

[60] S. Bhattacharya, M. Schiavone, S. Chakrabarti, S.K. Bhattacharya. CO<sub>2</sub> hydration by immobilized carbonic anhydrase. *Biotechnology and Applied Biochemistry* 38 (2003) 111-7.

[61] S.H. Zhang, Z.H. Zhang, Y.Q. Lu, M. Rostam-Abadi, A. Jones. Activity and stability of

immobilized carbonic anhydrase for promoting CO<sub>2</sub> absorption into a carbonate solution for post-combustion CO<sub>2</sub> capture. *Bioresource Technology* 102 (2011)10194-201.

[62] E.V. Kupriyanova, A.G. Markelova, N.V. Lebedeva, L.M. Gerasimenko, G.A. Zavarzin, N.A. Pronina. Carbonic anhydrase of the alkaliphilic cyanobacterium *Microcoleus chthonoplastes*. *Microbiology* 73 (2004) 255-9.

[63] B.K. Kanth, K. Min, S. Kumari, H. Jeon, E.S. Jin, J. Lee, et al. Expression and Characterization of Codon-Optimized Carbonic Anhydrase from *Dunaliella* Species for CO<sub>2</sub> Sequestration Application. *Applied Biochemistry and Biotechnology* 167 (2012) 2341-56.

[64] P.S. Martin Borchert. Heat Stable Carbonic Anhydrases and Their Use. In: U.S.P.T.O, (Ed.). *Novozymes A/S2010*.

[65] U.K. Bageshwar, L. Premkumar, I. Gokhman, T. Savchenko, J.L. Sussman, A. Zamir. Natural protein engineering: a uniquely salt-tolerant, but not halophilic, alpha-type carbonic anhydrase from algae proliferating in low- to hyper-saline environments. *Protein Engineering Design & Selection* 17 (2004) 191-200.

[66] K.S. Smith, J.G. Ferry. A plant-type (beta-class) carbonic anhydrase in the thermophilic methanoarchaeon *Methanobacterium thermoautotrophicum*. *Journal of Bacteriology* 181 (1999) 6247-53.

[67] A.Y. Shekh, K. Krishnamurthi, S.N. Mudliar, R.R. Yadav, A.B. Fulke, S.S. Devi, et al. Recent Advancements in Carbonic Anhydrase-Driven Processes for CO<sub>2</sub> Sequestration: Minireview.

Critical Reviews in Environmental Science and Technology 42 (2012) 1419-40.

[68] L. Premkumar, U.K. Bageshwar, I. Gokhman, A. Zamir, J.L. Sussman. An unusual halotolerant alpha-type carbonic anhydrase from the alga *Dunaliella salina* functionally expressed in *Escherichia coli*. Protein Expression and Purification 28 (2003) 151-7.

[69] W.F. Lee, Y.C. Chen. Effect of hydrotalcite on the physical properties and drug-release behavior of nanocomposite hydrogels based on poly[acrylic acid-co-poly(ethylene glycol) methyl ether acrylate] gels. Journal of Applied Polymer Science 94 (2004) 692-9.

[70] L.H. Cheng, L. Zhang, H.L. Chen, C.J. Gao. Hollow fiber contained hydrogel-CA membrane contactor for carbon dioxide removal from the enclosed spaces. Journal of Membrane Science 324 (2008) 33-43.

[71] Y.T. Zhang, T.T. Zhi, L. Zhang, H. Huang, H.L. Chen. Immobilization of carbonic anhydrase by embedding and covalent coupling into nanocomposite hydrogel containing hydrotalcite. Polymer 50 (2009) 5693-700.

[72] Y.T. Zhang, X.G. Dai, G.H. Xu, L. Zhang, H.Q. Zhang, J.D. Liu, et al. Modeling of CO<sub>2</sub> mass transport across a hollow fiber membrane reactor filled with immobilized enzyme. Aiche Journal 58 (2012) 2069-77.

[73] Y.T. Zhang, L. Zhang, H.L. Chen, H.M. Zhang. Selective separation of low concentration CO<sub>2</sub> using hydrogel immobilized CA enzyme based hollow fiber membrane reactors. Chemical Engineering Science 65 (2010) 3199-207.

- [74] M.R. Banki, T.U. Gerngross, D.W. Wood. Novel and economical purification of recombinant proteins: Intein-mediated protein purification using in vivo polyhydroxybutyrate (PHB) matrix association. *Protein Science* 14 (2005) 1387-95.
- [75] K.L. Kadam. Plant flue gas as a source of CO<sub>2</sub> for microalgae cultivation. Economic impact of different process options. *Energy Conversion and Management* 38 (1997) S505-S10.
- [76] A. Richmond, S. Karg, S. Boussiba. Effects of Bicarbonate and Carbon Dioxide on the Competition between *Chlorella Vulgaris* and *Spirulina Platensis*. *Plant and Cell Physiology* 23 (1982) 1411-7.
- [77] R.D. Gardner, E. Lohman, R. Gerlach, K.E. Cooksey, B.M. Peyton. Comparison of CO<sub>2</sub> and bicarbonate as inorganic carbon sources for triacylglycerol and starch accumulation in *Chlamydomonas reinhardtii*. *Biotechnology and Bioengineering* 110 (2013) 87-96.
- [78] R.D. Gardner, K.E. Cooksey, F. Mus, R. Macur, K. Moll, E. Eustance, et al. Use of sodium bicarbonate to stimulate triacylglycerol accumulation in the chlorophyte *Scenedesmus sp* and the diatom *Phaeodactylum tricorutum*. *Journal of Applied Phycology* 24 (2012) 1311-20.
- [79] A.G. Miller, D.H. Turpin, D.T. Canvin. Growth and photosynthesis of the cyanobacterium *Synechococcus leopoliensis* in HCO<sub>3</sub><sup>-</sup>-limited chemostats. *Plant Physiology* 75 (1984) 1064-70.
- [80] S. Malisarad, M. Friedlander, R. Benarie, A.E. Richmond. Alkalinity-Induced Aggregation in *Chlorella vulgaris* .1. Changes in Cell Volume and Cell Wall Structure. *Plant and Cell Physiology* 21 (1980) 27-35.

- [81] L. Semerjian, G.M. Ayoub. High-pH magnesium coagulation-flocculation in wastewater treatment. *Advances in Environmental Research* 7 (2003) 389-403.
- [82] K.C. Park, C. Whitney, J.C. McNichol, K.E. Dickinson, S. MacQuarrie, B.P. Skrupski, et al. Mixotrophic and photoautotrophic cultivation of 14 microalgae isolates from Saskatchewan, Canada: potential applications for wastewater remediation for biofuel production. *Journal of Applied Phycology* 24 (2012) 339-48.
- [83] R.L. Hawkins. Utilization of xylose for growth by the eukaryotic alga, *Chlorella*. *Current Microbiology* 38 (1999) 360-3.
- [84] A.-D. Gonzalez-Delgado, V. Kafarov. Microalgae based biorefinery: Issues to consider. *CT&F-Ciencia Tecnologia y Futuro* 4 (2011) 5-22.
- [85] V.H. Work, S. D'Adamo, R. Radakovits, R.E. Jinkerson, M.C. Posewitz. Improving photosynthesis and metabolic networks for the competitive production of phototroph-derived biofuels. *Current Opinion in Biotechnology* 23 (2012) 290-7.
- [86] G. Bernat, N. Waschewski, M. Rogner. Towards efficient hydrogen production: the impact of antenna size and external factors on electron transport dynamics in *Synechocystis* PCC 6803. *Photosynthesis Research* 99 (2009) 205-16.
- [87] R. Davis, A. Aden, P.T. Pienkos. Techno-economic analysis of autotrophic microalgae for fuel production. *Applied Energy* 88 (2011) 3524-31.
- [88] T. Key, A. McCarthy, D.A. Campbell, C. Six, S. Roy, Z.V. Finkel. Cell size trade-offs govern

light exploitation strategies in marine phytoplankton. *Environmental Microbiology* 12 (2010) 95-104.

[89] E. Lee, R.L. Heng, L. Pilon. Spectral optical properties of selected photosynthetic microalgae producing biofuels. *Journal of Quantitative Spectroscopy & Radiative Transfer* 114 (2013) 122-35.

[90] M.P. Dudukovic, F. Larachi, P.L. Mills. Multiphase reactors - revisited. *Chemical Engineering Science* 54 (1999) 1975-95.

## CHAPTER 2 : MICROALGAE FOR TWO-STAGE CULTIVATION PART 1:

### BIO-PROSPECTING

#### 2.1. Abstract

Mass outdoor cultivation of microalgae for biofuels and co-products faces challenges of low lipid productivity, contamination, inefficient CO<sub>2</sub> supply, and difficulties in harvesting. A two-stage cultivation process was developed to address these challenges. This involves culturing microalgae in a fermentor heterotrophically or photobioreactor mixotrophically as first-stage to rapidly obtain high cell densities for inoculating a phototrophic open-pond culture featuring high levels of NaHCO<sub>3</sub>, pH, and salinity as second-stage. A microalgae that is tolerant of these phototrophic conditions, can use organic carbon, and can prolifically produce oil is key to the success of such a two-stage process. Two oleaginous, haloalkaline-tolerant, and dual-trophic green *Chlorella sp.* microalgae from soda lakes were isolated, identified, and compared in this study using a multi-instrument approach as candidates for such process. A model TAG was developed for rapid, non-destructive lipid quantitation using liquid-state <sup>1</sup>H NMR. A two-stage cultivation system and a high pH-mediated auto-flocculation method were tested on the selected strain ALP2 with a 1 L fermentor and 40 L open-tank. In unoptimized conditions, the strain achieved a final DCW of 0.978 g/L, lipid content of 39.78% DCW, and auto-flocculation harvesting efficiency of 64.1%.

**Keywords:** Microalgae; Lipid; Mixotrophic; NMR; pH; Bicarbonate

## 2.2. Introduction

Lipids from biomass are precursors for renewable fuels like biologically-derived synthetic paraffin kerosene (Bio-SPK) for aviation [1] and biodiesel for electrical power generation [2] and ground transportation [3]. The National Renewable Energy Laboratory's (NREL) Aquatic Species Program during the 1970-90s identified oleaginous photosynthetic microalgae as a biomass feedstock for such lipid-based fuels [4]. These algae accumulate neutral lipid as triacyl-glycerides [TAGs] in lipid bodies, typically under nitrogen or phosphate depletion stress conditions [4]. However, commercialization of microalgal biofuel involving large-scale, outdoor open-ponds is still constrained by low lipid productivity [5], contamination by airborne invasive species [6, 7], unsustainable supply of nutrients (e.g.; nitrogen [8, 9] and phosphorous) and inorganic carbon [10], limited available acreage for inoculum and primary cultures [7, 11], and inefficient harvesting [4, 12].

Use of a microalgae that can be efficiently cultured under heterotrophic or mixotrophic conditions [10] for inoculum and phototrophically for biomass growth and lipid accumulation was proposed as a two-stage cultivation strategy to address the challenges associated with long growth times and contamination [13] in large-scale open-pond operations. Heterotrophic or mixotrophic culture conditions in a closed reactor in the first stage enables the use of organic carbon substrates [11] to rapidly achieve high densities as inoculum for the outdoor phototropic open-pond culture that harnesses sunlight for lipid accumulation in the second stage. With a larger

inoculum and reduced growth time, the microalgae in the second-stage phototrophic open-pond culture could more likely outcompete or withstand undesirable environmental contaminants [10]. Low-maintenance, low surface area-volume ratio industrial fermentors currently used for commercial production of medicines, beverages, food additives, and energy [14, 15] could be used for such first-stage heterotrophic cultivation without light-limitation. Additionally, the organic carbon used in the first-stage heterotrophic cultivation could be derived from various waste sources, including cellulosic sugars from agricultural crop residues[16], acetate from pyrolyzed forestry residues[17], and crude glycerol from trans-esterification processes [18].

Challenges associated with outdoor contamination [19], low volumetric lipid productivity [20], harvesting [12, 21], and supply of inorganic carbon to second stage open-pond phototrophic cultures [10] could also be overcome by using high levels of bicarbonate salts that maintain a moderately high pH via bicarbonate buffering. For instance, high salinity and alkalinity (i.e. 17 g/L bicarbonate and pH 9-10) have been shown to limit contamination of cultures of *Spirulina sp.* in outdoor open-ponds [19]. Alkaline conditions in phototrophic cultures also support MgOH<sub>2</sub>-mediated auto-flocculation of cells and facilitate harvesting [12, 21]. Furthermore, addition of bicarbonate has reportedly enhanced microalgal growth and lipid accumulation [20]. For example, carbon-limited *Syecococcus lkopoliensis* grown in chemostats exhibited a very high photosynthetic affinity for HCO<sub>3</sub><sup>-</sup> over CO<sub>2</sub> during the growth phase [22]. Supplementation of HCO<sub>3</sub><sup>-</sup> to nitrogen-starved, CO<sub>2</sub>-sparged *Chlamydomonas reinhardtii* microalgal cultures

reportedly triggered a photosynthetic increase in their neutral TAG-lipid accumulation [20]. Using bicarbonate salts that are more soluble and storable at night when least needed compared to CO<sub>2</sub> gas has been additionally advocated. This represents a way to avoid the inefficient gas-liquid mass transfer [10], outgassing losses, medium acidification, and low one-pass 25-30% capture [23] associated with supplying concentrated CO<sub>2</sub> from flue-gas emissions to large, highly evaporative, second-stage open-pond phototrophic cultures [10].

Such a two-stage mass-cultivation process, however, requires identification of a microalgal strain that is suitable for these special conditions. Specifically, the ideal algae strain will grow well under heterotrophic, mixotrophic, and phototrophic conditions, tolerate strongly-alkaline conditions, use bicarbonate salts as a carbon source during both growth and lipid accumulation, and efficiently produce significant quantities of lipid. There have been no previous efforts to identify and propagate an algal species meeting these criteria. The purpose of this study was then to fill this technical gap. Two oleaginous, multi-trophic, halo-alkaline-tolerant microalgae from soda lakes, Alkali Lake and Soap Lake, in the State of Washington, U.S.A., were isolated and identified as candidates for this application. A two-stage cultivation featuring fermentor and open-tank photobioreactor (PBR) and auto-flocculation strategy were then demonstrated using one of the strains, ALP2.

## 2.3. Materials and Methods

### 2.3.1. Microalgal and Cyanobacterial Strain Isolation

Water and rock samples were collected with transparent screw-cap 0.5 L plastic bottles during spring (April 15, 2010) and summer (June 21, 2010), respectively, from the shallow shores of Alkali Lake (Latitude = 47.5165° N and Longitude = -119.5009° W) and the meromictic and terminal Soap Lake (Latitude = 47.4050° N and Longitude = -119.4975° W, elevation = 330.71 m, and total depth = 4.27 m) in the lower Grand Coulee of Grant County, Washington, U.S.A. Soap Lake phytoplankton population density is reportedly highest in the spring when it thermally stratifies via a metalimnion layer and when grazing zooplankton population density is lower [24, 25]. Clear lake water or visibly phototrophic green mats that were scraped with wire-brush from rocks were used within 24 hrs to inoculate 0.25 L flasks containing a previously described 2NBH medium [26] supplemented with 1 g/L NaHCO<sub>3</sub> and adjusted to pH 9.60 to mimic enriched soda lake water. The high pH cultures were grown for 20 days at 130 rpm agitation on orbital shaker under 70 μmole m<sup>-2</sup> s<sup>-1</sup> of poly-chromatic light intensity from overhead fluorescent bulbs set on a 16 hr-light/8hr-dark diurnal cycle with a timer. As visualized under an optical light microscope, two green coccoidal phototrophs, ALP2 from Alkaline Lake, and SLP2 from Soap Lake, were sorted from the spring lake water-inoculated cultures using a FACS Vantage SE fluorescence activated cell sorter (BD Immunocytometry Systems, San Jose, CA) equipped with FACSDiva v.2008 software. These two isolates were then streaked and grown on 2% (w/v) agar plates

containing modified 2NBH medium. Single ALP2 and SLP2 phototrophic colonies were then cloned and loop-inoculated into 10 ml glass tubes containing modified 2NBH for phototrophic axenic cultivation. A freshwater cyanobacterial strain, *Synechococcus PCC7942* (Targeted Growth, Inc, Seattle, WA.), was later used to co-inoculate an ALP2 flask culture for flow-cytometrically monitoring contamination experiments. Additional characterization work, subsequent two-stage cultivation, and  $^1\text{H}$  NMR model development were conducted using the more promising ALP2 strain that yielded higher biomass than SLP2 during organic carbon screening experiments.

### 2.3.2 Microalgal Strain Identification

Genomic DNA was isolated from SLP2 and ALP2 cultures grown in BG-11 medium [27] as previously described [26]. A TD-700 Nanodrop fluorometer (Turner Designs, Inc., Sunnyvale, CA) was used to measure DNA concentration and  $\text{OD}_{260/280}$  purity ratio. Full segments of internal transcribed spacer regions 1 and 2 and 5.8S rDNA with fragment segments of 18S rDNA and 28S rDNA were PCR amplified using ITS1 forward and ITS4 reverse primers as previously described using a DNA Engine Peltier Thermal-Cycler (Bio-Rad, Hercules, CA) with the exception that 20  $\mu\text{g}/\text{ml}$  of template DNA was used [26]. PCR reactions were run alongside a 2-log DNA ladder on a 1% (w/v) agarose gel at 95V electrophoresis. Single-band PCR products were visualized by ethidium bromide staining and with a Universal Hood II UV-light exposure (Bio-Rad, Hercules, CA) and cleaned with a PCR clean-up kit (Qiagen, Venlo, Netherlands). The

products were then subjected to a dideoxy big-dye incorporation thermal-cycler reaction and then cleaned by centrifugation through a size-exclusion chromatography elution column, vacuum evaporated for 30 min, and then directly distinguished and sequenced with capillary electrophoresis at the WSU Sequencing Center. Sequences were cleaned and edited using Geneious software version 5.0 bioinformatic software (Biomatters, Ltd., Auckland, New Zealand). A contig assembly was generated, from which nucleotide BLAST searches were performed with NCBI GenBank. BLAST results in the form of GenBank accession numbers were ranked according to e-value and query match percentage.

### *2.3.3. Microalgal Carbon and Trophic Mode Screening Experiments*

To initially test the effects of carbon source and light intensity conditions during heterotrophic, mixotrophic, and phototrophic conditions, SLP2 and ALP2 from maintenance cultures were washed 4x in PBS and inoculated at an  $OD_{680} = 0.035$  into 0.25 L flasks containing 0.10 L of BG-11 medium adjusted to pH 7.0 and supplemented with 4.0 g C/L from various candidate carbon sources (glucose (10.0 g/L), xylose (10.0 g/L), glucose + xylose (5.0 g/L + 5.0 g/L), glycerol (11.0 g/L), potassium acetate (13.4g/L), arabinose (5.0 g/L), mannose (5.0 g/L),  $NaHCO_3$  (28.0 g/L)). Cultures were agitated at 150 rpm on orbital shaker in foam-capped flasks for 10 days at 21°C, either side by side or at different times under phototrophic/mixotrophic ( $70 \mu\text{mol m}^{-2}\text{s}^{-1}$  of continuous polychromatic light intensity from overhead fluorescent bulbs) or heterotrophic (flasks covered with aluminum foil except for the top for gas exchange) conditions. Stock solutions of

NaNO<sub>3</sub> were autoclaved separately from glucose to avoid inhibitory Mehler-reaction by-products. Samples of 1ml were aseptically removed for measurements of OD<sub>680</sub>, OD<sub>750</sub>, and monomer sugar content. On the final culture days, the remaining biomass was sampled for measurement of dry cell weight (DCW). The minimal Na<sub>2</sub>CO<sub>3</sub> in BG-11 medium was not included in calculations of total NaHCO<sub>3</sub> supplemented to phototrophic cultures.

#### *2.3.4. Demonstration of Two-Stage Cultivation Process*

A small-scale two-stage cultivation system was evaluated with the ALP2 strain using 0.25 L flasks. ALP2 was inoculated at OD<sub>680</sub> = 0.50 and grown heterotrophically for 8 days at 28°C in an incubator at 130 rpm on orbital shaker on BG-11<sub>0</sub> medium [27] supplemented with 10.0 g/L glucose and 0.529 g/L urea at an initial pH of 7. This first stage culture was then used to inoculate at an OD<sub>680</sub> = 0.50 (corresponding to an initial cell density of 2.40 x 10<sup>7</sup> cells/ml) a second stage 0.25 L flask culture connected to a <sup>1</sup>H NMR flow cell [26] and grown phototrophically for 8 days on BG-11<sub>0</sub> medium supplemented with 10.0 g/L NaHCO<sub>3</sub> and 0.032 g/L urea at pH 9 adjusted daily with HCl. A similar two-stage process was conducted but with the second stage flask supplied 0.529 g/L urea and co-inoculated with cyanobacteria at an OD<sub>750</sub> = 0.25 to evaluate control of competing contamination.

A larger-scale two-stage cultivation system was then evaluated using a first stage 1 L fermentor and second stage 40 L open-tank PBR. A 1 L BioFlo 110 fermentor (New Brunswick Scientific, NJ) was inoculated with ALP2 at an OD<sub>680</sub> = 0.15 at a working volume of 0.75 L of

BG-11<sub>0</sub> medium supplemented with 10.0 g/L glucose and 0.529 g/L urea with the following set-points (pH=7 controlled by 1.0 M HCl/NaOH peristaltic pump addition, agitation = 300 rpm controlled by Rushton-type impeller, O<sub>2</sub> saturation = 50% with cascading DO control to agitation speed, aeration rate = 1 vvm air inlet). A thin layer of aluminum foil was used to keep conditions heterotrophic. No anti-foam was used or needed. Based on average thermocouple readings, the fermentor temperature was maintained at room temperature (20°C). The fermentor culture was then directly inoculated at an OD<sub>680</sub> = 0.12 at an initial cell density of 4.88 x 10<sup>6</sup> cells/ml into an oval, black open-tank PBR with working volume of 40 L and 0.15 m depth, in BG-11<sub>0</sub> medium supplemented with 17.0 g/L NaHCO<sub>3</sub> and 0.133 g/L urea and adjusted to pH 9. A pH 9 was subsequently maintained by daily adjustment with HCl acid during growth, prior to the onset of a matured, urea nitrogen-starvation induced stationary phase. After 653 hrs of total two-stage cultivation time, glacial acetic acid was used instead [28]. The culture was grown phototrophically indoors at approximately 21°C under 70 μmoles m<sup>-2</sup>s<sup>-1</sup> polychromatic light intensity delivered by overhead fluorescent bulbs. The culture was agitated by an RW-16 rotary impeller (IKA Works, Inc., Wilmington, NC) to simulate a paddle wheel. A total of 44 L of unfiltered, distilled deionized water was supplemented to this indoor culture via four additions to compensate for evaporative losses. One liter of the indoor culture was transferred to a magnetically stirred graduated cylinder. MgOH<sub>2</sub> was first supplemented to 0.058 g/L, and then 3.35 g Ca(OH)<sub>2</sub>/g-biomass was added to raise the pH to 12 and auto-flocculate the cells based on a previously described procedure [12].

Final  $OD_{680}$  measurements were taken from the mid-zone of the cylinder and compared to the initial  $OD_{680}$  of the open-tank PBR, from which harvesting recovery was estimated as follows:

$$\% \text{ Recovery} = \frac{OD_{680 \text{ initial}} - OD_{680 \text{ final}}}{OD_{680 \text{ initial}}} \times 100 \quad (2.1)$$

### 2.3.5 Biomass and Extracellular Concentration Measurements

Dry cell weight (DCW) was measured by drying and weighing a 0.05 L culture sample that was centrifuged and washed 4x in 0.5M  $NH_3HCO_3$  to remove glucose,  $NaHCO_3$ , and other impurities and drying it overnight at 105°C in an oven [29]. The ammonium cation and bicarbonate anion of  $NH_3HCO_3$  used to maintain osmolarity and prevent cell lysis and/or lipid leakage volatilizes or decomposes to  $CO_2$  and water vapor at high oven temperatures, leaving virtually no salt residue behind that would otherwise distort dry cell weight measurement[29]. Optical density (OD) at 680 nm for algae and 730/750nm for cyanobacteria was measured for cultures using a fixed-wavelength 20 Genesys spectrophotometer (Spectronics Instruments, Rochester, NY) and appropriate medium blanks. Cell density was determined visually with a light microscope and Spencer AO Bright-Line Neubauer haemocytometer (Sigma-Aldrich, St. Louis, MO). A standard curve correlating  $OD_{680}$  with cell density (X) for ALP2 was also developed:

$$X(\text{cells} / \text{mL}) = OD_{680} \times (3 \times 10^7) + (9 \times 10^6), R^2=0.9144 \quad (2.2)$$

Specific growth rate during a period between an initial ( $t_1$ ) and final ( $t_2$ ) time was calculated from the corresponding cell densities,  $X_1$  and  $X_2$ , as follows:

$$\mu = \frac{\ln(X_2) - \ln(X_1)}{t_2 - t_1} \quad (2.3)$$

Chlorophyll a/b and carotenoid content of ALP2 was determined via a modification of a methanol extraction method [30] that used a combined 20 min ultrasonication at 47 kHz and 5 min bead-beating. Methanol extracts were then analyzed for absorbance readings at 665, 652.5, and 470 nm corresponding to chlorophyll-a, b, and carotenoids, respectively, via a multi-wavelength, 0.5 nm resolution UV-2550 spectrophotometer (Shimadzu, Kyoto, Japan) with previously described equations [31]. Gram-staining was performed on a sample from the indoor open-tank PBR culture at the mid-point time (481 hrs) of total two-stage cultivation using microscope slides and Difco crystal violet, iodine, ethanol de-colorizer, and safarin stains (Becton, Dickinson, and Company, Franklin Lakes, NJ). Extracellular pH of culture samples and soda lake water were measured with an Accumet AB15 pH meter (Thermo Fisher Scientific, Inc., Waltham, MA) three-point calibrated daily at pH 4.00, 7.00, and 10.00. Light intensity was measured with a LI-283A PAR sensor (LI-COR, Lincoln, NE). Extracellular content of C5 (i.e. xylose, mannose, ribose) and C6 (glucose, galactose) sugars from first-stage mixotrophic or heterotrophic cultures was measured by a Dionex ICS-3000 Ion-exchange HPLC equipped with amperimetric detector and Chromeleon 6.8 software (Thermo Scientific, Sunnyvale, CA) as previously described [32]. Alkalinity of lake water was measured using a T-150 alkalinity meter (Mettler-Toledo, Columbus, OH). Total ammonia in soda lake water and effluent was measured using 2300 Kjeltac Analyzer Unit (Tecator, Boulder, CO).

### *2.3.6 Flow-Cytometric Measurements*

A benchtop FACSCalibur flow cytometer equipped with CellQuest software (BD Immunocytometry Systems, San Jose, CA.) was used to assess relative cell dimensions, granularity, and cell densities of populations of chlorophyll-fluorescent, microalgal ALP2 and co-inoculated, contaminating, phycocyanin-fluorescent cyanobacteria [33]. Chlorophyll and phycoerythrin are excited with a 488-nm argon laser and fluoresce at 690 nm (red) and 570nm (orange), respectively. Phycocyanin is excited at 620nm and emits at 640 nm, needing detection by a red-emitting laser [33, 34]. A silica-bead 1 $\mu$ m-size standard (Duke Standards- Thermo Scientific, Sunnyvale, CA) was used for single-point calibration. For quantifying cell density in ALP2 cultures co-inoculated with contaminating cyanobacteria, 1x-PBS-washed samples were immediately re-suspended and fixed in 1% formaldehyde in PBS, vortexed, and stored at -80°C until examined by flow cytometry. Cell populations were gated, and a wet cell concentration or cell density was calculated from the number of events acquired in each gated population for 15 sec. Sheath fluid was then replaced with spent BG-11 medium in a polystyrene flow tube and aspirated for 1 min. The volume difference between the initial and final sample volume divided by the elapsed time was then used to estimate the flow rate [34]. Flow data were analyzed using FCS Express v.3 software (De Novo Software, Los Angeles, CA).

### *2.3.7 Neutral Lipid Concentration and Fatty-Acid Profile Measurements*

Liquid-state static and HR-MAS  $^1\text{H}$  NMR spectroscopy were used to rapidly and

non-destructively assess microalgal lipid content in single-time point static culture suspensions, or under continuous flow cell conditions, as previously described [26]. All  $^1\text{H}$  NMR spectra were recorded on either a Varian Inova 500 MHz spectrometer (499.84 MHz  $^1\text{H}$  frequency), a Varian 400-MR 400 MHz spectrometer (399.76 MHz  $^1\text{H}$  frequency) or a Varian VNMRS 600 MHz spectrometer (599.69 MHz  $^1\text{H}$  frequency) using acquisition parameters previously described. Dried cells from a 13-day old 0.05 L ALP2 culture grown phototrophically on BG-11<sub>0</sub> supplemented with 0.133 g/L urea and 10.0 g/L  $\text{NaHCO}_3$  at HCl-adjusted pH 9 were extracted with 2:1  $\text{CHCl}_3/\text{CH}_3\text{OH}$  and subsequently fractionated on a silica column as previously described [26]. These fractions were subsequently analyzed by FAME-GC and  $^1\text{H}$  NMR to develop a model TAG for ALP2, which provided a statistically-derived proton count and molecular weight for use in converting NMR integrals to grams lipid/ml culture [26]. In addition, the fractions containing TAG were pooled, and the combined fractions were used to analyze the distribution of poly-unsaturated to mono-unsaturated and saturated fatty acids by  $^1\text{H}$  NMR using the methods developed by Miyake et al. [35] and Knothe et al.[36]. The mole fractions of poly-unsaturated to mono-unsaturated to saturated fatty acids were then used to develop an additional model TAG which was compared to the model developed from the FAME-GC analysis. The total weight of the isolated neutral lipids was used to gravimetrically validate total neutral lipid content as measured in-vivo by static  $^1\text{H}$  NMR. The fatty-acid profile for the raw ALP2 culture grown in the open-tank 2<sup>nd</sup>-stage PBR was assessed via the aforementioned FAME

GC-based procedure [37].

### *2.3.8 Microscopy for Cell Count, Identification, and Detection of Lipid Body*

A LSM 510 Meta confocal microscope (Carl Zeiss Group, Oberkochen, Germany) was used to obtain images of Nile Red-stained ALP2 and its chloroplasts and spherical lipid bodies at 63x with no oil-immersion. For this, a blue helium laser excitation at 488 nm was employed, TAG lipid fluorescence was detected at 560 nm, and chlorophyll auto-fluorescence was detected at 650 nm with a long-pass filter. ALP2 cells growing on BG-11<sub>0</sub> medium supplemented with 10.0 g/L NaHCO<sub>3</sub> and 0.133 g/L urea, pH 9.0 were diluted to 0.50 x 10<sup>6</sup> cells/ml (200µl cells) with ultra-pure RO-H<sub>2</sub>O (650µl), supplemented with 15% DMSO (150µl) , stained with a Nile Red (Sigma-Aldrich, St. Louis, MO) stock solution of 0.6 mg/ml acetone (8µl) at a final working solution of 4.8 µg/ml, and incubated in the dark at 21°C for 10 min prior to imagery[38]. A VanGuard 1200MM optical light microscope (New York Microscope Company, Hicksville, NY.) was used to observe general cell features, identify contamination, and count densities with 10x ocular lens and either 10x, 40x, or 100x objective lens for 100x, 400x, and 1000x total magnification.

## **2.4. Results and discussion**

### *2.4.1. Microalgal Isolation and Identification*

Primary cultures of water samples taken from the shores of the proximate Alkali Lake and Soap Lake, chosen as initial prospecting sites, yielded preparations containing green,

non-filamentous, and phototrophic organisms. Prospecting and sample collection were undertaken to find dual-trophic, oleaginous, halo-alkaline tolerant microalgae that would likely be compatible with a proposed two-stage cultivation strategy for algae biomass bearing lipid-precursors to biofuel and valuable co-products. Soda lakes, like Mono Lake, CA, Lake Manito, Canada, and Lake Magadi, Kenya represent rare, diverse sources of such phototrophs, as they are characterized by high pH (i.e. pH 11-12 for Lake Magadi, Kenya), alkalinity, and salinity [25, 39]. For instance, Alkali Lake was the source of *Halomonas campisalis* sp. nov., a denitrifying and haloalkaliphilic bacterium exploitable for treatment of saline, alkaline waste during ion exchange resin regeneration [40]. A mixotrophic microalgal strain variant of *Chlorella minutissima* with tolerance to 1.6 g/L equivalent  $\text{NaHCO}_3$  and pH (8-9) was also isolated from Lake Magadi in Kenya, but was not subsequently characterized for neutral lipid accumulation [41]. The shore water pH, alkalinity, and ammonia-N content of Soap Lake, which uniquely also has the highest diverse mineral content of any water body on earth [42], were measured to be pH 9.86, 6.81 g/L, and 0.006 g/L, respectively. Those of Alkali Lake were pH 8.65, 1.02 g/L, and 0.073 g/L, respectively.

Flow Assisted Cell Sorting (FACS) of culture samples yielded two isolates, ALP2 and SLP2. A fluorescent population P2 was separated from contaminating debris designated as P3 and P4 (Figure 2.1). The flow-cytometric parameters of side and forward light scatter corresponding to size and granularity and those for fluorescence corresponding to chlorophyll and phycobillin (i.e. phycocyanin, phycoerythrin, allophycocyanin) pigmentation enabled FACS to discriminate and

isolate phototrophs, like microalgae and cyanobacteria from debris [33].

The isolated ALP2 and SLP2 strains were preliminarily surmised to be eukaryotic and photosynthetic, based on their microscopically-observed green coloration and presence of what appeared to be membrane-enclosed organelles (i.e. nuclei, chloroplasts, and mitochondria). ALP2 and SLP2 had single-cell, coccoidal morphology with average diameters of approximately 5 $\mu$ m. The detection of neutral lipid contained in ALP2 and SLP2 by liquid-state  $^1\text{H}$  NMR relies on the presence and accumulation of mobile and spheroidal lipid bodies [26]. These appeared as yellow regions inside Nile-Red stained ALP2 cells using laser confocal microscopy (Figure 2.2), even under non-N-starved conditions. This further established ALP2's microalgal and oleaginous identity, as lipid bodies are generally absent in native cyanobacteria.

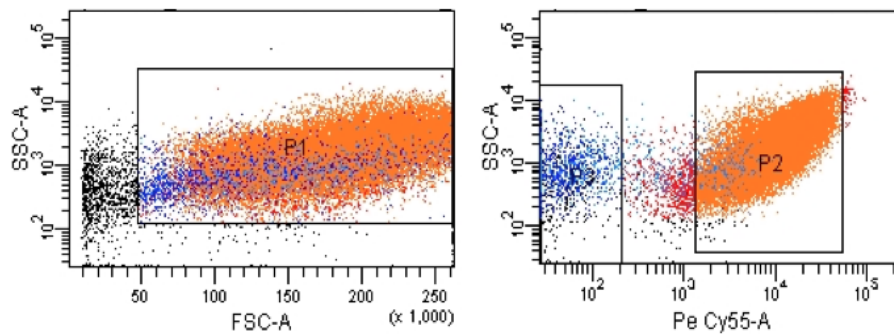


Figure 2.1. Plot depicting (Left) forward-scatter vs. side-scatter and (Right) fluorescent PE-Cy5.5 channel vs. side-scatter during Flow Assisted Cell Sorting (FACS) of ALP2 microalgae

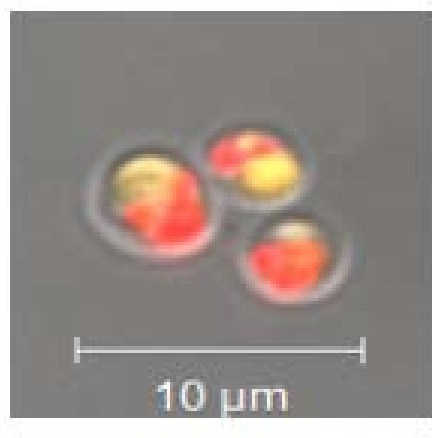


Figure 2.2. Laser-confocal image of ALP2 cells stained with Nile-Red for TAG-lipid fluorescence

Microalgal identity for ALP2 was further substantiated by the absence of absorption peaks at 565nm corresponding to the cyanobacterial pigment phycoerythrin from spectrophotometric absorption scans of intact cells from a phototrophic culture and its extracted pigments (Figure 2.3). Spectral analysis of the methanol extract of an ALP2 alkaline culture revealed that the photosynthetic pigments were predominantly chlorophylls a and b and carotenoids, with overlapping peak absorbances at 436.5/665 nm, 452.5/652.5 nm, and 470 nm, and that phycobillins phycoerythrin at 565nm and phycocyanin were absent. The ratio of chlorophyll-a and -b content was 2.15, which is lower than the 4-7 ratio of prochlorophytes but typical of green microalgae [41].

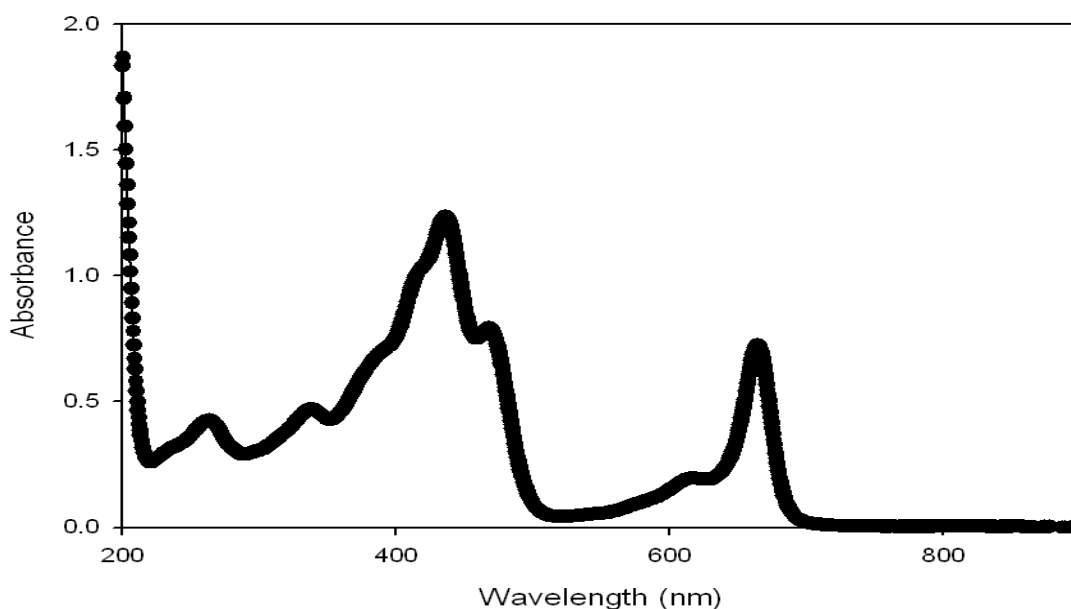


Figure 2.3. UV-Vis multi-wavelength absorbance spectra of ALP2 methanol extracts

ALP2 and SLP2 were more definitively identified via the polymerase chain reaction (PCR) and sequencing analysis [39]. The PCR band products for amplified rDNA sequences and ITS1 and ITS2 regions of ALP2 and SLP2 used for sequencing are shown (Figure 2.4). Accession number results from a nucleotide BLAST search using the PCR-amplified sequences generated for ALP2 were EU038291: *Auxenochlorella protothecoides* strain F-2, EU038289: *Chlorella pyrenoidosa* strain F-9, EU038288: *Chlorella pyrenoidosa* strain F-5, and FM205881: *Micractinium* sp. CCAP 248/14. Those for SLP2 were HQ404895: *Chlorella* sp. CCCryo297-06, DQ057340: *Chlorella* sp. NC64A, FM205862: *Chlorella* sp. UTEX 938, AY591514: *Chlorella vulgaris* strain CCAP 211/11F, AB260897: *Chlorella* sp. IFRPD 1014. Based on an e-value of

$7 \times 10^{-7}$  and query match of 94% and 88%, the ALP2 and SLP2 isolates were determined to be strains of *Chlorella pyrenoidosa* and *Chlorella vulgaris*, respectively. Such isolation of *Chlorella* is consistent with the observation that, in springs and winters, planktonic eukaryotic algae of *Xanthophyta*, *Chlorophyta*, and *Heteroconta* dominate the highly productive soda lakes [43]. *Chlorella sp.* are well known to be capable of high phototrophic neutral lipid productivity [44], as well as and high heterotrophic productivity of high-value nutraceuticals like astaxanthin and lutein using organic carbon sources [15, 45].



Figure 2.4. UV-irradiated agarose gel depicting electrophoretically migrated PCR amplicons for ALP2 (lane 2), SLP2 (lane 3) run alongside a 2-log DNA ladder (lane 1)

#### 2.4.2 Microalgal Screening on Carbon Sources and Trophic Modes

Both ALP2 and SLP2 strains were capable of heterotrophic and mixotrophic growth on glucose, and glucose was the highest yielding substrate in terms of biomass (Table 2.1). Both strains also yielded higher final DCW when cultured mixotrophically, rather than heterotrophically,

on glucose. Even in un-optimized conditions, these exceeded a previously reported 2.4 g/L DCW from heterotrophic growth of *Chlorella* on 10.0 g/L glucose in flasks [44]. The final cell densities obtained mixotrophically and heterotrophically using glucose were  $3.67 \times 10^8$  cells/ml and  $2.98 \pm 0.03 \times 10^8$  cells/ml, respectively. Between days 1 and 5, ALP2 achieved mixotrophically a higher specific growth rate of  $0.777 \text{ days}^{-1}$  than the  $0.481 \pm 0.017 \text{ days}^{-1}$  achieved heterotrophically, and this represents reduced operating time for inoculation of the second phototrophic stage. Such observed advantages of mixotrophy over heterotrophy [44] are likely due, in part, to both photosynthesis and oxidative phosphorylation-based metabolism, where waste  $\text{CO}_2$  from one metabolic process is thought to be consumed by another. Consistent with industrial practices, heterotrophic cultivation in fermentor was nonetheless used in place of mixotrophic cultivation in PBR for the first of a two-stage strategy demonstrated here. IC-HPLC data revealed an ALP2 glucose consumption rate of  $1.78 \text{ g L}^{-1} \text{ day}^{-1}$  and  $0.49 \text{ g L}^{-1} \text{ day}^{-1}$  for mixotrophic conditions of supplemented 10.0 g/L glucose and 5.0 g/L glucose + 5.0 g/L xylose, respectively.

ALP2 and SLP2 also grew on glycerol and potassium acetate, but only under mixotrophic conditions (Table 2.1). Such light-requirement for growth was absent in the previously observed heterotrophy of *Chlorella* on glycerol [18]. Interestingly, the SLP2 biomass yield (30.18 %) on potassium acetate was much higher than that of ALP2 (4.60 %). In contrast to a previously described *Chlorella* strain [46], no ALP2 growth was observed on xylose, nor was there any observed ALP2 growth on arabinose or mannose. ALP2 grew mixotrophically to a final DCW of

2.297 g/L on a 1:1 mixture of glucose and xylose. That this mixture initially containing 50% of the glucose found in the 100% glucose mixotrophic condition resulted in 43.50% of its final DCW suggests that xylose uptake transporters and consumption were not induced by the presence of glucose. IC-HPLC data also verified a decrease of glucose concentration and a negligible decrease of xylose concentration. Therefore, ALP2 likely could consume the C6 glucose but not any of the C5 monomer sugars present in enzymatic hydrolysates of ligno-cellulosic biomass [16].

Phototrophic growth of ALP2 and SLP2 was also observed under concentrations of bicarbonate as high as 28 g/L NaHCO<sub>3</sub> (Table 2.1). In one run, the pH of these cultures increased to pH 10.16 and 10.30, respectively, presumably due to photosynthetic consumption of bicarbonate buffer. The ability of ALP2 and SLP2 to grow on a relatively high NaHCO<sub>3</sub> level to high culture pH indicates that both isolates were haloalkaline-tolerant. The corresponding 20.3 g/L bicarbonate level for this run greatly exceeds the 0.075 g/L level used to optimally grow a typical *Chlorella sp.* [47] and the 4.2 g/L level above which an increasingly growth-inhibiting effect was observed for *Chlorella vulgaris* [19]. Note that the 28.0 g/L bicarbonate level used here exceeds the 16.8 g/L level used to limit open-pond contamination of *Spirulina sp.* [19] and represents a salinity that is the same order of magnitude as the 0.42 M combined salts used to optimally grow a haloalkaline-tolerant *Neochloris oleoabundans* algae [48]. Its alkalinity also approaches those measured from Soap Lake and Alkaline Lake waters.

Table 2.1. Final dry cell weights (DCW) of ALP2 and SLP2 microalgae cultivated for 10 days under different trophic modes on BG-11 medium supplemented with various carbon sources at 4.0 g C/L

Trophic Cultivation Mode	ALP2 Microalgae Final DCW (g L <sup>-1</sup> )	SLP2 Microalgae Final DCW (g L <sup>-1</sup> )
<b>Mixotrophic</b>		
Glucose	5.410	4.075
Glycerol	1.595±0.145	1.420
K-Acetate	0.622±0.054	3.678
Xylose	0.010	0.052
Xylose/Glucose	2.297	N/A
Mannose	0.041	N/A
Arabinose	0.028	N/A
<b>Heterotrophic</b>		
Glucose	3.956±0.068	3.032
Glycerol	0.044	0.074
K-Acetate	0.070	0.039
<b>Phototrophic</b>		
NaHCO <sub>3</sub>	1.561±0.011	1.593±0.057

A previously described closed-loop integrated system [10] could generate the necessary bicarbonate for open-ponds by scrubbing the CO<sub>2</sub> from cooled waste boiler flu-gas or anaerobic-digester bio-gas point emissions, and converting these to bicarbonate. Both the proximity of CO<sub>2</sub>-bicarbonate conversion reactors to open-pond reactors, as well as microalgal tolerance to extreme, near-saturation bicarbonate levels, were deemed necessary to maximize the efficiency of such processes [10]. The 28.0 g/L NaHCO<sub>3</sub> that ALP2 and SLP2 grew on represents

roughly 27.94 % saturation at 25°C. Although a haloalkaliphilic cyanobacterium *Euhalotheca ZM001* thrived at higher near-saturation levels of 1.0M NaHCO<sub>3</sub>/Na<sub>2</sub>CO<sub>3</sub> and would be more suitable for this process from this perspective [49], it did not accumulate any significant level of useful TAG-biofuel pre-cursors.

#### *2.4.3. Development of the Model TAG for Lipid Quantitation*

A model TAG was developed for rapid, sensitive, accurate, and non-destructive microalgal lipid quantitation for this and future optimization studies. The DCW of 0.05 L of raw ALP2 culture sample grown on BG-11<sub>0</sub> supplemented with 0.133 g/L urea and 10.0 g/L NaHCO<sub>3</sub> at HCl-adjusted pH 9 was 104.1 mg, and total 2:1 CHCl<sub>3</sub>/CH<sub>3</sub>OH extracted lipid weighed 41.6 mg, amounting to 39.9 % total extractable lipids. The crude extract was fractionated on a silica column [26] with each fraction checked for neutral lipid content by <sup>1</sup>H NMR. Fractions coming off the column with either CH<sub>2</sub>Cl<sub>2</sub> or CHCl<sub>3</sub> were almost exclusively TAG, and a fraction coming off the column at the point where the solvent was being switched to acetone contained mostly DAG which was highly enriched in ω-3 fatty acids. These fractions were combined to yield 32.8 mg of total neutral lipid representing 79% of total lipid content. The pooled fractions were evaporated and re-dissolved in CDCl<sub>3</sub> to give a solution of 6.0 ± 0.2 mg/ml. A <sup>1</sup>H NMR spectrum of this solution (Figure 2.5) was recorded using a previous method [26], and the integral region from 2.85-0.3 ppm was compared against the integral for the TMSP standard. Knowing the solution concentration in g/ml, a scaling factor of 0.0001219 was obtained relating the ratio of the integral of the sample

region to the integral of the standard (49.201:1). The fatty acid profile via GC-FAME analysis of the pooled neutral lipid fractions yielded a model TAG having a proton count of 88 for the integral region measured and molecular weight of 851 g/mole. The GC-FAME method used was a slight modification of the procedure previously used [26] wherein the incubation time and temperature were decreased to 20 min and increased to 85°C, respectively. Using these values, a scaling factor of 0.0001158 for determining neutral lipid content in g/ml via the NMR samples region: capillary standard integral ratio. Using this scaling factor a neutral lipid concentration of 5.64 mg/ml was calculated for the pooled fractions. This value differed from the gravimetrically-determined concentration by -6%.

The pooled neutral lipid NMR spectrum was also analyzed via a method that used the ratio of the different  $^1\text{H}$  multiplets to determine the ratio of unsaturated fatty acids to polyunsaturated fatty acids to saturated fatty acids [35, 36]. This analysis resulted in mole fractions of 10.9%  $\omega$ -3 fatty acid, 29.4% polyunsaturated, 21.4% monounsaturated and 38.3% saturated. Using linolenic, linoleic, oleic, and palmitic as the model fatty acids for these categories, an alternative model TAG was constructed giving 86 protons in the integrated region (2.85-0.3 ppm) and a molecular weight of 852 g/mole. These values resulted in a scaling factor of 0.0001187 to relate the sample integral region to the TMS standard integral. The resulting concentration of 5.78 mg/ml for the neutral lipid pool was calculated from this relationship and differed from the gravimetric value by -3.7%. In keeping with our previous work [26], the scaling factor derived from the FAME GC-analysis

was used to estimate the ALP2 neutral lipid content from the  $^1\text{H}$  NMR integral values.

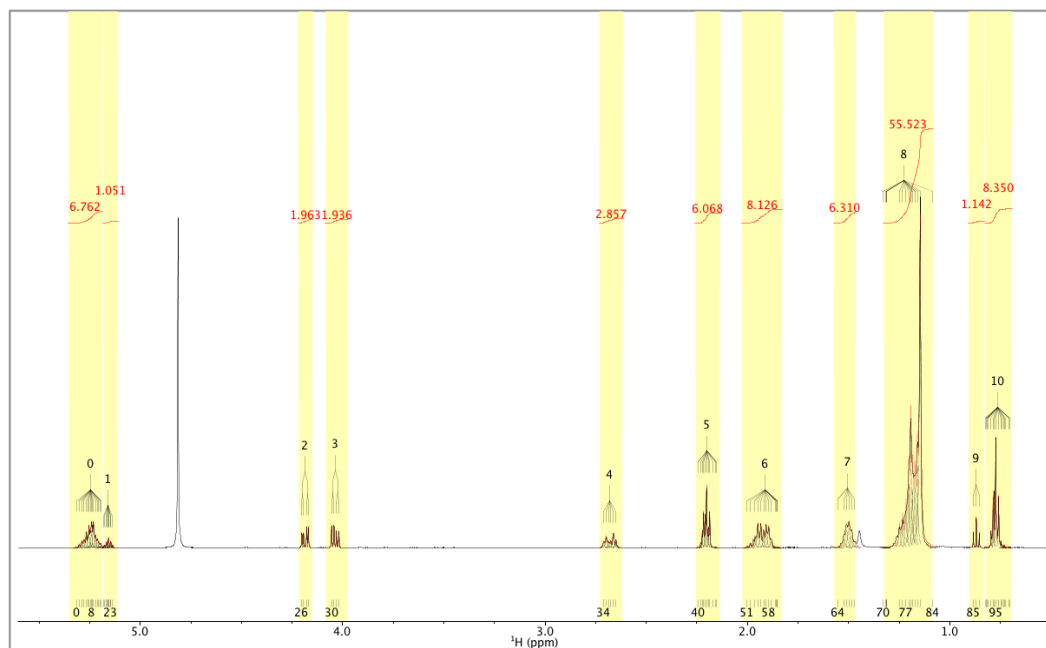


Figure 2.5. Static liquid-state  $^1\text{H}$  NMR spectra of isolated and pooled neutral lipid fractions in  $\text{CDCl}_3$  for ALP2 cells grown in BG-11<sub>0</sub> medium supplemented with 10 g/L  $\text{NaHCO}_3$  and 0.133 g/L urea at HCl-adjusted pH 9. Integral values shown in red above respective peaks including glycerol protons were used to determine the ratio of poly-unsaturated to mono-unsaturated to saturated fatty acids for the isolated TAGs

As a final validation for the  $^1\text{H}$  NMR method, the  $^1\text{H}$  spectrum of the culture that was used to isolate the neutral lipid fractions was taken, and the adjusted integral value (integral value of the algae sample minus the integral value for a sample where the algae cells were removed from the media via centrifugation) for the 2.85-0.3 ppm region was found to be 6.242 relative to the external

standard as 1.000. Using the scaling-factor of 0.0001158 derived from the GC-FAME analysis, the amount of neutral lipid in 0.050L of the culture as measured by  $^1\text{H}$  NMR was found to be 36.1 mg. This differs from the gravimetric value of 32.8 mg by +9% and is most likely reflective of losses in neutral lipid during the isolation process.

#### 2.4.4. Demonstration of Two-Stage Cultivation System

The two-stage cultivation of ALP2 was performed first in small flasks and monitored with both flow-cytometry and liquid-state  $^1\text{H}$  NMR spectroscopy. The heterotrophic culture on glucose achieved a cell density of  $2.22 \times 10^8$  cells/ml before inoculation of the second stage phototrophic flask. Static  $^1\text{H}$  NMR spectra revealed net peak areas in the 2.85-0.30 ppm chemical shift region corresponding to intra-cellular neutral lipids which had accumulated heterotrophically and were then diluted down upon inoculation of the second stage flask (Figure 2.6). Based on the  $^1\text{H}$  NMR model developed, the volumetric neutral lipid concentration of this heterotrophic first stage culture immediately prior to inoculation of the second stage was estimated to be 0.670 g/L, and that of the second stage upon its inoculation was estimated to be 0.042 g/L.

This study therefore reports for the first time the use of rapid, non-destructive liquid-state static  $^1\text{H}$  NMR spectroscopy to monitor intra-cellular neutral lipid accumulation in heterotrophic microbial cultures. Heterotrophic cultivation has been considered analogous to phototrophic cultivation in N-starved conditions as way to alter the C:N ratio and boost *Chlorella protothecoides* lipid productivity by as much as 400% [4].

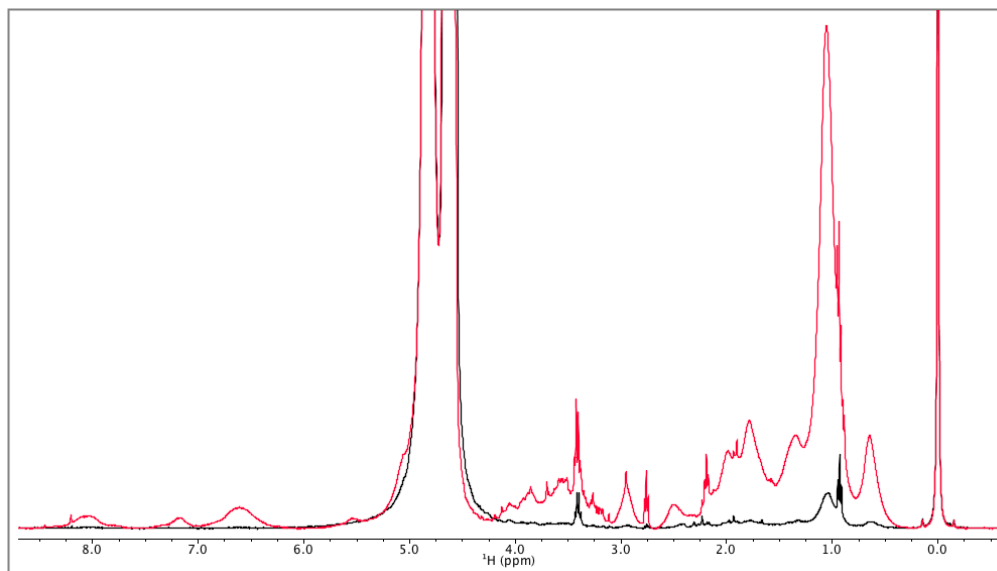


Figure 2.6. Liquid-state  $^1\text{H}$  NMR spectra of ALP2 1<sup>st</sup>-stage flask culture (Red Line)

heterotrophically cultivated in BG-11<sub>0</sub> medium supplemented with 10 g/L glucose and 0.529 g/L urea immediately prior to inoculation of second-stage flask culture (Black Line) phototrophically cultivated in BG-11<sub>0</sub> medium supplemented with 10 g/L NaHCO<sub>3</sub> and 0.032 g/L urea, pH 9

Such heterotrophic cultivation for high lipid content as opposed to high cell density in commercial operations should however be further justified by a more rigorous and comprehensive economic analysis. Although beyond the scope of this work, this would require reconciling capital costs (i.e. land, equipment, reactors, etc.) and operating costs (i.e. water, fertilizer nutrients, labor, gas supply, electricity, etc.) with revenues (i.e. volume and price of biofuel and nutraceuticals produced, CO<sub>2</sub>-carbon credits, etc.) for operations involving stainless-steel fermentors or open-ponds for microalgal lipid production. Until then, the two-stage cultivation for biofuel that is

demonstrated in this work is based on the following premise: Even with availability of the largest capital-intensive fermentors or mixotrophic PBRs, the scale needed to make a lipid-based biofuel commodity profitable is currently achievable only in large, albeit less efficient, open-ponds[13].

Automated flow-cell  $^1\text{H}$  NMR acquisition of a continuously circulating sample of the aforementioned phototrophic second-stage ALP2 flask culture that was inoculated from the heterotrophic first-stage and subsequently grown revealed the dynamic increase of intra-cellular neutral lipid peaks over time (Figure 2.7). Very low initial neutral TAG lipid levels were apparent in the  $^1\text{H}$  NMR spectrum during the initial (time = 0-92 hrs) stages of the phototrophic culture (Figure 2.7A). By 120 hrs there was a measurable amount of TAG which was monitored hourly for the next 42 hours (Figure 2.7B). During this time period, 0.5 ml aliquots were taken from the flask and measured separately on a 400 MHz spectrometer to obtain an independent measure of neutral lipid content. The overall increase in neutral lipid content accelerated as nitrogen became more limited. A final DCW of 0.984 g/L was achieved in the second-stage flask.

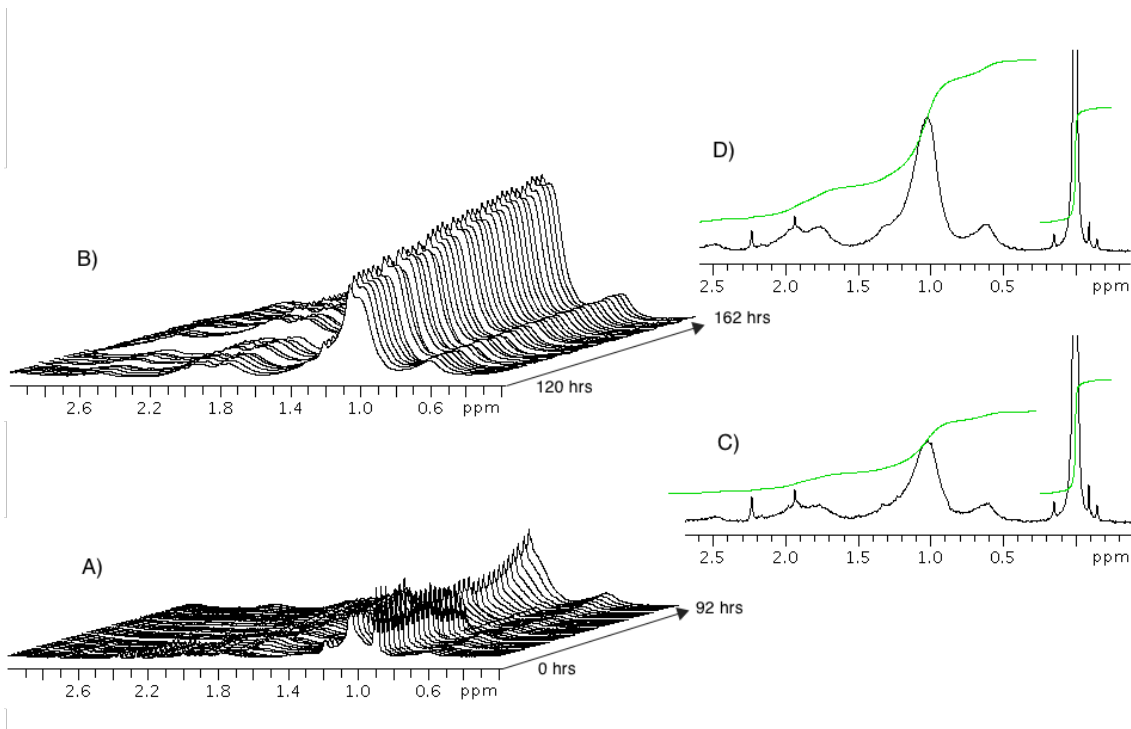


**Figure 2.7.** (A) Stacked plot of continuous flow-cell liquid-state  $^1\text{H}$  NMR spectra of ALP2 second-stage flask culture phototrophically cultivated in flask containing BG-11<sub>0</sub> supplemented with 10 g/L  $\text{NaHCO}_3$  and 0.032 g/L urea, pH 9 during initial 92 hour period. Initial sharp peaks at early time points are primarily due to small molecule contaminants in the culture medium. (B) Stacked plot of spectra taken during lipid accumulation stage from 120 hours to 162 hours. Spectra were taken hourly. (C) Static  $^1\text{H}$  NMR spectrum of a sample of culture taken at 92 hours. (D) Static  $^1\text{H}$  NMR spectrum of a sample of culture taken at 162 hours

The ability of high pH, high  $\text{NaHCO}_3$ , and high inoculation cell density to limit contamination of ALP2 in a second-stage phototrophic flask culture was also demonstrated. Flow cytometric plots of the fixed samples from initial and 7-day cultivation time points revealed two distinct

populations corresponding to the microalgae ALP2 and the co-inoculated model contaminant cyanobacterium *Synechococcus PCC7942* (Figure 2.8). These two species could be segregated by both fluorescence (i.e. FL3 and FL4 channels) due to chlorophyll and cyanobacteria-specific phycoerythrin and phycocyanin pigments and by size and granularity. Based on literature and the bead standard used, the smaller cyanobacterium was estimated to be about 1.5  $\mu\text{m}$  in size. An inoculation cell density of  $2.42 \times 10^6$  ALP2 cells/ml and  $1.09 \times 10^6$  cells/ml cyanobacterial cells/ml at the beginning of the culture corresponded to 67.42 % and 32.53 % of all events, respectively. However, after 7 days of culture, the cyanobacterial population represented only 1.57 % of all events compared to 98.41 % for ALP2, indicating that the high pH, salinity, and  $\text{NaHCO}_3$  levels helped limit this cyanobacterial contamination, and allowed the microalgae ALP2 to dominate.

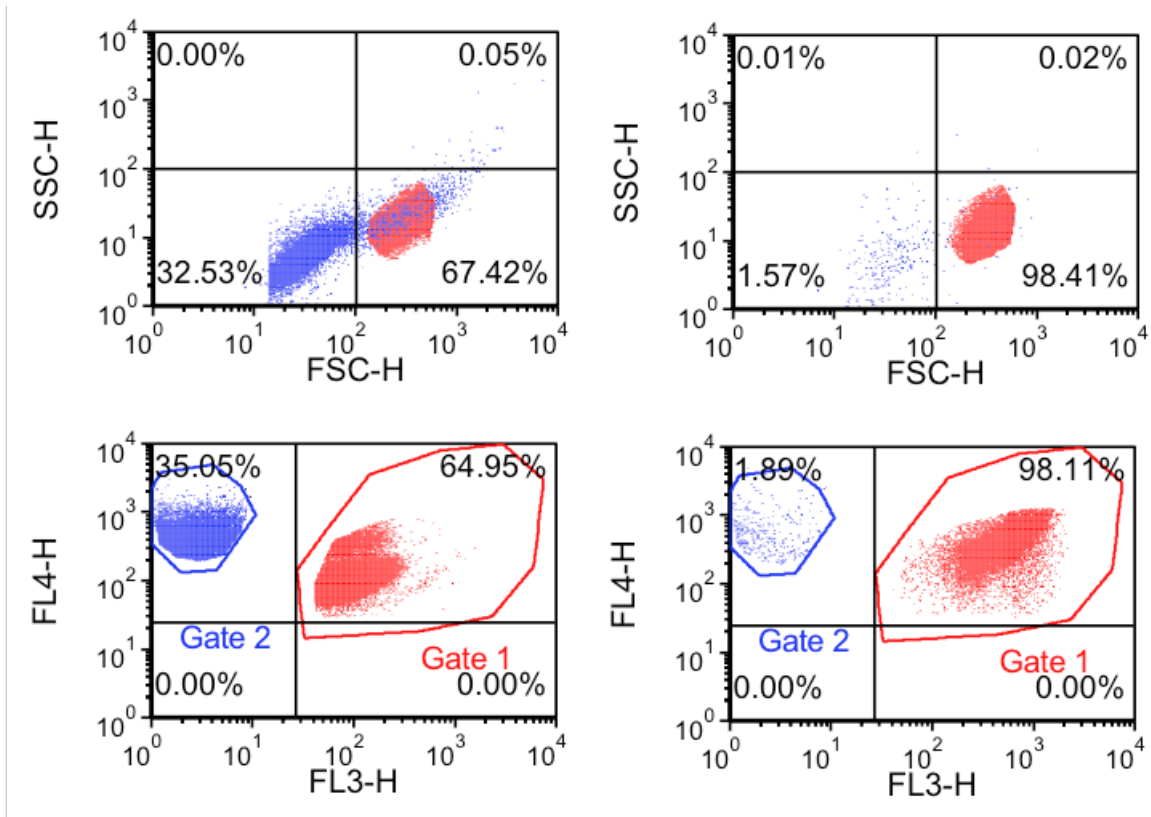


Figure 2.8. Flow cytometric plots for ALP2 (red population) and contaminating cyanobacteria (blue population) phototrophically grown on BG-11<sub>0</sub> medium supplemented with 10.0 g/L NaHCO<sub>3</sub> and 0.032 g/L urea with HCl-adjusted pH 9 during second-stage of small-scale flask two-stage process. Forward (FSC-H) and side (SSC-H) scatter for cultures at (Top Left) time = 0 days and (Top Right) time = 7 days are depicted. FL3 (FL3-H) and FL4 (FL4-H) fluorescence for cultures at (Bottom Left) time = 0 days (Bottom Right) time = 7 days are depicted

Growth curves for the larger-scale two-stage cultivation of ALP2 are shown (Figure 2.9). The first stage heterotrophic culture grew rapidly during the first 120 hrs at a specific growth rate of 0.034 hr<sup>-1</sup> to 2.76 x 10<sup>8</sup> cells/ml and was used to inoculate the second stage open-tank PBR at a cell

density of  $4.88 \times 10^6$  cells/ml. The second-stage phototrophic culture then grew for 200 hrs at a specific growth rate of  $0.011 \text{ hr}^{-1}$ . Microscopic observation of gram-stained samples taken at around the 481 hrs mid-point time of total two-stage cultivation revealed uptake of red stain by the ALP2 microalgae but not by other organisms. This and the absence of relatively smaller gram-negative blue populations indicated that bacterial contamination of the culture was limited.

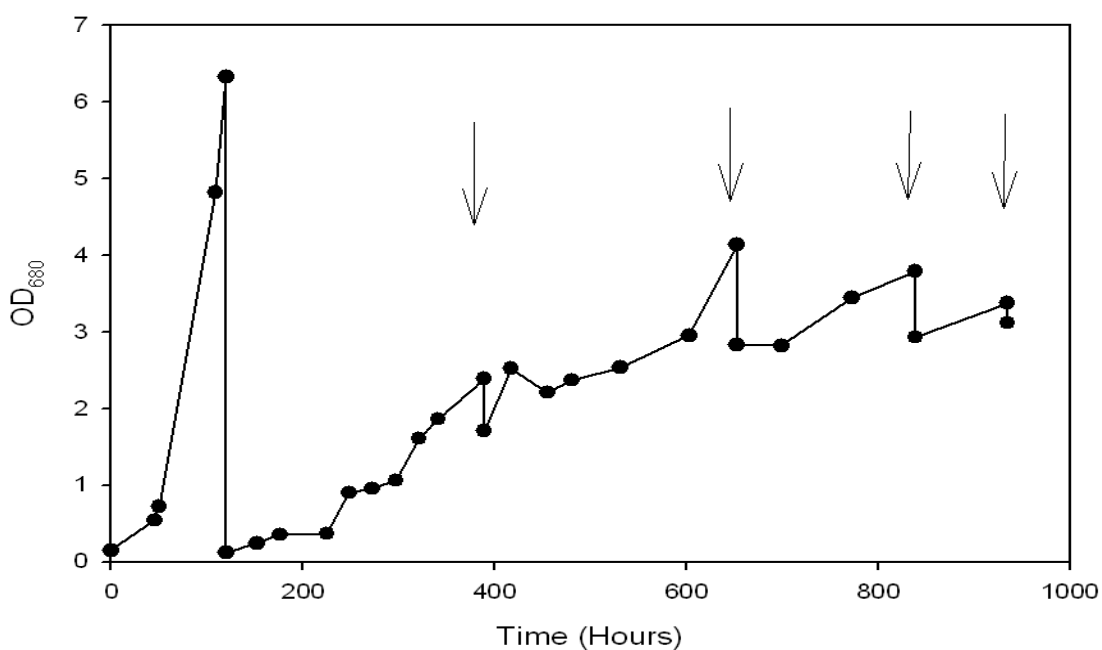


Figure 2.9. OD<sub>680</sub> as function of time for ALP2 cultivated in first-stage 1 L fermentor followed by second-stage indoor 40-L open-tank PBR. Arrows designate addition of H<sub>2</sub>O to compensate for evaporative losses

Based on the net <sup>1</sup>H NMR spectral proton peak area in the chemical shift range of 2.85-0.3 ppm for the phototrophic open-tank culture for a sample taken at 935 hrs (39 days) of total

two-stage cultivation, following a probable N-starvation-induced stationary phase, the final, pre-flocculation volumetric neutral lipid concentration was 0.389 g/L. The corresponding final fatty acid methyl ester (FAME) GC-based fatty-acid profile is presented (Table 2.2).

Table 2.2. Final Fatty Acid Methyl Ester (FAME)-GC-based fatty acid profile of raw ALP2

open-tank PBR culture phototrophically grown on BG-11<sub>0</sub> supplemented with 17.0 g/L NaHCO<sub>3</sub> and 0.133 g/L urea at HCl-adjusted pH 9

<b>Identified Fatty Acid</b>	<b>% Total</b>
C14:0 (Myristic)	0.23
C14:1n3(Tetradecanoic)	0.24
C14:2n6 (Tetradecadienoic)	0.88
C16:0 (Palmitic)	26.31
C16:1n9(Hexadecenoic)	4.30
C16:1n7 (Palmitoleic)	3.87
C16:2n6 (Hexadecadienoic)	4.00
C18:0 (Stearic)	3.88
C18:1n9 (Oleic)	29.14
C18:2n6 (Linoleic)	20.76
C18:3n3 (Linolenic)	6.39

A phototrophic volumetric lipid productivity was estimated to be 0.011 g L<sup>-1</sup>day<sup>-1</sup>, although this would have likely been much higher had it been instead based on earlier lipid measurements not taken. The final DCW before auto-flocculation of the open-tank second-stage was 0.978 g/L. The final DCW was about four times higher than that achieved by a Lithuanian *Chlorella sp.* under highly saline conditions [50]. However, this was also at least two times lower than that obtained in

smaller 0.25 L flasks [51]. Insufficient agitation and a light intensity used ( $70 \mu\text{moles m}^{-2} \text{s}^{-1}$ ) that was much lower compared to measured outdoor average solar intensities could account for this. The lipid content thus represented 39.78% DCW, which exceeded the 12.80 % DCW lipid content previously achieved under  $\text{CO}_2$ -sparged conditions [11].

The water evaporation rate was estimated at 1.09 L/day, and a total 44 L of water was added throughout to compensate. The harvesting efficiency at terminal pH 12 was 64.1%. The EDTA present in the BG-11<sub>0</sub> medium did not completely interfere with the  $\text{Mg}^{2+}$  mediated auto-flocculation at high pH and alkalinity as previously reported [12]. Importantly, no  $\text{CO}_2$  gas or air was ever bubbled into the open-tank throughout the culture run. Both the biomass and lipid productivities could be increased in the future with higher light intensity, additional optimization of culture conditions, and PBR design. This study demonstrates that ALP2 and SLP2 microalgae are suitable candidates for further exploring a two-stage process designed to address various challenges associated with microalgal mass cultivation.

## 2.5. Conclusions

Two new oleaginous, multi-trophic, halo-alkaline tolerant microalgae, ALP2 and SLP2, were isolated from soda lakes in Washington State, U.S.A. and screened as candidates for a two-stage cultivation process designed to address various challenges associated with large-scale outdoor cultivation. ALP2 and SLP2 were oleaginous *Chlorella sp.* able to grow on multiple carbon sources (i.e. glycerol, acetate, glucose, bicarbonate), as well as at high pH (i.e. 9-10) and high

NaHCO<sub>3</sub> levels (i.e. 17-28 g/L). A two-stage cultivation and auto-flocculation process was validated at larger scale using 1 L fermentor for the first stage and a 40 L open-tank photobioreactor (PBR) as a model for the second stage using ALP2. These novel ALP2 and SLP2 strains and two-stage process offers technological advancement in mass cultivation of microalgae.

### **Acknowledgements**

Financial support for this work was provided by the US Department of Energy (EE0003112).

Special thanks to the WSU Microscopy Center and Dr. Gary Anderson.

## 2.6. References

- [1] M. Elmoraghy, I.H. Farag. Green Approach to Produce Bio-jet Fuel from Microalgae. AIChE 2012 Annual Meeting American Institute of Chemical Engineers, 2012.
- [2] J. Glanz. Data Barns in a Farm Town, Gobbling Power and Flexing Muscle. In: N.Y. Times, Times-Mirror Company, New York City, NY, 2012.
- [3] Y. Chisti. Biodiesel from microalgae. *Biotechnology Advances* 25 (2007) 294-306.
- [4] S.A. Scott, M.P. Davey, J.S. Dennis, I. Horst, C.J. Howe, D.J. Lea-Smith, et al. Biodiesel from algae: challenges and prospects. *Current Opinion in Biotechnology* 21 (2010) 277-86.
- [5] K.K. Sharma, H. Schuhmann, P.M. Schenk. High Lipid Induction in Microalgae for Biodiesel Production. *Energies* 5 (2012) 1532-53.
- [6] N.R. Moheimani, M.A. Borowitzka. The long-term culture of the coccolithophore *Pleurochrysis carterae* (Haptophyta) in outdoor raceway ponds. *Journal of Applied Phycology* 18 (2006) 703-12.
- [7] V. Patil, K.Q. Tran, H.R. Giselrod. Towards sustainable production of biofuels from microalgae. *International Journal of Molecular Sciences* 9 (2008) 1188-95.
- [8] E.D.G. Danesi, C.D.O. Rangel-Yagui, J.C.M. de Carvalho, S. Sato. An investigation of effect of replacing nitrate by urea in the growth and production of chlorophyll by *Spirulina platensis*. *Biomass & Bioenergy* 23 (2002) 261-9.
- [9] D. Soletto, L. Binaghi, A. Lodi, J.C.M. Carvalho, A. Converti. Batch and fed-batch cultivations of *Spirulina platensis* using ammonium sulphate and urea as nitrogen sources. *Aquaculture* 243 (2005) 217-24.
- [10] Z.Y. Chi, J.V. O'Fallon, S.L. Chen. Bicarbonate produced from carbon capture for algae culture. *Trends in Biotechnology* 29 (2011) 537-41.
- [11] Y.B. Zheng, Z.Y. Chi, B. Lucker, S.L. Chen. Two-stage heterotrophic and phototrophic culture strategy for algal biomass and lipid production. *Bioresource Technology* 103 (2012) 484-8.

- [12] D. Vandamme, I. Foubert, I. Fraeye, B. Meesschaert, K. Muylaert. Flocculation of *Chlorella vulgaris* induced by high pH: Role of magnesium and calcium and practical implications. *Bioresource Technology* 105 (2012) 114-9.
- [13] C.U. Ugwu, H. Aoyagi, H. Uchiyama. Photobioreactors for mass cultivation of algae. *Bioresource Technology* 99 (2008) 4021-8.
- [14] O. Perez-Garcia, F.M.E. Escalante, L.E. de-Bashan, Y. Bashan. Heterotrophic cultures of microalgae: Metabolism and potential products. *Water Research* 45 (2011) 11-36.
- [15] F. Bumbak, S. Cook, V. Zachleder, S. Hauser, K. Kovar. Best practices in heterotrophic high-cell-density microalgal processes: achievements, potential and possible limitations. *Applied Microbiology and Biotechnology* 91 (2011) 31-46.
- [16] P.L. Li, X.L. Miao, R.X. Li, J.J. Zhong. In Situ Biodiesel Production from Fast-Growing and High Oil Content *Chlorella pyrenoidosa* in Rice Straw Hydrolysate. *Journal of Biomedicine and Biotechnology* (2011) 1-8.
- [17] Y. Liang, X. Zhao, Z. Chi, M. Rover, P. Johnston, R. Brown, et al. Utilization of acetic acid-rich pyrolytic bio-oil by microalga *Chlamydomonas reinhardtii*: Reducing bio-oil toxicity and enhancing algal toxicity tolerance. *Bioresource Technology* 133 (2013) 500-6.
- [18] J. O'Grady, J.A. Morgan. Heterotrophic growth and lipid production of *Chlorella protothecoides* on glycerol. *Bioprocess and Biosystems Engineering* 34 (2011) 121-5.
- [19] A. Richmond, S. Karg, S. Boussiba. Effects of Bicarbonate and Carbon-Dioxide on the Competition between *Chlorella vulgaris* and *Spirulina platensis*. *Plant and Cell Physiology* 23 (1982) 1411-7.
- [20] R.D. Gardner, E. Lohman, R. Gerlach, K.E. Cooksey, B.M. Peyton. Comparison of CO<sub>2</sub> and bicarbonate as inorganic carbon sources for triacylglycerol and starch accumulation in *Chlamydomonas reinhardtii*. *Biotechnology and Bioengineering* 110 (2013) 87-96.
- [21] S. Malisarad, M. Friedlander, R. Benarie, A.E. Richmond. Alkalinity-Induced Aggregation in *Chlorella vulgaris*. 1. Changes in Cell Volume and Cell Wall Structure. *Plant and Cell Physiology*

21 (1980) 27-35.

[22] A.G. Miller, D.H. Turpin, D.T. Canvin. Growth and photosynthesis of the cyanobacterium *Synechococcus leopoliensis* in  $\text{HCO}_3^-$ -limited chemostats. *Plant Physiology* 75 (1984) 1064-70.

[23] J.L. Milne, Jeffrey C. Cameron, Lawrence E. Page, Sally M. Benson, Himadri B. Pakrasi. Algal Technologies for Biological Capture and Utilization of  $\text{CO}_2$  Require Breakthroughs in Basic Research. *Perspectives on Biofuels: Potential Benefits and Possible Pitfalls*. American Chemical Society 1116 (2012) 107-41.

[24] K.F. Walker. The seasonal phytoplankton cycles of two saline lakes in central Washington. *Limnology and Oceanography* 20 (1975) 40-53.

[25] P.A. Dirnithiu, H.C. Pinkart, B.M. Peyton, M.R. Mormile. Spatial and temporal patterns in the microbial diversity of a meromictic soda lake in Washington State. *Applied and Environmental Microbiology* 74 (2008) 4877-88.

[26] P.T. Davey, W.C. Hiscox, B.F. Lucker, J.V. O'Fallon, S. Chen, G.L. Helms. Rapid triacylglyceride detection and quantification in live micro-algal cultures via liquid state  $^1\text{H}$  NMR. *Algal Research* 1 (2012) 166-75.

[27] J.C. Meeks. <http://microbiology.ucdavis.edu/meeks/BG11medium.html>. 2013.

[28] K.L. Yeh, C.Y. Chen, J.S. Chang. pH-stat photoheterotrophic cultivation of indigenous *Chlorella vulgaris* ESP-31 for biomass and lipid production using acetic acid as the carbon source. *Biochemical Engineering Journal* 64 (2012) 1-7.

[29] C.J. Zhu, Y.K. Lee. Determination of biomass dry weight of marine microalgae. *Journal of Applied Phycology* 9 (1997) 189-94.

[30] Aris Hosikian, S. Lim, R. Halim, M.K. Danquah. Chlorophyll Extraction from Microalgae: A Review on the Process Engineering Aspects. *International Journal of Chemical Engineering* 2010 (2010) 1-11.

[31] A.R. Wellburn. The Spectral Determination of Chlorophyll-a and Chlorophyll-b, as well as Total Carotenoids, Using Various Solvents with Spectrophotometers of Different Resolution.

Journal of Plant Physiology 144 (1994) 307-13.

[32] Y. Zheng, X. Yu, J. Zeng, S. Chen. Feasibility of filamentous fungi for biofuel production using hydrolysate from dilute sulfuric acid pretreatment of wheat straw. *Biotechnology for Biofuels* 5 (2012) 50-63.

[33] M. Cellamare, A. Rolland, S. Jacquet. Flow cytometry sorting of freshwater phytoplankton. *Journal of Applied Phycology* 22 (2010) 87-100.

[34] D. Marie, N. Simon, D. Volaut. Phytoplankton Cell Counting By Flow Cytometry. In: R.A. Andersen, (Ed.) *Algal Culturing Techniques*, Elsevier Academic Press, Burlington, MA., 2005.

[35] Y. Miyake, K. Yokomizo, N. Matsuzaki. Determination of unsaturated fatty acid composition by high-resolution nuclear magnetic resonance spectroscopy. *Journal of the American Oil Chemists Society* 75 (1998) 1091-4.

[36] G. Knothe, J.A. Kenar. Determination of the fatty acid profile by <sup>1</sup>H NMR spectroscopy. *European Journal of Lipid Science and Technology* 106 (2004) 88-96.

[37] J.V. O'Fallon, J.R. Busboom, M.L. Nelson, C.T. Gaskins. A direct method for fatty acid methyl ester synthesis: Application to wet meat tissues, oils, and feedstuffs. *Journal of Animal Science* 85 (2007) 1511-21.

[38] T.T.Y. Doan, J.P. Obbard. Improved Nile Red staining of *Nannochloropsis sp.* *Journal of Applied Phycology* 23 (2011) 895-901.

[39] H.C. Rees, W.D. Grant, B.E. Jones, S. Heaphy. Diversity of Kenyan soda lake alkaliphiles assessed by molecular methods. *Extremophiles* 8 (2004) 63-71.

[40] M.R. Mormile, M.F. Romine, T. Garcia, A. Ventosa, T.J. Bailey, B.M. Peyton. *Halomonas campisalis sp nov.*, a denitrifying, moderately haloalkaliphilic bacterium. *Systematic and Applied Microbiology* 22 (1999) 551-8.

[41] L.M. Gerasimenko, A.V. Dubinin, L.L. Mityushina, G.A. Zavarzin. A microscopic green alga from soda lakes. *Microbiology* 68 (1999) 610-4.

[42] K. Kiefer. Soap Lake-A Mineral Lake In The Heart of Washington. JACOL FilmWorks 2004.

- [43] L.M. Gerasimenko, O.S. Mikhodyuk. Halophilic Algal-Bacterial and Cyanobacterial Communities and Their Role in Carbonate Precipitation. *Paleontological Journal* 43 (2009) 940-57.
- [44] Y.N. Liang, N. Sarkany, Y. Cui. Biomass and lipid productivities of *Chlorella vulgaris* under autotrophic, heterotrophic and mixotrophic growth conditions. *Biotechnology Letters* 31 (2009) 1043-9.
- [45] Z.Y. Wu, C.B. Qu, X.M. Shi. Biochemical System Analysis of Lutein Production by Heterotrophic *Chlorella pyrenoidosa* in a Fermentor. *Food Technology and Biotechnology* 47 (2009) 450-5.
- [46] R.L. Hawkins. Utilization of xylose for growth by the eukaryotic alga, *Chlorella*. *Current Microbiology* 38 (1999) 360-3.
- [47] C.R. Devgoswami, M.C. Kalita, J. Talukdar, R. Bora, P. Sharma. Studies on the growth behavior of *Chlorella*, *Haematococcus* and *Scenedesmus sp* in culture media with different concentrations of sodium bicarbonate and carbon dioxide gas. *African Journal of Biotechnology* 10 (2011) 13128-38.
- [48] A.M. Santos, M. Janssen, P.P. Lamers, W.A.C. Evers, R.H. Wijffels. Growth of oil accumulating microalga *Neochloris oleoabundans* under alkaline-saline conditions. *Bioresource Technology* 104 (2012) 593-9.
- [49] Z. Chi, Y. Xie, F. Elloy, Y. Zheng, Y. Hu, S. Chen. Bicarbonate-based Integrated Carbon Capture and Algae Production System with alkalihalophilic cyanobacterium. *Bioresource Technology* 133 (2013) 513-21.
- [50] V. Makarevičienė, V. Andrulevičiute, V. Skorupskaitė, J. Kasperoviciene. Cultivation of *Chlorella sp.* and *Scenedesmus sp.* as Potential Biofuel Feedstock. *Environmental Research, Engineering, and Management* 57 (2011) 21-7.

**CHAPTER 3 : MICROALGAE FOR TWO-STAGE CULTIVATION PART II:  
OPTIMIZATION AND CHARACTERIZATION OF BIOMASS AND LIPID  
ACCUMULATION**

**3.1. Abstract**

An oleaginous, haloalkaline-tolerant, dual-trophic green microalgae, ALP2, from a soda lake was previously isolated, identified, and screened as candidate for a two-stage cultivation process designed to address challenges of mass outdoor cultivation. This involved growing microalgae in a fermentor heterotrophically or photobioreactor mixotrophically (first stage) to rapidly obtain high cell densities for inoculating a phototrophic open-pond culture (second stage) that used high levels of NaHCO<sub>3</sub>, pH, and salinity. The effects of carbon and nitrogen sources and levels, temperature, pH, diurnal light intensity, and HCl-mediated pH control were determined in this study. Optimal first-stage conditions involved cultivation on BG-11<sub>0</sub> medium supplemented with 10.0 g/L glucose and 0.529 g/L urea at 28°C, where ALP2 achieved 1.7 x 10<sup>8</sup> cells ml<sup>-1</sup>day<sup>-1</sup> cell productivity. Optimal second-stage conditions involved cultivation on BG-11<sub>0</sub> medium supplemented with 17.0 g/L NaHCO<sub>3</sub> and 0.133 g/L urea at HCl-mediated pH 9, where ALP2 replicated before nitrogen-starvation and achieved 0.078 g L<sup>-1</sup>day<sup>-1</sup> lipid productivity. With increasing NaHCO<sub>3</sub> levels in BG-11<sub>0</sub> media with 0.529 g/L urea at pH 9, ALP2 cellular size and granularity increased, carotenoid/chlorophyll ratio decreased, and chlorophyll-fluorescence parameters F<sub>v</sub>/F<sub>m</sub>, Psi<sub>II</sub>, and NPQ remained relatively constant. Photosynthetic state transition

occurred upon 33.6 g/L NaHCO<sub>3</sub> addition. Results characterized ALP2 two-stage cultivation.

### 3.2. Introduction

Mass cultivation of microalgae in outdoor open-ponds for biofuels and co-products faces challenges of low lipid productivity [1], contamination [2, 3], inefficient CO<sub>2</sub> [4] and unsustainable nutrient [5, 6] supplies, and difficulties in harvesting [7-9]. A multi-trophic, oleaginous, and haloalkaline-tolerant green microalgae, ALP2, was previously isolated, identified, and screened as candidate for developing a two-stage cultivation strategy designed to address some of these challenges[9]. The two-stage cultivation in a photosynthetic biorefinery involves cultivating microalgae in an enclosed fermentor heterotrophically or photobioreactor mixotrophically on organic carbon (first-stage) to rapidly obtain high cell densities for inoculation of a phototrophic, oleaginous open-pond culture (second stage). The contamination control effect can be further enhanced by using high levels of NaHCO<sub>3</sub>, pH, and salinity in the second stage.

Previous studies have examined how carbon and nitrogen sources, C:N ratio, and temperature affect biomass and lipid productivity under heterotrophic conditions [10]. Studies have also been conducted to evaluate how increased levels of inorganic carbon (i.e. CO<sub>2</sub> [11] and bicarbonate [12, 13]), salinity [14], potassium [15], and external pH [16] influence the photosynthetic apparatus, lipid productivity, and other functions in microalgae and cyanobacteria under phototrophic conditions. Results on bicarbonate-mediated mechanisms that trigger cessation of replication, and increase in pH, cell size, and intra-cellular accumulation of neutral TAG lipids in microalgal cultures that were initially sparged with CO<sub>2</sub> for growth were reported [17].

To extend these studies and gain further insight into the halo-alkaline tolerant and

heterotrophic growth characteristics of ALP2 with regards to its potential use in a two-stage mass culture system, experiments were here conducted to evaluate how ALP2 was influenced by heterotrophic conditions and the relatively higher salinity and alkalinity (i.e. 17.0 g/L NaHCO<sub>3</sub> and pH 9-12) used to limit open-pond contamination [18] and induce auto-flocculation harvesting of phototrophic cultures [13]. If microalgal photosynthetic and replicative growth were possible at these highly saline and alkaline conditions, and subsequently lipid accumulation were to proceed once nitrogen is depleted, then microbial contamination could be limited, the additional problem of supplying adequate amounts of dissolved CO<sub>2</sub> to open-ponds for growth could be eliminated, and harvesting could be simplified. Specifically, questions on how these simultaneously influenced cellular photosynthetic parameters, dimensions, replication, and lipid and biomass productivity of a nitrogen-depleted, oleaginous, haloalkaline-tolerant microalgae were of interest. To answer these questions, variations in carbon and nitrogen source and level, temperature, pH, diurnal light intensity, and pH-adjusting acid were tested for process suitability and optimization for both heterotrophic first-stage and phototrophic second-stage cultivation.

### **3.3. Materials and Methods**

#### *3.3.1. Microalgal Growth Experiments*

Heterotrophic growth experiments were conducted on previously isolated *Chlorella sp.* ALP2 microalgae [9] to evaluate the effects of glucose concentration, nitrogen source and concentration, and temperature as first-stage culture. ALP2 cultures were grown heterotrophically for 8 days at

21°C in aluminum foil-covered, foam-capped 0.25 L flasks containing 0.10 L of BG-11 medium [19] initially adjusted to pH 7 and supplemented with different glucose concentrations (0, 1, 5, 10, 20 g/L) and agitated at 130 rpm on orbital shaker. In a second experiment, ALP2 cultures were grown in a BG-11<sub>0</sub> medium [19] supplemented with 10 g/L glucose as the organic carbon source and different nitrogen sources, including 1.500 g/L NaNO<sub>3</sub>, 0.529 g/L urea, or 22.0 % (v/v) effluent from anaerobically-digested food waste, corresponding to the 0.247 g N/L of NaNO<sub>3</sub> in BG-11 medium at three temperatures, 21°C, 28°C, and 37°C using incubators for temperature control. In a third experiment, ALP2 cultures were grown in a dark room at approximately 18°C on BG-11<sub>0</sub> medium supplemented with 10 g/L glucose and different concentrations of the chosen nitrogen-source urea (0, 0.133, 0.265, 0.529, 1.058, 1.587, 3.070 g/L).

Phototrophic growth experiments were next conducted on ALP2 to evaluate the effects of bicarbonate concentration, nitrogen source and concentration, diurnal light intensity, pH, and pH-adjusting acid as second-stage culture. In general, conditions resulting in the highest biomass yield after a single-variable change were then used to evaluate the effects of subsequent variables. All phototrophic growth experiments occurred in 0.25 L foam-capped flasks containing 0.10 L medium and agitated at 130 rpm on orbital shaker. The growth medium was neither filtered nor autoclaved because NaHCO<sub>3</sub> will decompose to CO<sub>2</sub> and H<sub>2</sub>O above 70°C and also because costly filtration membranes and high autoclaving temperatures and pressures were to be avoided for larger-scale operations. The minimal Na<sub>2</sub>CO<sub>3</sub> in BG-11 medium was not included in calculations

of total  $\text{NaHCO}_3$  supplemented to cultures.

To determine the effect of bicarbonate concentration, ALP2 was inoculated at  $\text{OD}_{680} = 0.035$  into four separate flasks containing each BG-11 medium, having 1.500 g/L  $\text{NaNO}_3$  as the nitrogen source, supplemented with varying concentrations (1.4, 7.0, 14.0, and 28.0 g/L) of  $\text{NaHCO}_3$ , initially adjusted to pH 7, and grown phototrophically for 8 days under continuous  $70 \mu\text{moles m}^{-2} \text{s}^{-1}$  light intensity delivered by overhead fluorescent polychromatic light bulbs. To determine the effect of nitrogen source, ALP2 cultures were grown phototrophically in a similar manner, except using BG-11<sub>0</sub> medium, supplemented with 7.0 g/L  $\text{NaHCO}_3$  and either 1.500 g/L  $\text{NaNO}_3$ , 0.529 g/L urea, or 22.0% (v/v) anaerobically-digested food waste effluent corresponding to the 0.247 g N/L of  $\text{NaNO}_3$  in regular BG-11, and initially adjusted to pH 7. (The effluent also served to replace phosphates from BG-11 phosphates stock solution). To determine the effects of urea concentration, ALP2 cultures were grown phototrophically in a similar manner except using a BG-11<sub>0</sub> medium supplemented with 7.0 g/L  $\text{NaHCO}_3$  and a range of urea concentrations (0, 0.133, 0.265, 0.529, 1.058, 1.587, 3.070 g/L), and initially adjusted to pH 7. To test the effect of pH control, ALP2 cultures were similarly grown phototrophically except on BG-11<sub>0</sub> medium supplemented with 7 g/L  $\text{NaHCO}_3$  and 1.058 g/L urea with a range of starting pH (7, 8, 9, 10, and 11) that was either left unadjusted or adjusted back to the starting level every 24 hours with either 0.5M HCl acid or glacial acetic acid.

It was found that the best source of supplementary nitrogen, overall, was urea, and that pH

control to pH 9 by periodic addition of HCl acid resulted in the higher biomass accumulation than that without pH adjustment. Based on these observations, and to gain additional insight on the effects of NaHCO<sub>3</sub> concentration, pH adjustment, and diurnal light intensity, four ALP2 cultures were then inoculated at OD<sub>680</sub> = 0.90 into flasks containing BG-11<sub>0</sub> medium supplemented with 0.133 g/L urea and grown phototrophically under 45 μmole m<sup>-2</sup> s<sup>-1</sup> of poly-chromatic light on a 16 hr-light/8hr-dark diurnal cycle approximated by covering with aluminum foil at selected times. The four cultures were established with either 1.4 g/L or 17.0 g/L NaHCO<sub>3</sub>, and with or without pH adjustment with 0.5M HCl acid (initial pH = 9 in all cases). Over the course of the experiment, for the two pH-adjusted flasks, a total of 0.56 mls and 3.77 mls of 0.5M HCl acid were used to maintain pH 9 in the 1.4 g/L and 17.0 g/L NaHCO<sub>3</sub> flasks, respectively.

An additional experiment was performed to simultaneously evaluate the effects of NaHCO<sub>3</sub>, urea, and acid-adjusted pH levels. To simulate an actual two-stage process, ALP2 cultures were inoculated at OD<sub>680</sub> = 0.33 at an initial cell density of 6.55 x 10<sup>6</sup> cells/ml from an exponentially-grown heterotrophic maintenance culture that was washed 2x in PBS to remove residual glucose and urea, into flasks containing BG-11 medium supplemented with various NaHCO<sub>3</sub> concentrations (0.7, 1.4, 3.5, 10.0, 17.0, 25.0, 42.0, 63.0 and 84.0 g/L) and urea concentrations (0.133 and 0.529 g/L), with starting pH of 7, 8, 9, or 10 adjusted daily with either 37% (v/v) HCl or glacial acetic acid. These cultures were illuminated under 70 μmole m<sup>-2</sup> s<sup>-1</sup> of poly-chromatic light intensity from overhead fluorescent bulbs on a 16 hr-light/8hr-dark diurnal

cycle. Samples of 1 ml were taken for chlorophyll and carotenoid content, flow cytometric, and photosynthetic measurements during mid-exponential phase on day 6. Samples were taken for dry cell weight (DCW), <sup>1</sup>H NMR-based lipid content, cell count, total N, and total organic/inorganic carbon, respectively, on day 13.

### 3.3.2. Biomass, Lipid, and Extracellular Concentration Measurements

Dry cell weight (DCW), chlorophyll a/b and carotenoid content, extracellular pH, light intensity, optical density (OD) were measured as previously described [9]. Absorbance maxima at OD<sub>680</sub> corresponding to algal chlorophyll was not found to be correlated to absorbance minima at OD<sub>750</sub>. Separate standard curves were generated for heterotrophic and phototrophic cultures because OD<sub>680</sub> depends on dynamic microalgal optical properties (i.e. Mie-scattering and Beer's Law absorption extinction cross-sections, which are related to chlorophyll LHC<sub>II</sub> antenna size and cellular dimensions) that, in turn, are dependent on the incident light intensity [20]. A standard curve correlating heterotrophic OD<sub>680</sub> and DCW for ALP2 was therefore developed with linear regression as follows:

$$DCW(g/L) = OD_{680} \times 0.4007 - 0.0172, R^2=0.9734 \quad (3.1)$$

Similarly, a standard curve correlating phototrophic OD<sub>680</sub> and DCW for ALP2 was developed:

$$DCW(g/L) = OD_{680} \times 0.3713 + 0.1617, R^2=0.9068 \quad (3.2)$$

Specific growth rates during the exponential growth phase between initial (t<sub>1</sub>) and final (t<sub>2</sub>) time points were calculated as previously described [9]. Total carbon and inorganic carbon in

supernatant were measured using a TOC-5000 analyzer (Shimadzu, Kyoto, Japan). Total nitrogen was measured using a spectrometer and total high-range (10-150 mg/L) colorimetric reagent Test N Tube kits (Hach Company, Loveland, CO). An un-inoculated flask containing BG-11<sub>0</sub> medium, adjusted to pH 9 and supplemented with 2.5% (v/v) effluent and 17.0 g/L NaHCO<sub>3</sub>, was agitated to determine its ammonia volatilization rate, based on periodic measurement of total nitrogen in the medium. Neutral lipid content was assessed for the majority of ALP2 cultures via <sup>1</sup>H NMR, as previously described [9]. Lipid content and fatty-acid profiles for ALP2 cultures grown heterotrophically at 28°C and 21°C at 10 g/L and 20 g/L glucose, or phototrophically on food waste effluent, were assessed by a previously described FAME GC-based procedure [21].

### *3.3.3. 77K, Chlorophyll Fluorescence, and O<sub>2</sub> Evolution/Respiration Measurements*

77K spectrofluorimetry was used to measure the short-term effects of transitioning ALP2 from low to high NaHCO<sub>3</sub> levels. For this, ALP2 algal cultures that were initially grown and adapted to 70 μmoles m<sup>-2</sup> s<sup>-1</sup> light intensity in BG-11 medium supplemented with 0.84 g/L NaHCO<sub>3</sub>. Confirming first that the algae were at an OD<sub>680</sub> corresponding to a chlorophyll concentration below a critical 0.25 μg/ml to avoid re-absorption, they were then supplemented step-wise to 33.64 g/L NaHCO<sub>3</sub>. The algae was then frozen down in liquid-N<sub>2</sub> in sealed-glass Pasteur pipettes at the start and then at 2 min, 15 min, 60 min, and 3 days after the NaHCO<sub>3</sub> step changes. The intensities of frozen samples and medium blank were acquired on a MaxiFluor-4 spectrofluorometer (Horiba Jobin Yvon, Inc., Kyoto, Japan) at 435 and 475 nm excitation with 1

nm slit width from 600-800 nm, and later blank-normalized using an .xfm script. Chlorophyll fluorescence and O<sub>2</sub>-evolution/respiration photosynthetic measurements were done to elucidate the effects of pH and NaHCO<sub>3</sub> on mid-exponentially growing cells that were pre-adapted to darkness for 30 min to induce an equilibrium state for the photosynthetic electron transport. F<sub>v</sub>/F<sub>m</sub>, PSII efficiency (Psi<sub>II</sub>), non-photochemical quenching (NPQ), and the operational quantum yield (qL) was measured as previously described [22] using an FMS/2S Pulse-Amplitude-Modulated (PAM) chlorophyll fluorimeter (Hansatech Instruments, Ltd., Norfolk, England) and trace-conversion .xfm script. O<sub>2</sub> evolution and respiration were measured using an Oxy-Lab Clark-type electrode probe unit (Hansatech Instruments, Ltd., Norfolk, England) with sodium thiosulfate dissolved-O<sub>2</sub> calibration, stirrer speed set to 200 rpm, and temperature set to 28°C.

#### *3.3.4. Preparation of Effluent from Anaerobic Digestion of Food Waste*

Effluent was derived from processing of Washington State University (WSU) cafeteria food waste in a system comprised of a high-solids anaerobic digester with recycling seed (SADRS) for hydrolysis and an Up-Flow Anaerobic Sludge Blanket (UASB) reactor for methanogenesis [23]. To initially test if effluent alkalinity and salinity sufficiently prevented ammonia volatilization losses at high temperatures, the effluent was autoclaved for 25 min at 121°C and 100 kPa above atmospheric pressure and analyzed.

#### *3.3.5 Statistical Analysis*

Preliminary heterotrophic and phototrophic cultivation experiments were performed using

balanced duplicate replication, randomization, and negative-controls. Data were statistically analyzed by one-way analysis of variance (ANOVA) using statistical tables. Statistical significance was evaluated by estimation of the descriptive level (p), where results were considered statistically significant when  $p < 0.05$  ( $\alpha = 0.05$ , confidence level of 95%).

### **3.4. Results and Discussion**

#### *3.4.1. Microalgal Screening on Heterotrophic First-Stage Conditions*

ALP2 was observed during heterotrophic experiments to grow to final DCW of  $0.035 \pm 0.003$  g/L,  $0.351 \pm 0.013$  g/L,  $1.676 \pm 0.020$  g/L,  $3.910 \pm 0.042$  g/L, and  $4.687 \pm 0.179$  g/L, at glucose concentrations of 0, 1, 5, 10, and 20 g/L, respectively (Figure 3.1). Although the highest final DCW and proportionately highest cell density of  $6.29 \times 10^8$  cells/ml at 20 g/L was most optimal to inoculate a phototrophic second-stage, the highest yield (39.10%) from 10 g/L glucose was used instead for later experiments because it represented a more efficient use of the sugars. The pH increased from 7.00 to 8.69, 8.68, and 8.41 for cultures grown on BG-11 supplemented with 1, 5, and 10 g/L glucose, respectively, because of consumption of nitrate.

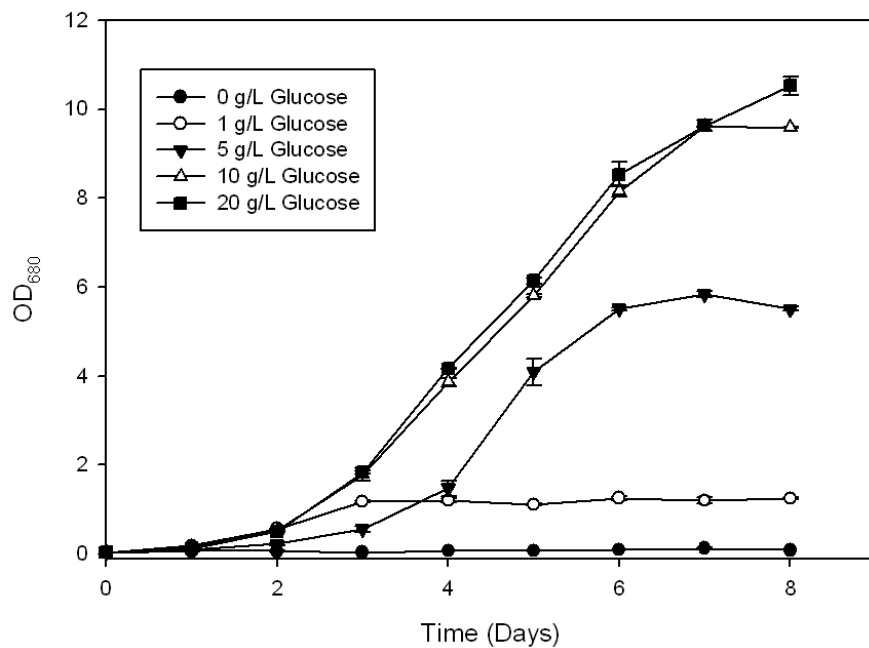


Figure 3.1.  $OD_{680}$  as function of time for ALP2 heterotrophically grown on BG-11 medium supplemented with 0, 1, 5, 10, and 20 g/L glucose at 21°C

Total lipid content and fatty-acid profile varied for ALP2 heterotrophic cultures previously grown on BG-11 medium supplemented with 10 g/L and 20 g/L glucose at 21°C. At 21°C and 10 g/L glucose, ALP2 grew to a higher final DCW of 4.208 g/L on 0.529 g/L urea than for  $NaNO_3$  (3.868 g/L on 1.500 g/L  $NaNO_3$ ) or anaerobically-digested food waste effluent (2.156 g/L on 22.0% (v/v) of the effluent) (Figure 3.2).

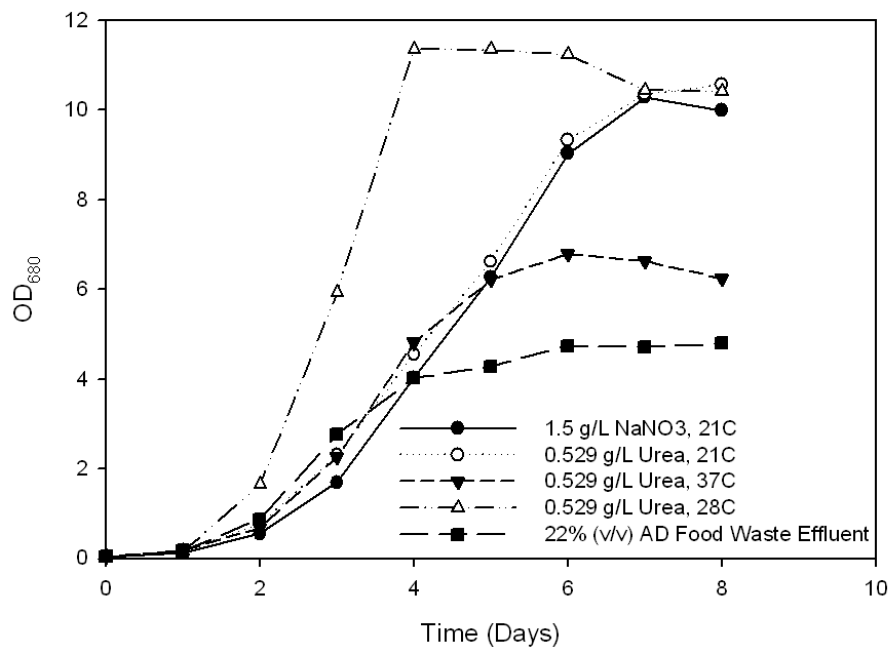


Figure 3.2. OD<sub>680</sub> as function of time for ALP2 heterotrophically grown on BG-11<sub>0</sub> medium supplemented with 10 g/L glucose and various nitrogen sources at different temperatures.

Effluent from waste represented a more cost-effective source of nitrogen and phosphates

However, the consumption of ammonia in the effluent led to a decrease in the pH to 3.77 and inhibited biomass yield even with some buffering alkalinity still present (Table 3.1). Also, when ALP2 was grown with 10 g/L glucose and 0.529 g/L urea at 28°C, the specific growth rate of 1.56 day<sup>-1</sup> and final DCW of 4.260 g/L were obtained, which were higher than that at 37°C or 21°C. This implies reduced operation time for heterotrophic cultivation used to inoculate a second-stage phototrophic culture. The highest DCW that ALP2 actually achieved at 28°C was actually 4.533

g/L in only 4 days, corresponding to a biomass yield of 45.33% and a cell density of  $6.78 \times 10^8$  cells/ml.

An increase in temperature had previously resulted in decreases in stearic, oleic, hexadecadienoic and linoleic free fatty acids even though total lipid content of ALP2 cultures grown at 28°C and 21°C were similar with that at 25.01% and 24.70%, respectively. This is consistent with findings that temperature influences biomass productivity, as well as membrane lipid free fatty acid profile, desaturation, and permeability.

Table 3.1. Anaerobically-digested food waste effluent properties

Effluent Component	Readings
<b>Pre-Autoclave</b>	
Alkalinity	7.04 g/L
Ammonia-N	0.89 g/L
Total-N	1.07 g/L
PO <sub>4</sub> <sup>3-</sup>	0.08 g/L
COD	6.64 g/L
pH	7.79
<b>Post-Autoclave</b>	
Alkalinity	5.90 g/L
Ammonia-N	0.66 g/L
pH	9.26

Final DCW for ALP2 grown on urea concentrations 0, 0.133, 0.265, 0.529, 1.058, 1.587, and 1.860 g/L were  $0.070 \pm 0.030$ ,  $1.909 \pm 0.115$ ,  $2.891 \pm 0.045$ ,  $3.149 \pm 0.075$ ,  $3.094 \pm 0.012$ ,  $3.200 \pm 0.068$ ,

and  $3.082 \pm 0.038$  g/L, respectively. These DCWs were relatively lower than those previously obtained because ALP2 in this series was cultivated in a relatively cool and dark room. Still, a minimal final DCW was reached at urea concentration of 0.133 g/L. The dissimilarities in final DCW for urea levels exceeding 0.133 g/L indicate that the C:N ratio influenced biomass yield ( $p < 0.001$ ). However, gains in final DCW at 1.587 g/L urea over that achieved at 0.529 g/L urea did not sufficiently justify the higher expenditure and risk of nitrogen-carryover into the next second phototrophic outdoor cultivation stage, where N-depletion conditions are desired for lipid productivity. Therefore, the optimal batch culture conditions for the first stage were determined to be heterotrophic growth on BG-11<sub>0</sub> medium, adjusted initially to pH 7 and supplemented with 10 g/L glucose and 0.529 g/L urea, at 28°C.

### *3.4.2. Microalgal Screening on Second-Stage Phototrophic Conditions*

#### *3.4.2.1. Effects of NaHCO<sub>3</sub> Levels and Nitrogen Sources on Biomass Productivity*

The final DCW of ALP2 achieved on 1.4, 7.0, 14.0, and 28.0 g/L NaHCO<sub>3</sub> without daily pH adjustment were  $0.697 \pm 0.005$ ,  $1.049 \pm 0.043$ ,  $0.991 \pm 0.031$ , and  $0.969 \pm 0.063$ , respectively (Figure 3.3). Growth limitation at 1.4 g/L NaHCO<sub>3</sub> may have resulted because relatively less NaHCO<sub>3</sub> inorganic carbon was initially supplemented and made available. Also, this may have occurred because relatively less buffering resulted in a fast photosynthetic increase of extra-cellular pH to levels that both limited the availability and uptake of HCO<sub>3</sub><sup>-</sup> due to bicarbonate-carbonate speciation and prevented maintenance of a suitable intra-cellular pH. Additional NaHCO<sub>3</sub>, even

beyond 7.0 g/L, did not result in a significant increase in final DCW when pH was left unadjusted.

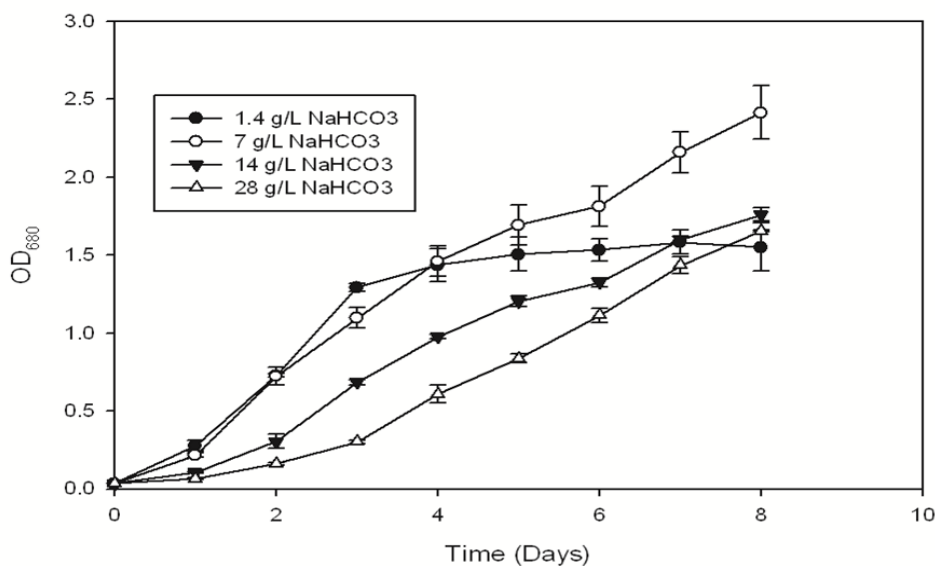


Figure 3.3. OD<sub>680</sub> as function of time for ALP2 phototrophically grown on BG-11 medium supplemented with 1.4, 7.0, 14.0, and 28.0 g/L NaHCO<sub>3</sub> levels with pH initially adjusted to 7 but subsequently left unadjusted

On an equivalent N-basis, ALP2 grew to a final DCW of  $1.220 \pm 0.068$  g/L on urea, slightly higher than  $0.840 \pm 0.054$  g/L on NaNO<sub>3</sub> and  $1.176 \pm 0.008$  g/L on the ammonia-containing 22.0% (v/v) anaerobically-digested food waste effluent with pH left unadjusted. Nitrogen source influenced final DCW ( $0.025 < p < 0.050$ ), and the pH increased to 10.89, 10.93, and 10.96 for cultures grown on effluent, urea, and nitrate, respectively, by the 2<sup>nd</sup> day. These growth performance results are consistent with reports of higher total biomass [24] and chlorophyll

content [6] on urea compared to  $\text{NaNO}_3$  in *Chlorella sp.* from Lithuanian lakes and *S. platensis*, respectively. They are also consistent with DNA microarray data suggesting that *Synechocystis* cells preferentially transport and assimilate ammonia, urea, and Arg under PSII light over nitrate [25].

At a concentration of 1.500 g/L,  $\text{NaNO}_3$  represents the most expensive and concentrated component of the traditional BG-11 medium, which is an inherently minimal formulation containing no vitamin B-12 thiamine or biotin. Although the market price of urea has historically been more volatile [26], it is generally lower than that of  $\text{NaNO}_3$  [6], which has significant implications regarding nutrient supply for large-scale open-ponds. Urea is also less metabolically expensive for microalgae in that either spontaneous hydrolysis to ammonia and potentially consumable  $\text{CO}_2$ , under alkaline conditions and/or a single urease-catalyzed step, is needed to convert it to more readily metabolized  $\text{NH}_4^+$  and  $\text{CO}_2$  [6]. This is in contrast to the 8 moles of reduced ferredoxin needed to convert 1 mol of nitrate to nitrite and then to  $\text{NH}_4^+$  by nitrate reductase and nitrite reductase, respectively [25].

This study also reports for the first time the use of anaerobically-digested food waste effluent as source of nitrogen and phosphates for phototrophic microalgal cultivation. With a light golden brown coloration, the food waste effluent optically allows greater phototrophic light penetration than the more turbid and common dairy manure effluents. The FAME-GC-based fatty-acid profile of a raw ALP2 cultured on the BG-11<sub>0</sub> medium supplemented with 7.0 g/L  $\text{NaHCO}_3$  and 22.0%

(v/v) anaerobically-digested food waste effluent is shown (Table 3.2). Interestingly, oleic, linoleic, and linolenic free fatty-acids comprised 52.47% of the total fatty acids. The high concentration of  $\omega$ -3 linolenic fatty acid in ALP2 approached levels found in flaxseed oil. In a culture grown phototrophically on BG-11<sub>0</sub> medium supplemented with 3.5 g/L NaHCO<sub>3</sub> and 0.035 g/L urea, HR-MAS probe <sup>1</sup>H NMR furthermore detected the presence of such  $\omega$ -3 compounds, as evidenced by a de-convoluted triplet methyl peak at 1.131 ppm (Figure 3.4). With such a favorable  $\omega$ -6/ $\omega$ -3 ratio of 1.17 and a poly-unsaturated fatty acid content representing 53.65% of the total, ALP2 biomass represents high potential nutrition for humans, livestock, or aquaculture. Conceivably, ALP2 biomass could be fed to nearby livestock whose manure waste is anaerobically-digested to generate biogas and effluent [27, 28], from which storable ammonium sulfate and phosphate salts are recovered via a patented nutrient recovery process [29].

Table 3.2. Fatty-acid profile of ALP2 phototrophically grown on BG-11<sub>0</sub> supplemented with 7.0 g/L NaHCO<sub>3</sub> and 22.0% (v/v) ADFW levels

<b>Fatty acid</b>	<b>Structure</b>	<b>Fatty Acid (%)</b>
Tetradecenoic	C14:1n3	2.29
Tetradecadienoic	C14:2n6	7.63
Palmitic	C16:0	15.95
Hexadecenoic	C16:1n9	2.75
Palmitoleic	C16:1n7	0.96
Hexadecadienoic	C16:2n6	7.22
Hexadecatrienoic	C16:3n3	3.67
Oleic	C18:1n9	9.71
Linoleic	C18:2n6	22.93
Linolenic	C18:3n3	19.83
<b>Fractions</b>		
Saturated		15.95
MUFA		23.34
PUFA		53.65
Total Fat		7.13
ω-3		25.79
ω-6		30.15
ω-6:3 Ratio		1.17
Identified		92.95
Unknown		7.05

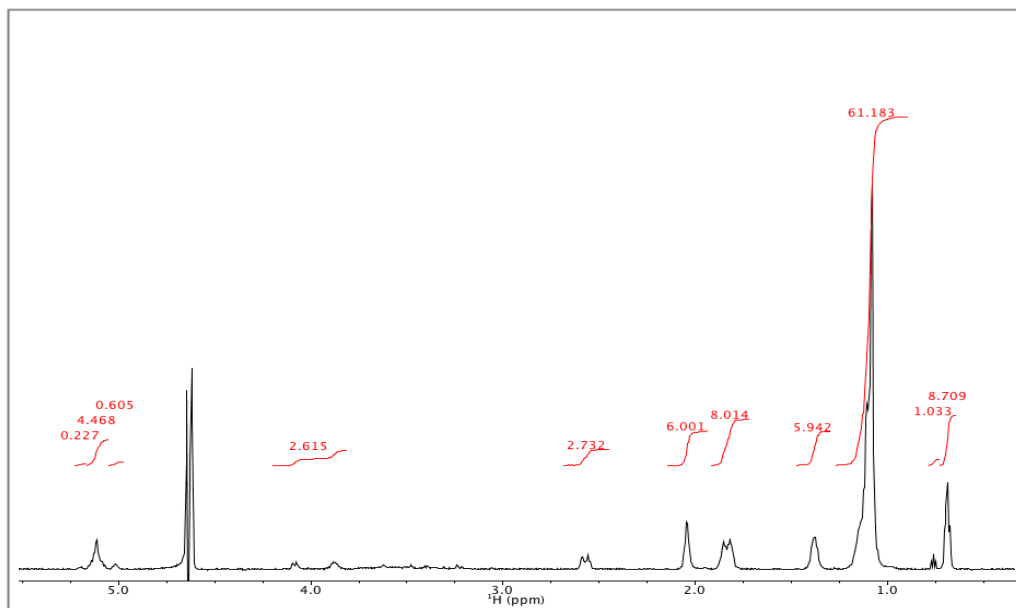


Figure 3.4. High-resolution magic angle-spinning (HR-MAS)  $^1\text{H}$  NMR spectra of raw ALP2 culture phototrophically grown on BG-11<sub>0</sub> supplemented with 3.5 g/L  $\text{NaHCO}_3$  and 0.133 g/L urea at HCl-adjusted pH 9. Red integral values shown over respective peaks

Although the aforementioned benefits of using more cost-effective ammonia-containing effluents and urea nitrogen sources are clear, ammonia that is either inherently found in effluent, or results from urea degradation, at the proposed highly alkaline conditions of the second-stage open-pond cultivation, could volatilize and cause economic losses of nitrogen and pollution [30]. In this study, the sorbent properties [31] of ALP2 microalgae during cultivation, high  $\text{NaHCO}_3$ -mediated ionic strength [32], or unfiltered solutes that contributed to light coloration may have prevented total loss of ammonia during autoclaving (Table 3.1). An initial and final effluent total nitrogen volatilization rate of  $16.15 \text{ mg L}^{-1} \text{ day}^{-1}$  and  $3.66 \text{ mg L}^{-1} \text{ day}^{-1}$  were

measured. A relatively low overall equivalent  $O_2$ -mass transfer coefficient of  $24 \text{ hr}^{-1}$  was also previously estimated for similarly foam-capped 0.25 L shaker flasks [33].

Ammonia loss during hot summers would, however, likely be higher in the proposed larger-scale open-ponds with higher surface areas, temperatures, pH, and wind-speeds. High concentrations of protonated ammonia were also reportedly more toxic to the PSII photosynthetic apparatus of phototrophs at high pH, where uncontrollable, diffusive, non-active transport across the cell boundary occurs [34]. Therefore, a future urea (or effluent) fed-batch strategy at high pH in the proposed second stage culture should be developed with an exponentially increasing mass flow [6]. This would need to balance (1) the rate of urea (or effluent) supplementation required for both sufficient growth and terminal nitrogen starvation-induced lipid accumulation, with (2) the rate of ALP2 urea (or ammonia) consumption and (3) the rate of high pH-induced volatilization.

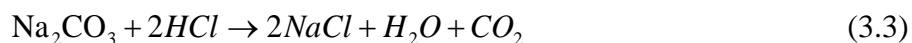
#### *3.4.2.2. Effects of Nitrogen and pH Levels and pH-Adjusting Acids on Biomass Productivity*

Using urea as the more available and better-performing nitrogen source, and dosing with 7.0 g/L  $\text{NaHCO}_3$ , ALP2 grew to final DCW of  $0.136 \pm 0.000$ ,  $0.910 \pm 0.002$ ,  $0.858 \pm 0.046$ ,  $0.980 \pm 0.044$ ,  $0.984 \pm 0.008$ ,  $1.076 \pm 0.064$ , and  $0.972 \pm 0.072$  g/L on 0, 0.133, 0.265, 0.529, 1.058, 1.587, 3.070 g/L urea, respectively, when the pH was left unadjusted. The final DCW increased to 1.216, 1.348, 1.304, and 1.380 g/L for 0.529, 1.058, 1.587, 3.070 g/L urea levels, respectively, when pH was adjusted daily to 9 with HCl acid. With daily glacial acetic acid pH adjustment, the final DCW slightly increased further to 1.220, 1.804, and 1.364 g/L for the 0.529, 1.058, and 1.587

g/L urea levels, respectively. At the 1.058 g/L urea level, growth enhancement with HCl acid-mediated pH control was also observed at higher pH, as DCW of 1.066, 1.031, 1.022, and 0.854 g/L were obtained at pH 7, 8, 9, and 10 when pH was unadjusted and 1.108, 1.520, 1.723, and 1.200 g/L at pH 7, 8, 9, and 10 when pH was adjusted with HCl, respectively. A premature stationary phase that resulted from a photosynthetic-increase in pH from 7.00 to 11.39 within 3 days, was prevented by daily control of pH. ALP2 growth was inhibited at pH 11 and only reached final DCW of 0.156 g/L with pH unadjusted. These results further established ALP2's alkaline-tolerance since it grew best at pH 9 adjusted daily with HCl acid.

Such enhancement of biomass productivity via HCl acid-mediated pH control may be attributed to increased bio-availability of the bicarbonate as the predominant inorganic carbon species, as well as maintenance of an intracellular pH at a lower, albeit highly alkaline, extracellular pH. Based on liquid-phase inorganic carbon equilibria, dissolved CO<sub>2</sub> dominates when pH < 5, bicarbonate dominates when 7 < pH < 9, and carbonate (which cannot itself be consumed by ALP2 microalgae) dominates when pH > 9. Bicarbonate can gain a proton to become carbonic acid or lose a proton to become carbonate. The bicarbonate-carbonic acid pK<sub>a</sub> is 6.30, and the bicarbonate-carbonate pK<sub>a</sub> is 10.25 at 25°C. Disregarding other complex factors influencing water chemistry, pH should therefore be periodically adjusted to a level sufficiently high for limiting contamination [18] and stressing cells [35], but low enough where bicarbonate is in the long-term the predominant inorganic carbon available for growth and lipid accumulation.

This can be achieved by adding a neutralizing HCl acid below the liquid surface. In the short-term, this could theoretically also generate a swarm of small, high-surface area CO<sub>2</sub> bubbles to rapidly dissolve with a high K<sub>L</sub>a mass transfer coefficient for microalgal uptake via the following reaction:



These aforementioned benefits to productivity arising from HCl-mediated pH adjustment should be considered in the context of open-pond mass cultivation where other potential issues must be considered.

When cultivating open-pond microalgae on such proposed bicarbonate inorganic carbon source, the high starting pH is expected to photosynthetically increase, and it may therefore be necessary to periodically lower the pH via addition of an acid like HCl to neutralize the base and make the bicarbonate available for uptake. However, introducing high levels of Cl<sup>-</sup> ions via HCl-mediated pH control may reduce microalgal tolerance to the outdoor freezing temperatures of wintry nights in a Midwest or Pacific Northwest location where year-round photosynthetic biorefinery operations are desired. Cl<sup>-</sup> ions, rather than Na<sup>+</sup> cations, that suddenly permeabilize the outer and thylakoidal membrane during freezes, were shown to specifically damage chloroplasts and PSII activity of a cold and salt tolerant *Dunaliella* microalgae from Antarctica in absence of protective extra-cellular glycerol. This occurred regardless of membrane fatty-acid desaturation and chain-lengthening during cold adaptation and intra-cellular accumulation of osmo-regulating

glycerol during correlated salt-adaptation. Cold adaptation was itself reportedly hindered by high salinity and high light intensity. Waste crude glycerol from lipid trans-esterification can therefore potentially be used as both cost-effective anti-freeze during cold-winters and additional organic carbon source for outdoor open-pond cultures of growing at the evidently-tolerable high salinity and high pH conditions. This salty anti-freeze can be supplemented at night to the outdoor 2<sup>nd</sup> cultivation stage when temperatures are at their lowest, particularly in the Pacific Northwest after fall seasonal wheat harvests, and when dark heterotrophic consumption is not possible as results here indicate. At daybreak when solar light intensity and temperatures begin to increase, could then consume this glycerol mixotrophically before bacterial contamination sets in. Alternatively, the acetic acid from torrefaction condensate could theoretically be supplemented to late, mature, open-pond cultures to adjust pH and provide additional metabolic pre-cursors to the Acyl-CoA lipid metabolism of microalgae. Acetic acid supplementation has previously been demonstrated to adjust for constant pH and boost lipid productivity.

*3.4.2.3. Effects of NaHCO<sub>3</sub> Levels, HCl-mediated pH Adjustment, and Diurnal Light Intensity on Biomass and Lipid Productivity, Nitrogen and NaHCO<sub>3</sub> Uptake, Cellular Replication and Dimensions*

Data are shown for a four-flask experiment where ALP2 was grown on diurnal light cycle on 1.4 and 17.0 g/L NaHCO<sub>3</sub> with pH either left unadjusted or adjusted daily to pH 9 (Figures 3.5). During the initial 44 hrs, with urea nitrogen still available in the growth medium,

biomass-correlated OD<sub>680</sub> increased. But neither the cell density, nor the <sup>1</sup>H NMR-based neutral lipid content increased. Also, high and nearly equivalent inorganic carbon uptake and/or neutralization rates of 25.18 and 24.80 mg<sup>-1</sup> C L<sup>-1</sup> hr<sup>-1</sup> were estimated during this initial 0-44 hrs period for 17.0 g/L NaHCO<sub>3</sub>, adjusted and unadjusted pH conditions, respectively. This and the uniformly negligible <sup>1</sup>H NMR-based lipid content at 18 hrs suggests that cells were early on potentially increasing in size by accumulating intra-cellular starch reserves before dividing. Average cell size was difficult to quantify visually with microscope, and flow cytometric forward light scatter plots of fixed cell samples could better confirm this as was done for the later factorial experiment. The pH also decreased during dark incubation of the diurnal cycle, and this decrease was most prominent at 1.4 g/L NaHCO<sub>3</sub> concentration compared to the more buffered 17.0 g/L level. The less buffered pH at 1.4 g/L NaHCO<sub>3</sub> quickly increased to pH 11.94 from photosynthetic consumption of bicarbonate after 44 hrs.

Between 44-116 hrs, all cultures increased in both OD<sub>680</sub> and cell density, suggesting an ability to replicate, even at high NaHCO<sub>3</sub> and high pH levels. As previously stated [9], this implies that the provision of acidifying CO<sub>2</sub> for growth of an open-pond culture prior to stress-induced lipid accumulation may not be necessary for this particular strain. Cultures initially supplemented with 1.4 and 17.0 g/L NaHCO<sub>3</sub> with daily-adjusted pH 9 had specific growth rates during 44-116 hrs of 0.015 hr<sup>-1</sup> and 0.021 hr<sup>-1</sup>, respectively, that exceeded those of 0.009 hr<sup>-1</sup> and 0.005 hr<sup>-1</sup>, respectively, when pH was left unadjusted. The specific growth rate at 17.0 g/L NaHCO<sub>3</sub> with pH

adjusted exceeded that with unadjusted pH by a factor of 4.20. Similarly, the inorganic carbon uptake and/or neutralization rate during 44-116 hrs of  $8.99 \text{ mg}^{-1} \text{ C L}^{-1} \text{ hr}^{-1}$  for the 17.0 g/L  $\text{NaHCO}_3$ , adjusted pH condition exceeded the  $2.82 \text{ mg}^{-1} \text{ C L}^{-1} \text{ hr}^{-1}$  rate for the 17.0 g/L  $\text{NaHCO}_3$ , unadjusted pH condition by a factor of 3.19. Inorganic carbon for the 1.4 g/L  $\text{NaHCO}_3$ , pH adjusted condition appeared nearly depleted, yet cell density and  $\text{OD}_{680}$  continued to increase. Higher initial urea nitrogen uptake rates at 17.0 g/L  $\text{NaHCO}_3$  conditions also resulted in relatively less available nitrogen than at 1.4 g/L  $\text{NaHCO}_3$  conditions. The nitrogen-uptake rate during 0-140 hrs was  $0.94 \text{ mg L}^{-1} \text{ hr}^{-1}$  and higher than the  $0.66 \text{ mg L}^{-1} \text{ hr}^{-1}$  at the lower 1.4 g/L  $\text{NaHCO}_3$  with pH left unadjusted. These observations suggested that higher  $\text{NaHCO}_3$  levels resulted in higher nitrogen uptake rates and that pH adjustment resulted in higher inorganic carbon uptake.

At 116 hrs,  $\text{OD}_{680}$  for the 17.0 g/L  $\text{NaHCO}_3$ , daily-adjusted pH 9 condition was 47.09% higher than that for 1.4 g/L  $\text{NaHCO}_3$ , daily-adjusted pH 9 condition. Microscopic observation revealed that percentage of “doublet cells” in cell division abeyance were 3.39 % and 7.89 % for the 1.4 g/L and 17.0 g/L  $\text{NaHCO}_3$ , adjusted pH 9 conditions, respectively, and 7.22 %, and 26.55 % for the 1.4 g/L and 17.0 g/L  $\text{NaHCO}_3$ , unadjusted pH conditions, respectively. Combined high pH and high  $\text{NaHCO}_3$  levels appeared to arrest cellular division for a greater proportion of cells, yet overall cell density continued to slightly increase beyond this point. Stagnation of cell density and a cessation of cellular replication occurred for the 1.4 g/L  $\text{NaHCO}_3$ , unadjusted pH condition still having sufficient nitrogen and inorganic carbon for growth. One possible explanation for this is

that virtually unbuffered pH was allowed to photosynthetically increase from bicarbonate consumption to an extremely high level of 11.93 where bicarbonate-carbonate speciation favored useless carbonate as primary inorganic carbon source.

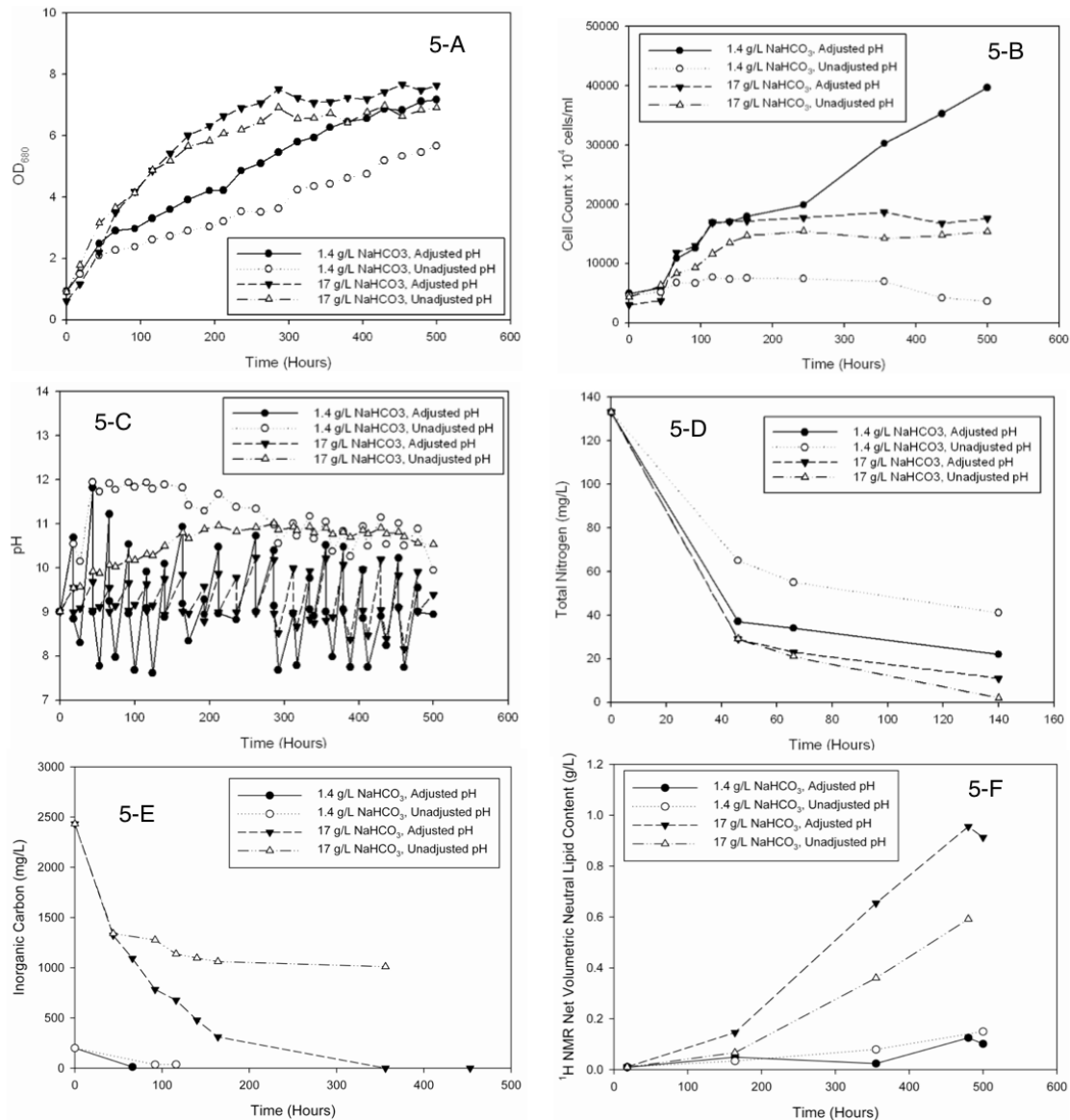


Figure 3.5. (A) OD<sub>680</sub>, (B) cell density, (C) pH, (D) total nitrogen remaining in medium, (E) total inorganic carbon remaining in medium, and (F) net <sup>1</sup>H NMR-based neutral lipid concentration as function of time for ALP2 cultures phototrophically grown in a diurnal light cycle on BG-11<sub>0</sub> supplemented with 0.133 g/L urea and either 1.4 or 17.0 g/L NaHCO<sub>3</sub>, with pH either left unadjusted or adjusted to 9

Between 140-164 hrs, total inorganic carbon still remained in supernatants of cultures at 17.0 g/L NaHCO<sub>3</sub>. This is despite cumulative microalgal uptake of the supplemented HCO<sub>3</sub><sup>-</sup>, which appeared to level off for the unadjusted pH condition, and periodic HCl-mediated neutralization for pH 9 adjustment. However, urea nitrogen in the supernatant was nearly depleted for these cultures at 140 hrs. Stagnation of cell density and cessation of cellular replication for this time likely resulted from a combination of full depletion of extra-cellular and intra-cellular nitrogen and high-pH stress. That this culture stagnated later compared to the culture at the 1.4 g/L NaHCO<sub>3</sub> unadjusted pH condition suggests the initial-supplemented NaHCO<sub>3</sub> level of 17.0 g/L was a stronger buffer and prevented even higher inhibitory pH and stress from being reached. Cellular replication notably ceased at these 17.0 g/L NaHCO<sub>3</sub> conditions even when OD<sub>680</sub> increased and inorganic carbon decreased, indicative of bicarbonate incorporation for neutral lipid accumulation.

At 164 hrs, the net <sup>1</sup>H NMR-based volumetric neutral lipid concentration were all higher for cultures with adjusted pH compared to unadjusted pH. The highest lipid content at 17.0 g/L NaHCO<sub>3</sub>, daily-adjusted pH 9 condition was also almost 3 times that for 1.4 g/L NaHCO<sub>3</sub>, daily adjusted pH 9. Therefore, higher supplemented inorganic bicarbonate levels, higher inorganic carbon uptake and/or neutralization rate, lower cellular replication due to N-starvation, and a pH adjusted to levels permitting inorganic bicarbonate uptake, may have all contributed to increased ALP2 cell size (confirmed flow cytometrically in Section 3.4.2.5), OD<sub>680</sub>, and neutral lipid accumulation from incorporated bicarbonate.

At 356 hrs, the 1.4 g/L NaHCO<sub>3</sub>, daily-adjusted pH 9 condition survived as the only one where cell density increased. Nitrogen was likely still available, and daily maintenance of pH 9 likely still permitted bicarbonate uptake under this condition to enable this growth. However, the initial precipitous decrease and final lack of detection of inorganic carbon in the supernatant at this 1.4 g/L NaHCO<sub>3</sub> condition indicates that another carbon source was responsible for increasing cell density. Three possible sources of such carbon are:

First, organic carbon from complex starches and other polysaccharides released into the supernatant during cell lysis and subsequently hydrolyzed to simpler sugars may have enabled mixotrophic growth and cellular replication. This culture, like the others, was never supplemented with organic carbon. However, the factorial experiment that follows in Section 3.4.2.5 confirmed the presence of 0.071 g/L of unidentified organic carbon in the supernatant of a similar culture. <sup>1</sup>H NMR spectra for supernatants at 356 hrs also revealed some lipids and starches leaked, which may have been caused by wide pH fluctuations and cell lysis during daily pH adjustment. Subsequent flocculation of lysed cells could potentially explain some long-term settling in NMR capillary tubes and a few “grape-like” clusters of cells and debris that were microscopically observed to interfere with haemocytometric cell enumeration. These may have in turn resulted from the shielding of otherwise repulsive negatively-charged microalgae by the intra-cellular polysaccharides released into the supernatant. However, cell debris was most evident in the cultures where pH was left unadjusted, and very little was observed at the 1.4 g/L NaHCO<sub>3</sub>

condition where pH was adjusted. Nevertheless, cell lysis and attraction of contaminants to large-scale open-pond cultures due to any leaked organic carbon could be prevented by adjusting pH to 9 throughout the majority of the culture run and only allowing pH to increase to extreme 11-12 levels at the end when harvesting via auto-flocculation.

Second, CO<sub>2</sub> resulting from intra-cellular hydrolysis of urea may have supplied the carbon necessary for cellular replication at the initially-supplemented 1.4 g/L NaHCO<sub>3</sub> condition. The relatively low buffer capacity of 1.4 g/L NaHCO<sub>3</sub> permitted the pH to fluctuate, reaching levels of 11.82 in some cases, before being re-adjusted daily to 9. These attained high extra-cellular pH levels may have resulted in high intra-cellular pH levels which, in conjunction with the urease enzyme activity, catalyzed the hydrolysis of incorporated urea to ammonia and CO<sub>2</sub> for photosynthesis. Thus, urea may have served both as a nitrogen and inorganic carbon source at these extreme conditions.

Third, the most likely carbon source enabling continued cellular replication and growth at 1.4 g/L NaHCO<sub>3</sub> with pH daily-adjusted was ambient CO<sub>2</sub> in the air that dissolved into the medium. CO<sub>2</sub> mass transfer rates were enhanced by the high pH of the medium and the high-velocity agitation, enough to overcome the bulk resistance of the foam plug of the flask which was periodically removed during daily pH adjustment.

At 286 hrs, the OD<sub>680</sub> of both the non-replicating 17.0 g/L NaHCO<sub>3</sub> adjusted and unadjusted pH flasks also finally stopped increasing. At 356 hrs, the net <sup>1</sup>H NMR neutral lipid concentration

achieved for the 17.0 g/L NaHCO<sub>3</sub>, daily-adjusted pH 9 culture condition was also almost 27 times that for 1.4 g/L NaHCO<sub>3</sub>, daily adjusted pH 9 but only 1.8 times that of the 17.0 g/L NaHCO<sub>3</sub> unadjusted pH culture condition. This suggests that NaHCO<sub>3</sub> levels influenced lipid accumulation more than pH level. At 480 hrs, net neutral lipid concentration of the 17.0 g/L NaHCO<sub>3</sub>, adjusted pH condition had reached a very high 0.955 g/L.

During the subsequent extended dark incubation between 480-500 hrs, net neutral lipid concentration decreased in the culture conditions involving 1.4 g/L NaHCO<sub>3</sub> and 17.0 g/L NaHCO<sub>3</sub>, with pH adjusted, by 19.02 % and 4.47%, respectively. As previously reported [36], this illustrates that respiratory pathways had catabolized accumulated lipid. The final DCW obtained for all cultures obtained were 1.773 g/L and 1.966 g/L for 1.4 g/L NaHCO<sub>3</sub> with pH adjusted and unadjusted, respectively, and 3.174 g/L and 2.691 g/L for 17.0 g/L NaHCO<sub>3</sub> with pH adjusted and unadjusted, respectively. Thus, the final lipid content achieved by the 17.0 g/L NaHCO<sub>3</sub> with pH adjusted culture was approximately 28.67 % DCW at a volumetric productivity rate of 0.044 g L<sup>-1</sup> day<sup>-1</sup>.

In summary, the results from this particular four-flask experiment showed that higher initially-supplemented NaHCO<sub>3</sub> concentration led to relatively higher OD<sub>680</sub>, DCW, neutral lipid content, and urea nitrogen uptake rate than at lower NaHCO<sub>3</sub> levels. Higher unadjusted pH also led to relatively lower cell count and replication, lower specific growth rates, and ultimately higher rates of cell lysis and death, than at the lower adjusted pH 9. Higher unadjusted pH only resulted in

proportionately higher neutral lipid content at low NaHCO<sub>3</sub> levels. The observation that ALP2 was able to divide under both low 1.4 g/L and high 17.0 g/L levels of NaHCO<sub>3</sub> agrees with the reported replication of the diatom *Phaedodactylum tricornutum* under 50 mM or 4.2 g/L NaHCO<sub>3</sub> alkaline conditions [36]. This again has serious implications with regards to there being no need to supply and bubble in CO<sub>2</sub> gas to large-scale open-pond cultures for initial growth. A unique uptake mechanism and metabolism, such as C<sub>4</sub>-photosynthesis, was previously postulated to explain why no replication in high NaHCO<sub>3</sub> or salinity was witnessed in other C<sub>3</sub>-photosynthesizing microalgae, like *Scenedesmus sp.*, *Chlamydomonas reinhardtii*, or *Chlorococcus sp.* [32, 33].

#### 3.4.2.4. Effects of NaHCO<sub>3</sub> and pH Levels on Net Photosynthesis and Photosystem Excitation

Photosynthesis experiments revealed the short-term effects of pH and NaHCO<sub>3</sub> levels on ALP2's PSII/PSI fluorescence ratio and O<sub>2</sub>-evolution and respiration. Based on a fixed chlorophyll content of 9.11 µg/ml for samples, ALP2's maximum net photosynthetic rate of 0.045 µmoles O<sub>2</sub> ml<sup>-1</sup> min<sup>-1</sup> at 25.2 g/L NaHCO<sub>3</sub> was higher than at 8.4 g/L (Figure 3.6). This maximum also occurred at an alkaline pH of approximately pH 8.50-9.00 that coincided with the measured pH 8.61 of Alkali Lake water from which ALP2 was originally isolated [9]. This response was consistent with that of the haloalkaline-tolerant microalgae previously isolated from Lake Magadi, Kenya [37].

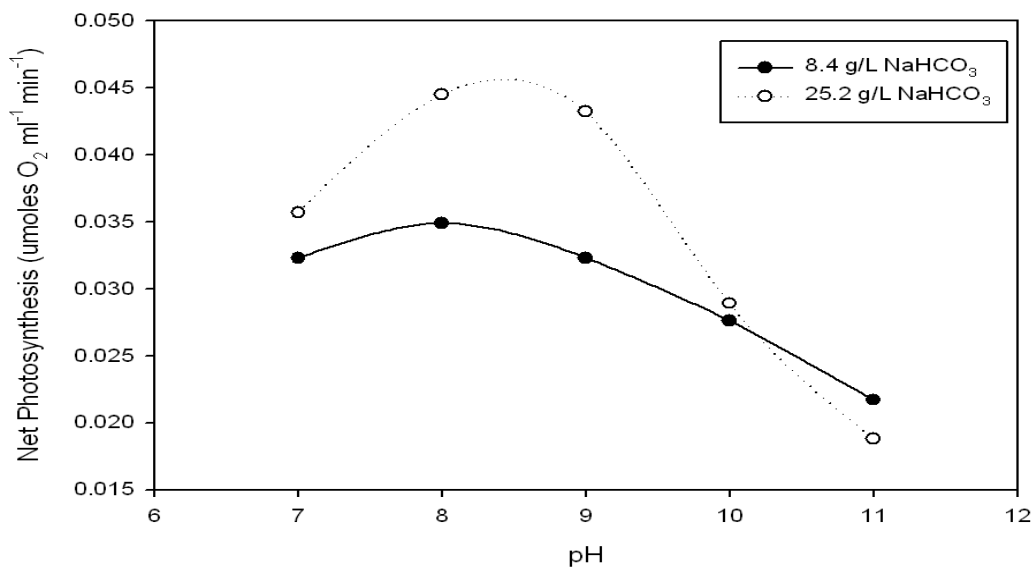


Figure 3.6. ALP2 net photosynthesis as function of pH and NaHCO<sub>3</sub> level

Upon transferring mid-exponentially growing ALP2 from 0.84 g/L to 33.64 g/L NaHCO<sub>3</sub>, low-temperature 77K chlorophyll fluorescence spectra (excitation at 435 nm) revealed a transient change in PSII emission (peaking at 685 nm, F685) to PSI emission (peaking around 720 nm, F720) ratio that initially decreased from 0.523 to 0.392 after 2 min, but then increased up to 0.538 and 0.740 after 15 and 60 min, respectively (Figure 3.7)

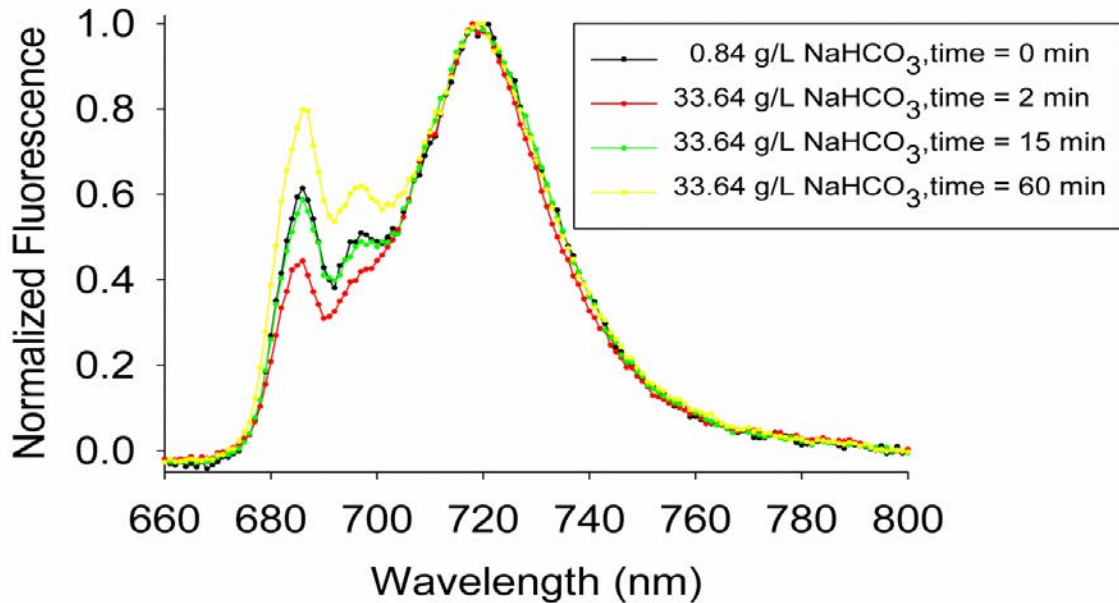


Figure 3.7. Normalized 77K-435 nm excitation wavelength as function of emittance for ALP2 transitioned from 0.84 to 33.64 g/L NaHCO<sub>3</sub>

Such initially-observed decrease in F685/F700 upon a step change to 33.64 g/L NaHCO<sub>3</sub> after only 2 min suggests a state 1 to state 2 transition (i.e. an increase in the PSI antenna size relative to PSII antenna size) via reversible post-translational protein phosphorylation. There is good evidence that in green algae state 2 represents an adaptive enhancement of cyclic electron transport around PSI, leading to higher ATP production [38]. As observed in *Spirulina sp.*[6], this ATP would power active transporters and regulate intra-cellular pH, salinity, and osmolarity once confronted with high pH and extremely high salinity from 33.64 g/L NaHCO<sub>3</sub>. Increased production of the osmo-regulant glycerol and glycine betaine for related reasons have also been

reported elsewhere [39]. The observed dynamic re-arrangement of ALP2's to state 2 mirrors that previously observed in high CO<sub>2</sub>-tolerant microalgae *Chlorococcum littorale* upon transfer from air to more acidifying 40% CO<sub>2</sub>, where PSII/PSI ratio initially decreased but eventually increased back as PSII function recovered [3]. This also agrees with the observed initial stimulation of the F<sub>v</sub>/F<sub>m</sub> ratio (optimal Psi<sub>II</sub> efficiency) in the cyanobacterium *Mycrocystis aeruginosa* after it was transferred from HCO<sub>3</sub><sup>-</sup> concentrations of 0.6 mM to 2.3 mM and 12.4 mM [4]. With all things considered, the maximal net photosynthesis at relatively high pH and NaHCO<sub>3</sub> levels, as well as the observed state transitions occurring upon a step-change in NaHCO<sub>3</sub>, suggest that ALP2 is well-adapted to extreme halo-alkaline culture conditions.

#### *3.4.2.5 Interplay of NaHCO<sub>3</sub>, pH, Nitrogen Levels and pH-Adjusting Acids on Lipid and Biomass Productivity and Photosynthetic Parameters*

The results of a factorial experiment done to evaluate the effects of simultaneous treatment of NaHCO<sub>3</sub>, urea, and acid-adjusted pH levels is summarized (Table 3.3). Regarding the effect of initial NaHCO<sub>3</sub> level, at a HCl-acid adjusted pH 9 and low 0.133 g/L urea level, ALP2 final DCW, <sup>1</sup>H NMR-based neutral lipid concentration and productivity after 13 days of cultivation increased with increasing NaHCO<sub>3</sub> (up to 17.0 g/L NaHCO<sub>3</sub>) to a maximum of 2.528 g/L, 1.009 g/L, and 0.078 g L<sup>-1</sup> day<sup>-1</sup>, respectively (Table 3.3). Beyond 17.0 g/L NaHCO<sub>3</sub>, these values decreased. Therefore, the optimal phototrophic second-stage conditions were found to be BG-11<sub>0</sub> medium supplemented with 17.0 g/L NaHCO<sub>3</sub> and 0.133 g/L urea, at a HCl-adjusted pH 9. The

highest DCW yields and percent lipid in dry biomass (42.78%-44.01%) occurred at very high 17-42 g/L NaHCO<sub>3</sub> concentrations (Table 3.3).

Table 3.3. Performance of ALP2 phototrophically cultivated on BG-11<sub>0</sub> supplemented with various NaHCO<sub>3</sub> levels, either 0.133 g/L or 0.529 g/L urea, and at HCl-mediated pH 9

NaHCO <sub>3</sub> (g/L)	0.133 g/L Urea				0.529 g/L Urea			
	Final DCW (g/L)	TAG (g/L)	Fat %	Lipid Productivity (g L <sup>-1</sup> day <sup>-1</sup> )	Final DCW (g/L)	TAG (g/L)	Fat %	Lipid Productivity (g L <sup>-1</sup> day <sup>-1</sup> )
0.7	1.114	0.050	4.48	0.004	1.296	0.018	1.39	0.001
1.4	1.232	0.044	3.60	0.003	1.478	0.016	1.10	0.001
3.5	1.848	0.277	15.01	0.021	2.030	0.045	2.21	0.003
10.0	2.260	0.776	34.34	0.060	2.612	0.123	4.71	0.009
17.0	2.528	1.009	39.92	0.078	2.252	0.186	8.25	0.014
25.0	2.502	0.962	38.44	0.074	2.186	0.298	13.65	0.023
42.0	1.166	0.513	44.01	0.039	1.368	0.160	11.70	0.012
63.0	0.600	0.257	42.78	0.020	0.718	0.051	7.05	0.004
84.0	0.182	0.022	12.32	0.002	0.145	0.011	7.77	0.001

At higher urea levels (i.e. 0.529 g/L), volumetric neutral lipid concentrations also increased with increasing NaHCO<sub>3</sub> levels, but to a relatively lower maximum of 0.298 g/L corresponding to an initially supplemented 25.0 g/L NaHCO<sub>3</sub>. Figure 3.8 shows an exemplary static <sup>1</sup>H NMR spectrum of an aliquot of ALP2 culture, showing the integrated peaks used for all volumetric neutral lipid determinations. These results support a previous observation of enhancement of lipid accumulation upon a step-change in NaHCO<sub>3</sub> at high pH during N-starvation conditions [37]. Bicarbonate levels above 25 g/L may be too saline for ALP2 to tolerate, and those below 17.0 g/L

may have provided insufficient amounts of inorganic carbon for robust growth and neutral lipid accumulation of ALP2.

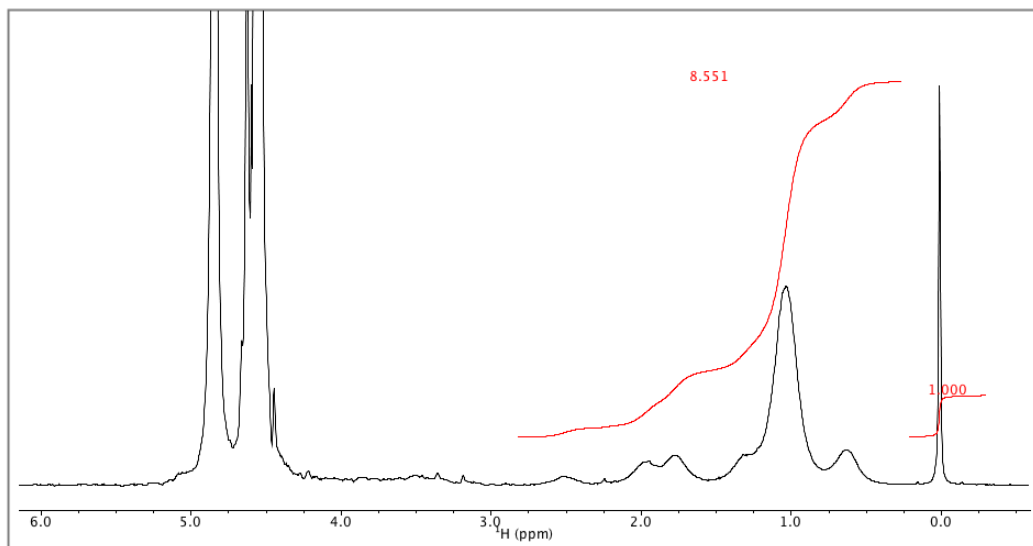


Figure 3.8. Liquid-state static  $^1\text{H}$  NMR spectra of raw ALP2 culture phototrophically grown on BG-11<sub>0</sub> supplemented with 10.0 g/L  $\text{NaHCO}_3$  and 0.133 g/L urea at HCl-adjusted pH 9. Blue integral values shown below respective peaks

The FSC vs. SSC and histogram flow-cytometric plots (Figure 3.9) of late culture samples from the factorial experiment for conditions at low 1.4 g/L and high 17 g/L  $\text{NaHCO}_3$  levels showed that the mean cell size, as designated by FSC axis, and cellular granularity, as designated by SSC axis, increased with increasing  $\text{NaHCO}_3$ . As ALP2 accumulated more neutral lipids at high  $\text{NaHCO}_3$  inorganic carbon levels and high pH under N-starvation conditions, the cell diameter and number of lipid bodies or vacuolar organelles present increased. At extremely high

(e.g. 42.0 g/L and 63.0 g/L)  $\text{NaHCO}_3$  concentrations, the FSC vs. SSC scatter plots were marked by a broader size distribution and tailings. This was likely a result of some cells lysing to create small debris in the extremely high salinity conditions. Detection of a relatively high organic carbon content in the supernatant of similarly treated cultures also supports this interpretation.

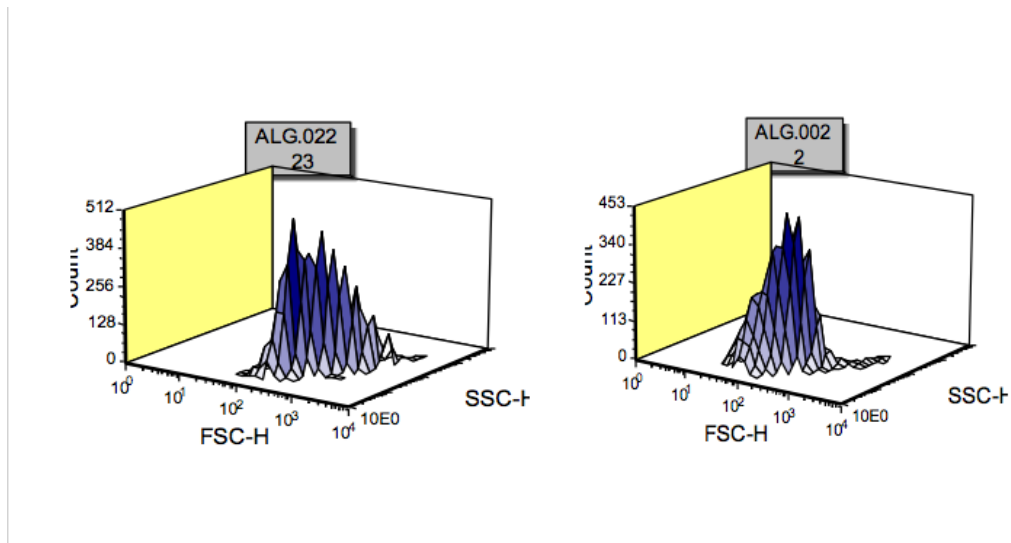


Figure 3.9. Three-Dimensional flow-cytometric plots depicting histogram (vertical axis), cellular size (FSC axis), and granularity (SSC axis) for ALP2 phototrophically grown on BG-11<sub>0</sub> medium supplemented with 0.133 g/L urea and either (Left) 1.4 g/L or (Right) 17.0 g/L  $\text{NaHCO}_3$  levels at HCl-adjusted pH 9

The long-term effects of initially supplemented  $\text{NaHCO}_3$  level on photosynthetic parameters NPQ,  $F_v/F_m$ ,  $q_L$ ,  $\text{Psi}_{II}$ , total carotenoid and chlorophyll, and chlorophyll a/b and carotenoid/chlorophyll ratios during the factorial experiment are also presented. Under pH 9 and 0.529 g/L urea conditions, ALP2 halalkaline-tolerance is evident in that impairment of PSII

activity (as measured by  $F_v/F_m$ ) and efficiency of linear electron flux between PSII and PSI (as measured by  $\Psi_{II}$ ) did not occur until relatively high  $\text{NaHCO}_3$  levels were reached (Figure 3.10).  $\Psi_{II}$  and  $F_v/F_m$  (maximal photochemical yield of PSII) were relatively constant until 25.0 g/L and 63.0 g/L  $\text{NaHCO}_3$ , respectively, beyond which they decreased with increasing  $\text{NaHCO}_3$  levels (Figure 3.10).  $q_L$  increased up to 10 g/L  $\text{NaHCO}_3$ , and its gradual downward trend beyond 10.0 g/L  $\text{NaHCO}_3$  suggests an increase in reduction level of the primary quinone acceptor of PSII, plastoquinone (PQ), between PSII and PSI due to increasing impairment of PSII-PSI linear electron flow beyond relatively high levels of  $\text{NaHCO}_3$ .

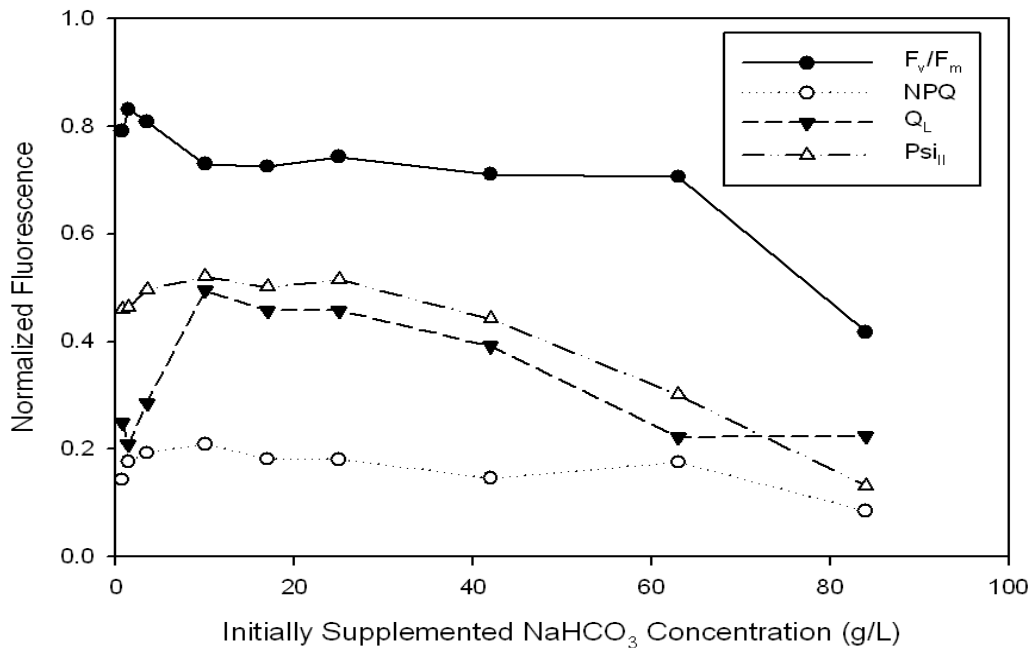


Figure 3.10. Chlorophyll fluorescence-based photosynthetic parameters of phototrophically grown ALP2 as function of NaHCO<sub>3</sub> levels initially supplemented to BG-11<sub>0</sub> medium, along with 0.529 g/L urea, at HCl-adjusted pH 9

The growth light intensity of 45  $\mu\text{mole m}^{-2} \text{s}^{-1}$  was likely not high enough to cause photo-oxidative damage or induce protective quenching and expression of the LHCsr3 protein [40], indicated by a relatively constant and low NPQ for a wide range of high NaHCO<sub>3</sub> levels. This differs from the previously observed increase in NPQ with salinity at high light in *Chlorococcum* sp. green algae [41]. Based on O<sub>2</sub>-evolution and respiratory measurements, the highest net photosynthesis for ALP2 occurred at relatively high 17.0 g/L NaHCO<sub>3</sub> and were 0.099 and 0.084  $\mu\text{moles O}_2 \text{ ml}^{-1} \text{ min}^{-1}$  at low (0.133 g/L) and high (0.529 g/L) urea levels, respectively. These

results agree with those from section 3.4.2.4 and again suggest that ALP2 is photosynthetically well-adapted to extreme halo-alkaline culture conditions

Consistent with DCW measurements, the total chlorophyll and carotenoid content both appeared to increase to maximal values occurring at relatively high 17.0 g/L NaHCO<sub>3</sub> (Figure 3.11).

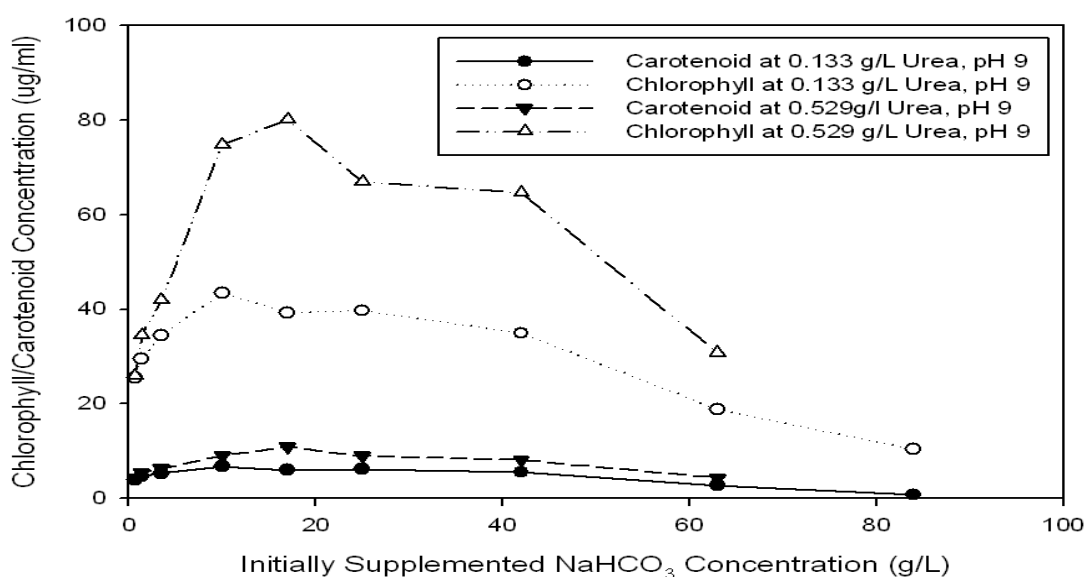


Figure 3.11. Total ALP2 chlorophyll and carotenoid content in methanol extracts from phototrophically grown ALP2 as function of NaHCO<sub>3</sub> and urea levels at HCl-adjusted pH 9

This agrees with previous reported increases in carotenoid (i.e. astaxanthin) content in *Chlorococcum sp.* green algae at 16.8 g/L salinity [41], and the algal *Haemotacoccus pluviialis* during red-stage cultivation at high salinity [42]. Interestingly, however, at a 0.529 g/L urea level sufficient for growth, the carotenoid/chlorophyll ratio generally decreased with increasing

NaHCO<sub>3</sub> (Table 3.4).

Table 3.4. Carotenoid/chlorophyll and chlorophyll a/b ratios of ALP2 phototrophically grown on BG-11<sub>0</sub> medium supplemented with 10.0 g/L NaHCO<sub>3</sub>

NaHCO <sub>3</sub> (g/L)	Urea (g/L)	Carotenoid/ Chlorophyll Ratio	Chlorophyll a/b Ratio
0.7	0.133	0.155	1.95
	0.529	0.166	1.84
1.4	0.133	0.157	2.28
	0.529	0.158	1.99
3.5	0.133	0.154	1.96
	0.529	0.151	2.03
10.0	0.133	0.156	1.95
	0.529	0.121	1.77
17.0	0.133	0.153	1.68
	0.529	0.136	2.07
25.0	0.133	0.156	1.82
	0.529	0.134	2.10
42.0	0.133	0.159	1.81
	0.529	0.127	1.82
63.0	0.133	0.148	1.99
	0.529	0.142	1.99
84.0	0.133	0.077	1.11
	0.529	N/A	N/A

An increase in the chlorophyll a/b ratio (i.e. decrease in the light-harvesting antenna size) at low 0.7-3.5 g/L NaHCO<sub>3</sub>, decrease at 10 g/L, and increase beyond that were also observed (Table 3.4). Upon transitioning from dark heterotrophic first stage to light phototrophic second stage, the

antenna size also appeared to have increased and recovered. These results have implications with regards to microalgal mass cultivation and production of high-value co-products like chlorophyll and astaxanthin, in addition to lipid-precursors to biofuel.

Regarding the effect of urea concentration in the factorial experiment, based on the observed chlorosis or yellowing coloration of late culture samples and the previously measured urea consumption rate, clearly the low urea level of 0.133 g/L resulted in later N-starvation conditions to induce higher neutral lipid accumulation in liposomes compared to cultures at 0.529 g/L urea (Table 3.3). The chlorophyll and carotenoid contents were generally lower at 0.133 g/L than at 0.529 g/L urea (Figure 3.11).

Regarding the effect of acetic acid for pH adjustment, cultures at 10.0 g/L  $\text{NaHCO}_3$  and 0.133 g/L urea that were pH-adjusted to 7 or 9 by manually supplementing acetic acid resulted in the highest neutral lipid content. For instance, at pH 7, these were 1.048 g/L and DCW of 2.110 g/L, respectively. But these cultures suffered from a cloudy bacterial contamination, particularly at pH 7. To minimize contamination, acetic acid could theoretically be supplemented instead to late, mature, open-pond cultures to adjust pH and also provide additional organic carbon and metabolic pre-cursors to microalgal Acyl-CoA lipid metabolism. Acetic acid supplementation was previously used to adjust pH and boost lipid productivity [43]. Regarding the effect of daily adjusted pH, at 10.0 g/L  $\text{NaHCO}_3$  and both a high 0.529 g/L and a low 0.133 g/L urea leading to N-starvation conditions, ALP2 cultures at pH 9 outperformed those at pH 7, 8, and 10 (Table 3.5).

Table 3.5. Performance of ALP2 phototrophically cultivated on BG-11<sub>0</sub> supplemented with 10.0 g/L NaHCO<sub>3</sub>, either 0.133 g/L or 0.529 g/L urea, at various HCl-adjusted pH levels

pH	Urea (g/L)	Final DCW (g/L)	TAG (g/L)	Fat %	Lipid Productivity (g L <sup>-1</sup> day <sup>-1</sup> )
7	0.133	1.928	0.489	25.35	0.038
	0.529	2.294	0.043	1.89	0.003
8	0.133	2.108	0.561	26.60	0.043
	0.529	2.396	0.058	2.42	0.004
9	0.133	2.260	0.776	34.34	0.060
	0.529	2.612	0.123	4.71	0.009
10	0.133	2.282	0.654	28.65	0.050
	0.529	1.477	0.080	5.40	0.006

This is further evidence of ALP2's halo-alkaline tolerance.  $q_L$  increased beyond pH 8, and both  $\Psi_{II}$  and  $F_v/F_m$  decreased beyond pH 9. Also, the chlorophyll a/b ratio was minimal and the total chlorophyll was maximal at pH 9. Net photosynthesis was highest at pH 8 and were 0.082 and 0.068  $\mu\text{moles O}_2 \text{ ml}^{-1} \text{ min}^{-1}$  at low (0.133 g/L) and high (0.529 g/L) urea levels, respectively. The actual extracellular pH of the cultures during O<sub>2</sub>-evolution measurements was likely higher due to any photosynthesis occurring between the time of pH adjustment and O<sub>2</sub>-evolution measurements. This again agrees with the previous experiment of section 3.2.4 showing maximal net photosynthesis pH 8.65 coinciding with the pH of Alkali Lake water [9].

### 3.5. Conclusions

Optimization of culture conditions and characterization of their effects on the growth and

lipid-accumulation of a recently discovered oleaginous, dual-trophic, and haloalkaline-tolerant *Chlorella sp.* ALP2 were undertaken. ALP2 possessed characteristics essential to a previously proposed two-stage cultivation process, designed to address challenges associated with outdoor mass cultivation of oleaginous microalgae.

ALP2 rapidly grew rapidly at a high rate of  $1.7 \times 10^8$  cells  $\text{ml}^{-1}\text{day}^{-1}$  cell in the first stage under optimized heterotrophic conditions comprising the use of BG-11<sub>0</sub> medium supplemented with 10.0 g/L glucose and 0.529 g/L urea at 28°C. pH-control (optimally at pH 9) with aqueous HCl acid, as well as use of urea and anaerobically-digested food waste nitrogen sources in place of  $\text{NaNO}_3$ , were found to further promote ALP2 phototrophic growth. ALP2 that was inoculated from a heterotrophic first-stage grew to a final DCW of 2.528 g/L and achieved a neutral lipid content and productivity of 39.92% of DCW and  $0.078 \text{ g L}^{-1} \text{ day}^{-1}$ , respectively, in the second-stage under optimized phototrophic conditions. These conditions comprised the use of BG-11<sub>0</sub> medium supplemented with 17.0 g/L  $\text{NaHCO}_3$  and 0.133 g/L urea, and maintenance of a pH 9 using aqueous HCl.

Relatively high levels of supplemental inorganic bicarbonate promoted ALP2 growth. High alkalinity, buffered by high concentration of bicarbonate ion, contributed to increased ALP2 cell size, granularity, optical density, and neutral lipid accumulation. ALP2 was found to be photosynthetically well-adapted to extreme haloalkaline culture conditions, based on observed state transition and the ability to maintain constant and high values for the photosynthetic

parameters  $F_v/F_m$ ,  $O_2$ -evolution and respiration, NPQ, and  $\Psi_{II}$  at high pH and  $NaHCO_3$  levels. ALP2 carotenoid/chlorophyll ratio decreased with increasing  $NaHCO_3$  levels. The ability of ALP2 to replicate at high  $NaHCO_3$  concentrations and high pH, and to use bicarbonate ion as a major carbon source in both growth and lipid accumulation phases of second-stage phototrophic growth is a significant development for the two-stage cultivation strategy. The additional ability of ALP2 to grow heterotrophically or mixotrophically rapidly to high cell densities makes it an ideal candidate for further optimization and scale-up of a highly productive two-stage cultivation process for commercial algal bio-oil production.

### **Acknowledgements**

Financial support for this work was provided by the US Department of Energy (EE0003112).

### 3.6. References

- [1] K.K. Sharma, H. Schuhmann, P.M. Schenk. High Lipid Induction in Microalgae for Biodiesel Production. *Energies* 5 (2012) 1532-53.
- [2] N.R. Moheimani, M.A. Borowitzka. The long-term culture of the coccolithophore *Pleurochrysis carterae* (Haptophyta) in outdoor raceway ponds. *Journal of Applied Phycology* 18 (2006) 703-12.
- [3] V. Patil, K.Q. Tran, H.R. Giselrod. Towards sustainable production of biofuels from microalgae. *International Journal of Molecular Sciences* 9 (2008) 1188-95.
- [4] Z.Y. Chi, J.V. O'Fallon, S.L. Chen. Bicarbonate produced from carbon capture for algae culture. *Trends in Biotechnology* 29 (2011) 537-41.
- [5] E.D.G. Danesi, C.D.O. Rangel-Yagui, J.C.M. de Carvalho, S. Sato. An investigation of effect of replacing nitrate by urea in the growth and production of chlorophyll by *Spirulina platensis*. *Biomass & Bioenergy* 23 (2002) 261-9.
- [6] D. Soletto, L. Binaghi, A. Lodi, J.C.M. Carvalho, A. Converti. Batch and fed-batch cultivations of *Spirulina platensis* using ammonium sulphate and urea as nitrogen sources. *Aquaculture* 243 (2005) 217-24.
- [7] D. Vandamme, I. Foubert, I. Fraeye, B. Meesschaert, K. Muylaert. Flocculation of *Chlorella vulgaris* induced by high pH: Role of magnesium and calcium and practical implications. *Bioresource Technology* 105 (2012) 114-9.

- [8] S.A. Scott, M.P. Davey, J.S. Dennis, I. Horst, C.J. Howe, D.J. Lea-Smith, et al. Biodiesel from algae: challenges and prospects. *Current Opinion in Biotechnology* 21 (2010) 277-86.
- [9] P. Wensel, G. Helms, B. Hiscox, W.C. Davis, H. Kirchhoff, M. Bule, et al. Microalgae for Two-Stage Cultivation: Part I Bio-prospecting (Submitted). *Algal Research* (2013).
- [10] T. Li, Y. Zheng, L. Yu, S. Chen. High productivity cultivation of a heat-resistant microalga *Chlorella sorokiniana* for biofuel production. *Bioresource Technology* 131 (2013) 60-7.
- [11] I. Iwasaki, Q. Hu, N. Kurano, S. Miyachi. Effect of extremely high-CO<sub>2</sub> stress on energy distribution between photosystem I and photosystem II in a 'high-CO<sub>2</sub>' tolerant green alga, *Chlorococcum littorale* and the intolerant green alga *Stichococcus bacillaris*. *Journal of Photochemistry and Photobiology* 44 (1998) 184-90.
- [12] L.J. Kang, X.J. Chen, X.J. Pan, F.Y. Chang, Y.D. Liu. Effect of Elevated Bicarbonate Concentration on Growth, Chlorophyll a Fluorescence and Ultra-Structure of *Microcystis Aeruginosa* (Cyanobacterium). *Fresenius Environmental Bulletin* 18 (2009) 687-93.
- [13] S. Masuda, T.A. Ono. Adenylyl cyclase activity of Cya1 from the cyanobacterium *Synechocystis sp* strain PCC 6803 is inhibited by bicarbonate. *Journal of Bacteriology* 187 (2005) 5032-5.
- [14] P.R. Sudhir, D. Pogoryelov, L. Kovacs, G. Garab, S.D.S. Murthy. The effects of salt stress on photosynthetic electron transport and thylakoid membrane proteins in the cyanobacterium *Spirulina platensis*. *Journal of Biochemistry and Molecular Biology* 38 (2005) 481-5.

- [15] B. Shukla, L.C. Rai. Potassium-induced inhibition of photosynthesis and associated electron transport chain of *Microcystis*: Implication for controlling cyanobacterial blooms. *Harmful Algae* 5 (2006) 184-91.
- [16] J.R. Coleman, B. Colman. Inorganic Carbon Accumulation and Photosynthesis in a Blue-Green-Alga as a Function of External pH. *Plant Physiology* 67 (1981) 917-21.
- [17] R.D. Gardner, E. Lohman, R. Gerlach, K.E. Cooksey, B.M. Peyton. Comparison of CO<sub>2</sub> and bicarbonate as inorganic carbon sources for triacylglycerol and starch accumulation in *Chlamydomonas reinhardtii*. *Biotechnology and Bioengineering* 110 (2013) 87-96.
- [18] A. Richmond, S. Karg, S. Boussiba. Effects of Bicarbonate and Carbon Dioxide on the Competition between *Chlorella vulgaris* and *Spirulina platensis*. *Plant and Cell Physiology* 23 (1982) 1411-7.
- [19] J.C. Meeks. <http://microbiology.ucdavis.edu/meeks/BG11medium.html>. 2013.
- [20] E. Lee, R.L. Heng, L. Pilon. Spectral optical properties of selected photosynthetic microalgae producing biofuels. *Journal of Quantitative Spectroscopy & Radiative Transfer* 114 (2013) 122-35.
- [21] J.V. O'Fallon, J.R. Busboom, M.L. Nelson, C.T. Gaskins. A direct method for fatty acid methyl ester synthesis: Application to wet meat tissues, oils, and feedstuffs. *Journal of Animal Science* 85 (2007) 1511-21.
- [22] K. Maxwell, G.N. Johnson. Chlorophyll fluorescence - a practical guide. *Journal of*

Experimental Botany 51 (2000) 659-68.

[23] L. Yu, Q.B. Zhao, J.W. Ma, C. Frear, S.L. Chen. Experimental and modeling study of a two-stage pilot scale high solid anaerobic digester system. *Bioresource Technology* 124 (2012) 8-17.

[24] V. Makarevičienė, V. Andrulėvičiūtė, V. Skorupskaite, J. Kasperoviciene. Cultivation of *Chlorella sp.* and *Scenedesmus sp.* as Potential Biofuel Feedstock. *Environmental Research, Engineering, and Management* 57 (2011) 21-7.

[25] A.K. Singh, M. Bhattacharyya-Pakrasi, T. Elvitigala, B. Ghosh, R. Aurora, H.B. Pakrasi. A Systems-Level Analysis of the Effects of Light Quality on the Metabolism of a Cyanobacterium. *Plant Physiology* 151 (2009) 1596-608.

[26] J.E. Kogel. *Industrial Minerals & Rocks: Commodities, Markets, and Uses* 7th ed. Littleton, Colorado, Society for Mining, Metallurgy, and Exploration, Inc. (SME), 2006.

[27] Y. Chisti. Biodiesel from microalgae. *Biotechnology Advances* 25 (2007) 294-306.

[28] D. Pleissner, W.C. Lam, Z. Sun, C.S.K. Lin. Food waste as nutrient source in heterotrophic microalgae cultivation. *Bioresource Technology* 1 (2013).

[29] S. Chen, C. Frear, A. Jiang, T. Zhang. Combined nutrient recovery and biogas scrubbing system integrated in series with animal manure anaerobic digester. In: USPTO, U.S.A, 2009.

[30] P.M. Ndegwa, A.N. Hristov, J. Arogo, R.E. Sheffield. A review of ammonia emission mitigation techniques for concentrated animal feeding operations. *Biosystems Engineering* 100

(2008) 453-69.

[31] K. Koirala, P.M. Ndegwa, H.S. Joo, C. Frear, J.H. Harrison, C.O. Stockle. Influence of Suspended Solids Adsorption Properties and Concentration on Ammonia Volatilization Mechanism from Liquid Dairy Manure. *Journal of Biosystems Engineering* 2 (2013) 1-12.

[32] F. Montes, C.A. Rotz, H. Chaoui. Process Modeling of Ammonia Volatilization from Ammonium Solution and Manure Surfaces: A Review with Recommended Models. *Transactions of the Asabe* 52 (2009) 1707-19.

[33] A. Gupta, G. Rao. A study of oxygen transfer in shake flasks using a non-invasive oxygen sensor. *Biotechnology and Bioengineering* 84 (2003) 351-8.

[34] M. Drath, N. Kloft, A. Batschauer, K. Marin, J. Novak, K. Forchhammer. Ammonia triggers photodamage of photosystem II in the cyanobacterium *Synechocystis sp* strain PCC 6803. *Plant Physiology* 147 (2008) 206-15.

[35] M. Giordano, J. Beardall, J.A. Raven. CO<sub>2</sub> concentrating mechanisms in algae: Mechanisms, environmental modulation, and evolution. *Annual Review of Plant Biology* 56 (2005) 99-131.

[36] R.D. Gardner, K.E. Cooksey, F. Mus, R. Macur, K. Moll, E. Eustance, et al. Use of sodium bicarbonate to stimulate triacylglycerol accumulation in the chlorophyte *Scenedesmus sp* and the diatom *Phaeodactylum tricornutum*. *Journal of Applied Phycology* 24 (2012) 1311-20.

[37] L.M. Gerasimenko, A.V. Dubinin, L.L. Mityushina, G.A. Zavarzin. A microscopic green alga from soda lakes. *Microbiology* 68 (1999) 610-4.

- [38] G. Finazzi, F. Rappaport, A. Furia, M. Fleischmann, J.D. Rochaix, F. Zito, et al. Involvement of state transitions in the switch between linear and cyclic electron flow in *Chlamydomonas reinhardtii*. *Embo Reports* 3 (2002) 280-5.
- [39] D.M.J. Dickson, G.O. Kirst. Osmotic Adjustment in Marine Eukaryotic Algae - The Role of Inorganic-Ions, Quaternary Ammonium, Tertiary Sulfonium and Carbohydrate Solutes .1. Diatoms and a Rhodophyte. *New Phytologist* 106 (1987) 645-55.
- [40] G. Peers, T.B. Truong, E. Ostendorf, A. Busch, D. Elrad, A.R. Grossman, et al. An ancient light-harvesting protein is critical for the regulation of algal photosynthesis. *Nature* 462 (2009) 518-U215.
- [41] J. Masojidek, G. Torzillo, J. Kopecky, M. Koblizek, L. Nidiaci, J. Komenda, et al. Changes in chlorophyll fluorescence quenching and pigment composition in the green alga *Chlorococcum sp* grown under nitrogen deficiency and salinity stress. *Journal of Applied Phycology* 12 (2000) 417-26.
- [42] C. Aflalo, Y. Meshulam, A. Zarka, S. Boussiba. On the relative efficiency of two- vs. one-stage production of astaxanthin by the green alga *Haematococcus pluvialis*. *Biotechnology and Bioengineering* 98 (2007) 300-5.
- [43] K.L. Yeh, C.Y. Chen, J.S. Chang. pH-stat photoheterotrophic cultivation of indigenous *Chlorella vulgaris* ESP-31 for biomass and lipid production using acetic acid as the carbon source. *Biochemical Engineering Journal* 64 (2012) 1-7.

## CHAPTER 4 : SIMULATION WITH COMPUTATIONAL FLUID DYNAMICS OF SUCCINIC ACID AND CO-PRODUCT BIOREFINERY PROCESS

### 4.1. Abstract

Succinic acid is a dicarboxylic acid with tremendous future market potential, and there is increasing interest to produce it from microorganisms using cheap renewable resources like biomass. However, commercialization of bio-succinic acid is currently challenged by limited profitability of processes devoted solely to succinic acid, high downstream process costs, and minimal available industrial-scale simulation. To address these limitations, a novel industrial-scale biorefinery process to convert corn-stover into succinic acid and co-products was simulated using an integrated mathematical model developed from reported laboratory-scale experimental data. The upstream section of the biorefinery featured handling, pre-treatment, conversion, and separation of corn stover feedstock into a liquid fraction for ethanol processing and a solids fraction containing mostly cellulose that was further hydrolyzed into glucose for succinic acid processing. Subsequent units of operation were then simulated for a baseline process: Microfiltration was used to remove residual insoluble lignin, and glucose was then continuously fermented by the strain *M. Succiniciproducens MBEL55E* to produce succinate and by-products acetate, lactate, and formate. Additional steps to recover and purify succinic acid included cell microfiltration for cell removal, moving-bed adsorption for sugar removal and decolorization, nanofiltration for separation of succinate primarily from other salts, ion exchange for acidification

and purification, and finally crystallization. The finite volume method of Computational Fluid Dynamics (CFD) was coupled with kinetic, stoichiometric, mass, and energy balance equations to simulate the effects of inlet temperature impeller speed, diameter, and spacing, as well as inlet temperature and fermentor volume, on fermentor cooling jacket heat transfer area. Predicted dissolved CO<sub>2</sub> concentrations in the fermentor were in agreement with those in literature. The effects of microfiltration recirculation rate, microfiltration stage numbers, and adsorber sorbent particle diameter on dimensional requirements and power consumption were additionally evaluated. Yields and estimated volume and area requirements for units of operation were obtained for the baseline process and for those involving the simulated variable changes. This work represents the first reported industrial-scale bio-succinic acid process model.

**Keywords:** Succinic acid, biorefinery; *Manheima succiniciproducens*; process simulation

## 4.2. Introduction

Succinic acid is a dicarboxylic acid which can be used as a C4 chemical building-block for manufacturing industrially valuable chemicals like adipic acid, N-methyl pyrrolidinone, 2-pyrrolidinone, succinate salts, 1,4-butanediol, maleic anhydride, tetrahydrofuran and gamma-butyrolactone, as well as ion-chelators, surfactants, detergents, synthetic resins, biodegradable polymers, pharmaceuticals, antimicrobials, food acidulants, flavor-enhancers, and green solvents [1-3]. Current succinic acid production ranges from 25,000–36,000 t/year, and market price ranges from \$5.90–9.00 (U.S.)/kg depending on purity [3, 4]. Succinic acid market and price were predicted to range from 180,000-27,000,000 t/year [1, 5], and from \$0.50-1.50(U.S.)/kg, respectively [2, 5].

Conventional production of succinic acid involves chemically processing fossil-based resources like petroleum through oxidation of n-butane or benzene via maleic anhydride, followed by hydrolysis and dehydrogenation [2, 6]. However, there is increased commercial and scientific interest to instead produce succinic acid from microorganisms using cheaper renewable resources like biomass. In 2004, the U.S. Department of Energy designated succinic acid as one of the top value-added chemicals from biomass [7]. Prospects of global bio-based succinic acid markets motivated companies such as Bioamber, DSM and Roquette, BASF and CSM, and Myriant to announce construction of new plants since 2010 [8-10]. Yu et al. [11] previously demonstrated a process involving pre-treatment and hydrolysis of inexpensive and renewable ligno-cellulosic

waste and residue like corncob from agricultural and food industries to yield substrates for microbial fermentative production of succinic acid and co-products.

Commercialization of bio-succinic acid is nonetheless currently challenged by limited profitability when a plant is devoted solely to succinic acid [5]. Succinic acid production should therefore occur in an integrated biorefinery, where co-production of ethanol, other carboxylic acids, and on-site steam and electricity via processing of recovered lignin residues enhance profitability. Commercialization is also challenged by high downstream costs associated with isolation, purification, and sterilization of end-products accounting for up to 80% of total production cost [12]. For example, succinic acid precipitation by  $\text{Ca}^{2+}$ -containing species results in excessive sludge waste and also adversely affects the fermented cellular metabolism and cell membrane fluidity and permeability [12-14]. Reactive extraction with tri-n-octylamine (TOA) [15] can remove glucose but suffers from organic solvent toxicity and waste. A promising batch laboratory-scale process involving four-acid products *Actinobacillus succinogenes* fermentation and downstream centrifugation, filtration, activated carbon adsorption, cation-exchange chromatography, vacuum distillation, crystallization, filtration, and drying achieved an 89.5% succinic acid yield from substrate and 99% purity [8]. However, a commercial-scale biorefinery should instead recover valuable and volatile lactic, acetic, and formic acid by-products rather than eliminate them at 60°C and pH 4 with vacuum distillation [16]. In contrast, a nanofiltration process achieved sharp and non-destructive separation of succinic acid from a quaternary mixture

containing pyruvic as opposed to lactic acid co-product but was not integrated with other purification steps [17].

Electrodialysis has been effectively used to concentrate and acidify succinic acid and other organic acids due to its environmental benignity, scalability, and ability to achieve high purity [18-27]. For instance, de-salting electrodialysis removed impurities and achieved a suitably concentrated, but undersaturated (< 25% weight) succinate solution for one process [22]. This undersaturated solution was then converted into a supersaturated succinic acid solution where ionized succinic acid was converted into undisassociated succinic acid by passing it through a water-splitting bipolar electrodialysis unit, from which an alkali NaOH stream was recycled to neutralize produced acids[22].Conventional electrodialysis was similarly integrated to a feed containing concentrated organic salt sodium gluconate to a bipolar membrane as a way to increase stability and limit a decrease in current efficiency and dramatic increase in energy consumption that frequently results at a high organic salts conversion rate in bipolar membranes due to salt depletion in feed compartments and organic acids diffusion [25]. Integration resulted in an apparent current efficiency higher than 100%, low energy consumption, and a predicted process cost of \$0.31 kg<sup>-1</sup>, which was less than the \$0.39 kg<sup>-1</sup> for the bipolar membrane [25].

Another process involving a succinic acid fermentation by *E.coli strain ATCC202021* used first nanofiltration and then desalting electrodialysis to further concentrate and purify succinate salts and remove small and large molecular weight nonionic or weakly ionic compounds like

sugars [26]. Severe membrane fouling was here alleviated by cleaning-in-place, reducing protein content in the fermentation broth, and raising its pH prior to microfiltration to denature the majority of proteins [26]. A mono-polar electro dialysis unit was also integrated with a continuous cell recycle fermentor for the production of succinic acid by *A. succinogenes* to continuously remove succinate and acetate from the permeate and recycle an organic acids-depleted solution back to the fermentor [19]. Compared to the cell recycle reactor system, this resulted in a five-fold increase in succinate concentration to 83 g/L at a high average succinate yield of 1.35 mol/mol and a slightly lower volumetric productivity of 10.4 g/ L<sup>-1</sup> h<sup>-1</sup>[19].

Nonetheless, a comparison between the technical feasibility of electro dialysis and that of other downstream methods must consider various factors like the cost of membrane and electrical energy consumption [8, 13, 18]. This may depend on purity levels and concentration profile, which in turn depends on water transport, the co-ion leakages through homopolar membranes, and the current density [28]. Also, to achieve higher succinic product fermentation concentrations than those obtained with NaOH, MgCO<sub>3</sub> has not only been used as a (1) pH controlling alkaline neutralizer to prevent acid product inhibition, but also as (2) a more soluble source of inorganic carbon than CO<sub>2</sub> gas requiring expensive compression, and (3) as a source of the co-factor Mg<sup>2+</sup> for the enzyme PEP carboxykinase that is essential for succinate synthesis [14]. The inability of downstream electro dialysis membranes for acidification and purification to effectively handle divalent Mg<sup>2+</sup> cation-containing species was therefore considered a major limitation [2].

Exploitation of the Donnan charge exclusion and the fixed charges of most nanofiltration membranes was also deemed more appropriate than electrodialysis for the separation of ionic by-product organic acid salts from succinate and for salt separation from organic electrolytes typically present in effluents produced by salt-generating reactions or by acid- or alkali-generating reactions followed by neutralization [17, 27]. Furthermore, the process costs and competitiveness of using either electrodialysis with bipolar membrane or ion exchange to acidify the carboxylic glucamonic acid were theoretically calculated by introducing two factors for environmental pollution and bipolar membrane prices and then compared [18]. Although these processes could be integrated to reduce environmental factors, results indicated that total process cost for ion-exchange was  $\$0.057 \text{ kg}^{-1}$  and less than that for bipolar membrane electrodialysis ( $\$0.085\text{--}0.407 \text{ kg}^{-1}$ ) [18].

There is also limited reported industrial-scale process simulation and economic analysis for bio-succinic acid fermentation, recovery, and purification [29]. For instance, experimentally-derived succinic acid crystal growth and nucleation kinetics [30], succinic acid and lactic acid liquid-solid sorbent equilibria [31], and rejection coefficients at specified transmembrane pressure and flux [17] were not then used to simulate integrated large-scale crystallizers, ion exchangers, or nanofilters, respectively. Model-predicted  $\text{CO}_2$  solubility and its experimentally observed effects on growth and succinic acid production during *M. succiniciproducens* fermentation were reported [32]. Kinetics for growth, glucose consumption,

carboxylic acid production, and product and substrate inhibition were also simulated and experimentally verified for small-scale batch *M. succiniciproducens* MBEL55E [6] and *A. succinogenes* [33] fermentations. However, a robust commercial-scale process model should involve continuous fermentors since their productivity will be at least 5.3 times greater than that of batch fermentors [34]. A continuous fermentor integrated with monopolar electro dialysis membrane for removal of cells and inhibitory levels of acetate and lactate was reported but not modeled [19].

A robust commercial-scale process model should also account for hydrodynamic phenomena in a continuous fermentor and its impact on heat and mass transfer, temperature and nutrient uniformity, and, when applicable, cell shear-sensitivity. For instance, growth inhibition of *M. succiniciproducens* MBEL55E was observed beyond an accumulated carboxylic acid concentration of 17.23 kg/m<sup>3</sup> in a small 5 L batch fermentor [6]. Growth inhibition was also observed below a dissolved CO<sub>2</sub> concentration of 8.74 mM in a small 6.6 L batch *M. succiniciproducens* fermentor [32]. Overcoming these pilot-scale limitations at more heterogeneous commercial scales via, for instance, addition of neutralizing MgCO<sub>3</sub> base and carbon source and higher inlet CO<sub>2</sub> partial pressures and agitation impeller speeds will be more systematically achieved by feeding and sparging strategies derived from hydrodynamic studies characterizing mixing times and gas-liquid mass transfer coefficients.

We here describe and simulate a novel commercial-scale succinic acid biorefinery process

featuring upstream corn-stover pre-treatment, hydrolysis, and cross-flow microfiltration and centrifugation for lignin recovery to yield sugars both for a co-ethanol fermentation and continuous *M. succiniciproducens* glucose fermentation for succinic acid, lactic, acetic, and formic acids production. These are then recovered by microfiltration for cell removal, adsorption for decolorization and glucose removal, nanofiltration for non-destructive separation of succinate, ion exchange chromatography, crystallization, filtration, and drying. A baseline process was assumed, but the effects of microfiltration recirculation rate, microfiltration stage numbers, fermentation productivity kinetics, and adsorber sorbent particle diameter on dimensional requirements and power consumption for capital and operating cost estimation were simulated. Effects of impeller speed and inlet temperature on fermentor power and cooling jacket heat transfer area were also simulated by coupling mass and energy balances and experimentally-derived kinetics to the finite volume method of Computational Fluid Dynamics (CFD).

CFD involves numerical solution of conservation equations for mass, momentum and energy in a flow geometry of interest, together with additional subsidiary sets of equations reflecting the considered problem [35]. Flow optimization via this tool represents significant potential savings in time and resources and increased profitability for a low profit margin, bio-commodity succinic acid process [35] by providing more data than physical trials and reducing the need for numerous and expensive experiments with prototype fermentors and probes. This is the first reported process simulation for industrial-scale bio-succinic acid production.

### **4.3. Materials and Methods**

#### **4.3.1 Software and General Refinery Description**

Microsoft Excel v. 2007 software was used for calculations associated with process mass and energy balances, unit simulation via variable changes, and cost and sensitivity analysis. CFD numerical procedure was conducted with commercial code FLUENT (v.6.3.26) [36]. The simulated biorefinery process is shown (Figure 4.1). Description of major process streams are listed (Table 4.1). The feedstock was corn stover containing approximately 40–45% cellulose, 30–35% hemicellulose, and 10–20% lignin [11]. The biorefinery was located in Iowa, a state accounting for 19% of total U.S. corn production having infrastructure to fulfill biorefinery requirement for co-production of corn-based ethanol. Capacity of 2,500 tons (wet basis) of corn stover/day was selected according to a National Renewable Energy Laboratory (NREL) model where raw material was collected within a 50 km radius [37]. This was the basis for the mass and energy balances and flow rates to simulate the succinic acid process units ranging from lignin microfiltration to crystallization.

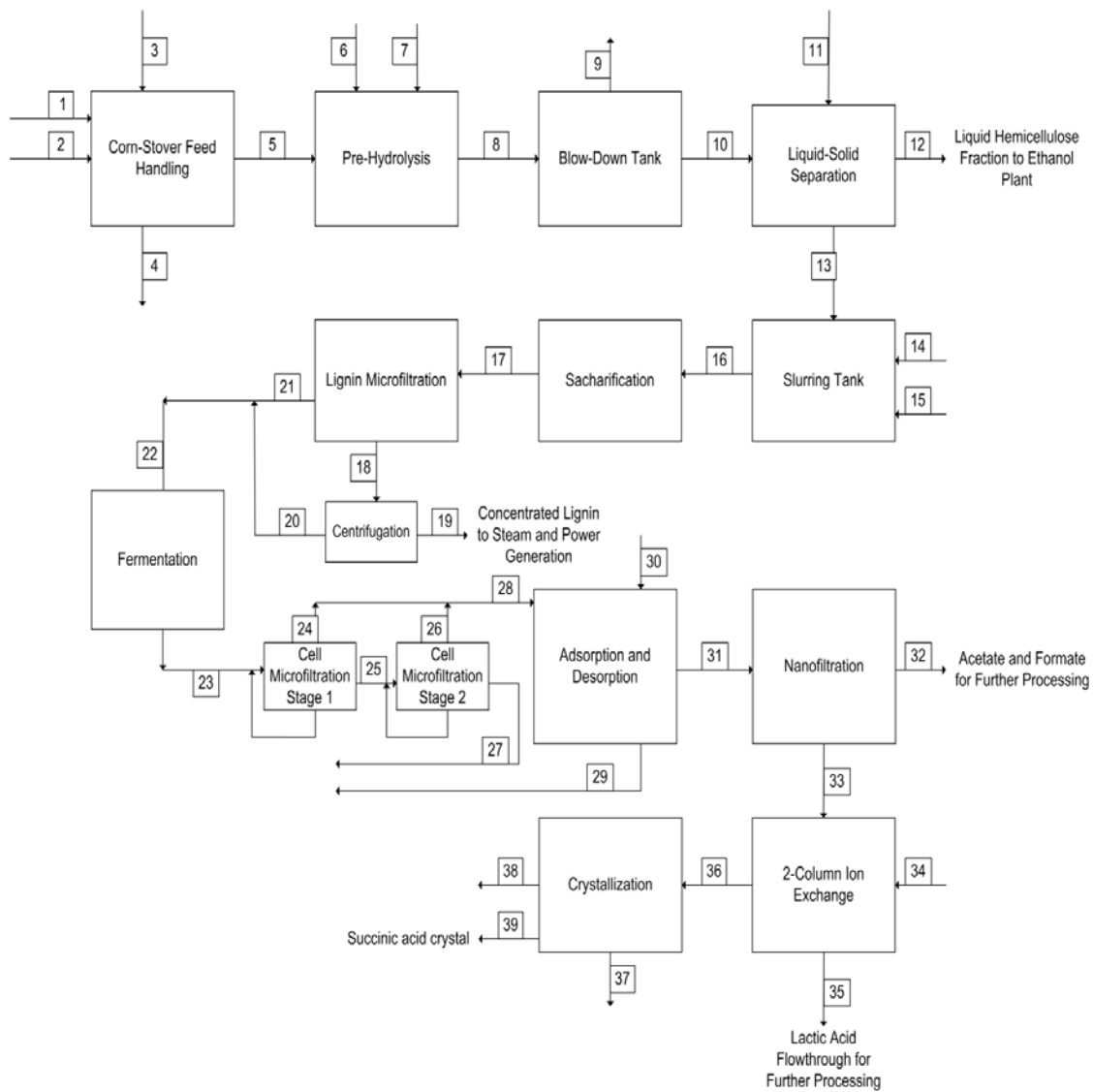


Figure 4.1. General flow diagram for succinic acid biorefinery

Table 4.1. Description of major process flow streams

Major Process Stream ID	Description
1	Corn Stover Feedstock (Dry Basis)
2	Corn Stover Feedstock Water Moisture Content
3	Losses
4	Supplemented Water
5	Shredded Corn Stover
6	Sulfuric Acid
7	Steam
8	Pre-treated Stover 1
9	Steam
10	Pre-treated Stover 2
11	Supplemented Water
12	Liquid Hemicellulose Fraction to Ethanol Plant
13	Solids Cellulose Fraction to Succinic Acid Plant
14	Calcium Hydroxide
15	Supplemented Water
16	Cellulose Fraction to Sacharification
17	Hydrolysate
18	Lignin Microfiltration Retentate
19	Concentrated Lignin to Steam and Power Generation
20	Centrifuged Retentate Flowthrough
21	Lignin Microfiltration Permeate
22	Combined Permeate Feed to Fermentation
23	Fermentation Product Streams (Cells, succinate, acetate, formate, and lactate)
24	Cell Microfiltration Stage#1 Permeate
25	Cell Microfiltration Stage#2 Retentate
26	Cell Microfiltration Stage#1 Permeate
27	Cell Microfiltration Stage#2 Retentate
28	Combined Permeate Feed to Adsorption and Desorption
29	Recovered Glucose Sugars
30	Regenerating Hot Water Solution
31	Nanofiltration Feed
32	Nanofiltration Permeate
33	Nanofiltration Retentate

---

34	Hot Water Regeneration Solution
35	Lactic Acid Flowthrough for Further Processing
36	Stripped Lactic Acid Eluant
37	Vented Water Vapor
38	Mother Liquor from Circulating Magma for Further processing
39	Succinic Acid Crystal

---

Unlike for plants devoted solely to ethanol fuel production, the generalized energy balance did not aim to show the extent that corn stover was converted into fuel energy since acid products were not fuels. Instead, energy losses and stream energy content were estimated:

$$E_{corn\_stover} = E_{electricity} + E_{ethanol} + E_{lactic} + E_{formic} + E_{succinic} + E_{steam\_hotwater} \quad (4.1)$$

Energy content was determined by multiplying mass flux by the corresponding High Heating Values (HHV) of 16, 29.7, 21.1, and 32.1 MJ/kg for corn stover, ethanol, lignin, and for each of the carboxylic acid products, respectively [38]. Electricity requirement was determined from estimates of electrical motor power consumption (i.e. for fermentor and crystallizer agitator), control systems, etc. Thermal energy requirement was determined from individual unit energy balances.

#### *4.3.2 Upstream processes including lignin microfiltration and centrifugation*

Upstream processes ranging from raw material corn stover feed handling to saccharification resembled those of a previous corn-based ethanol biorefinery [37], with the following major modifications and simplifying assumptions: First, pre-hydrolysis, the most thermal energy-consuming plant process, involved 1.2% diluted sulfuric acid and pressurized steam at

245°C, and 13.6 bar instead of ammonia fiber expansion (AFEX) to enable separation of liquid hemicellulose streams composed primarily of pentoses for ethanol fermentation and solid cellulose streams composed primarily of hexoses for glucose-based succinic acid fermentation. Second, the process included single-stage cross-flow tubular microfiltration units and centrifuge to remove and recover insoluble lignin from hydrolysate for combustion in a boiler and extra biorefinery steam and electricity.

Lignin-generated steam flow rate was calculated from lignin HHV, a boiler thermal efficiency of 0.65, specific enthalpy of steam at pre-hydrolysis conditions, and recovered lignin flow rate. For microfiltration, all insoluble lignin was retained, and the amount of glucose substrate partitioned to the retentate and permeate was 5% and 95% by mass, respectively. Retentate lignin concentration was specified based on a reported level 300 g/L of soluble lignin ultra-filtered in a pulp and mill plant [39]. To avoid rapid membrane caking or fouling, recirculation rate of 6 m/s was used for the baseline process but also varied for simulation, and specified inner diameter and length dimensions of the tubular module ensured turbulent Reynold's number. Assuming 40µm diameter spherical and insoluble lignin particles, inertial-lift theory [40] was used to calculate constant critical permeate flux representing 66% of the steady-state permeate flux [41] as follows:

$$J_c = \frac{0.024\rho_p r^3 \gamma_w^2}{\mu_p} \quad (4.2)$$

where  $J_c$  is critical permeate flux (m/s),  $\rho_p$  is permeate density (kg/m<sup>3</sup>),  $\mu_p$  is permeate viscosity (Pa\*s),  $r$  is lignin particle radius (m), and  $\gamma_w$  is tubular wall shear rate (s<sup>-1</sup>).

Microfiltration membrane area requirement was the ratio of mass balance-derived permeate flow rate to critical flux. Microfiltration power consumption was calculated [42]:

$$P_{micro-1} = \frac{0.04 \text{Re}^{-0.25} A_{micro-1} U_{micro-1}^3 \rho_p}{\eta_p} \quad (4.3)$$

where  $P_{micro-1}$  is pump power consumption (J/s),  $U_{micro-1}$  is recirculation rate (m/s),  $\eta_p$  is pump efficiency (Dimensionless),  $A_{micro-1}$  is the area requirement ( $\text{m}^2$ ), and Re is Reynold's Number (Dimensionless) calculated as follows:

$$\text{Re} = \frac{U_{micro-1}^3 d_{micro-1} \rho_p}{\mu_p} \quad (4.4)$$

where  $d_{micro-1}$  is tube inner diameter (m). The microfiltration retentate was then centrifuged to further de-water and concentrate its lignin prior to boiler combustion. A Sigma Factor  $\Sigma$  specifying disk-type centrifuge area requirement was calculated [40].

#### 4.3.3 Fermentation

The centrifuged and de-lignified retentate liquid stream containing glucose was then combined with microfiltration permeate, sterilized and cooled in external heat exchanger, and introduced to the continuous fermentor for succinic acid and co-production of lactic acid, acetic acid, and formic acid. The baseline process used the available batch kinetic parameters of *M. succiniciproducens MBEL55E* [6], a gram-negative capnophilic bacterium isolated from bovine rumen [32]. Succinic acid is metabolically both an intermediate of the reductive TCA cycle and fermentative end product for this and other anaerobic and facultative microorganisms. [32]. Some other strains [3]

have reportedly higher succinic acid yields and titers than *M. succiniciproducens* (Table 4.2). Some even have the flexibility of C5 and C6 sugar uptake [11] and Simultaneous Sacharification and Fermentation (SSF) [43]. However, their parameters were either unreported or less usable because yield and production terms were convoluted into single terms [33]. Nonetheless, the effect of substituting in an *A. succinogenes* succinic acid productivity term on overall succinic acid yield was simulated.

Table 4.2. Yields, reaction rates, and titers for *C. glutamicum*, *A. succinogenes*, and *M. succiniciproducens* [3]

<b>Microorganims</b>	<b>Y</b> (g/g glc)	<b>q<sub>succ</sub></b> (g/gDCW/h)	<b>r<sub>succ</sub></b> (g/l/h)	<b>Titer</b> (g/l)	<b>ResidenceTime</b> (h)
<i>C. glutamicum</i>	0.92	0.06	3.17	146	46
<i>A. succinogenes</i>	0.82	N.D.	1.36	105.8	78
<i>M. succiniciproducens</i>	0.76	0.72	1.80	52.4	30

An algorithm depicting the CFD-coupled model to predict the effect of impeller speed and inlet temperature on fermentor cooling jacket heat transfer area requirement is illustrated (Figure 4.2). To initially determine fermentor dimensions for such CFD simulation, an idealized Continuously Stirred Tank Reactor (CSTR) at steady-state with equivalent inlet and outlet flow rates was assumed. The fermentor was assumed to be cylindrical, free of headspace and internals, and sparged at the bottom by pure CO<sub>2</sub> gas from a clean, filtered, and recycled exhaust waste stream

integrated from biorefinery ethanol fermentors.

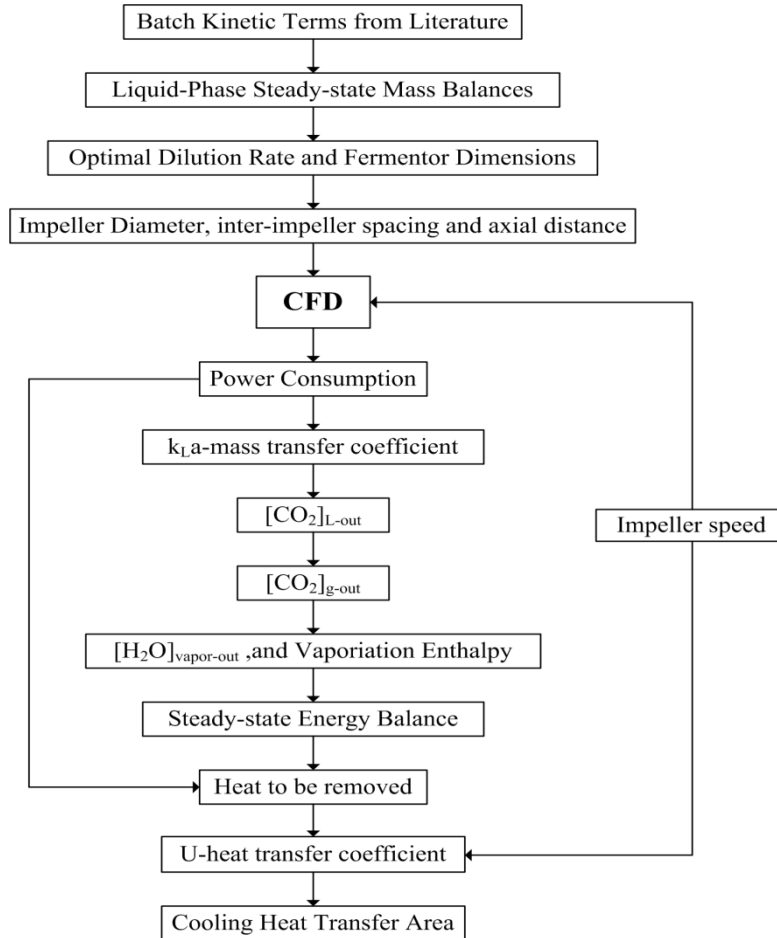


Figure 4.2. Algorithm of coupled CFD fermentor simulation

Steady-state liquid-phase mass balances for the component cell biomass, substrate, and carboxylic acid products using the available batch kinetic parameters of *M. succiniciproducens MBEL55E* [6] were therefore developed:

Viable Cell Liquid-Phase Mass Balance:

$$\frac{dX_{ss}}{dt} = 0 = \frac{F(X_0 - X_{ss})}{V_L} + \mu X_{ss} - k_d X_{ss} \quad (4.5)$$

where  $X_{ss}$  is steady-state cell biomass concentration (kg DCW/m<sup>3</sup>),  $X_0$  is initial feed cell biomass concentration (kg DCW/m<sup>3</sup>),  $\mu$  is specific growth rate (s<sup>-1</sup>),  $F$  is inlet/outlet volumetric flow rate (m<sup>3</sup>/s),  $V_L$  is fermentor liquid volume (m<sup>3</sup>), and  $k_d$  is specific death rate (s<sup>-1</sup>). Omitting substrate and product inhibition terms [6] and assuming Monod kinetics to avoid multiple non-washout steady-states [34],  $\mu$  was further expressed as:

$$\mu = \frac{\mu_{\max} S_{ss}}{K_S + S_{ss}} \quad (4.6)$$

where  $\mu_{\max}$  is maximum specific growth rate (s<sup>-1</sup>),  $K_S$  is glucose substrate half-saturation constant (kg/m<sup>3</sup>), and  $S_{ss}$  is steady-state glucose substrate concentration (kg/m<sup>3</sup>). Because feed was previously sterilized,  $X_0 = 0$  kg/m<sup>3</sup>. The recycle of cells back to the fermentor after downstream microfiltration recovery was for simplicity not simulated. A shear-dependent death rate term coupled with CFD simulation parameters was included as follows [44]:

$$k_d = \frac{c N_{impeller}^{2.25} d_{cell} D_{impeller}^{3.75}}{\nu_l^{1.25} V_L^{0.75}} \quad (4.7)$$

where  $N_{impeller}$  is rotational impeller speed (rps),  $d_{cell}$  is equivalent diameter for rodococcal *M. succiniciproducens* (m),  $D_{impeller}$  is impeller diameter (m),  $\nu_l$  is dynamic viscosity (m<sup>2</sup>/s),  $V_L$  is fermentor liquid volume (m<sup>3</sup>), and  $c$  is cell-dependent death rate constant (m<sup>3</sup>/s). However,  $k_d \approx 0$ , as *M. succiniciproducens*, unlike animal cells, likely had a very small death rate constant

since *E.coli* were reportedly damaged only at shear rates exceeding 1250 Pa [45].

Carboxylic Acids Product Liquid-Phase Mass Balances:

$$\frac{dP_{SA_{ss}}}{dt} = 0 = \alpha_{SA}\mu X_{ss} + \beta_{SA}X_{ss} - \frac{F(P_{SA_{ss}})}{V_L} \quad (4.8)$$

$$\frac{dP_{AA_{ss}}}{dt} = 0 = \alpha_{AA}\mu X_{ss} + \beta_{AA}X_{ss} - \frac{F(P_{AA_{ss}})}{V_L} \quad (4.9)$$

$$\frac{dP_{LA_{ss}}}{dt} = 0 = \alpha_{LA}\mu X_{ss} + \beta_{LA}X_{ss} - \frac{F(P_{LA_{ss}})}{V_L} \quad (4.10)$$

$$\frac{dP_{FA_{ss}}}{dt} = 0 = \alpha_{FA}\mu X_{ss} + \beta_{FA}X_{ss} - \frac{F(P_{FA_{ss}})}{V_L} \quad (4.11)$$

where  $P_{SA_{ss}}$ ,  $P_{AA_{ss}}$ ,  $P_{LA_{ss}}$ , and  $P_{FA_{ss}}$  are steady-state concentrations of succinic acid, lactic acid, acetic acid, and formic acid concentrations, respectively ( $\text{kg/m}^3$ ),  $\alpha_{SA}$ ,  $\alpha_{AA}$ ,  $\alpha_{LA}$ , and  $\alpha_{FA}$  are growth-associated productivity terms for succinic acid, acetic acid, lactic acid, and formic acid, respectively ( $\text{kg/kg}$ ),  $\beta_{SA}$ ,  $\beta_{AA}$ ,  $\beta_{LA}$  and  $\beta_{FA}$  are non-growth associated productivity terms for succinic acid, acetic acid, lactic acid, and formic acid, respectively ( $\text{kg/kg}$ ).

Glucose Substrate Liquid-Phase Mass Balance:

$$\frac{dS_{ss}}{dt} = 0 = \frac{F(S_0 - S_{ss})}{V_L} - \frac{\mu X_{ss}}{Y_{x/s}} - \frac{(\alpha_{SA}\mu X_{ss} + \beta_{SA}X_{ss})}{Y_{SA/s}} - \frac{(\alpha_{AA}\mu X_{ss} + \beta_{AA}X_{ss})}{Y_{AA/s}} - \frac{(\alpha_{LA}\mu X_{ss} + \beta_{LA}X_{ss})}{Y_{LA/s}} - \frac{(\alpha_{FA}\mu X_{ss} + \beta_{FA}X_{ss})}{Y_{FA/s}} - m_s X_{ss} \quad (4.12)$$

where  $S_0$  is initial glucose substrate feed concentration ( $\text{kg/m}^3$ ),  $m_s$  is glucose substrate maintenance term ( $\text{kg/kg}$ ),  $Y_{x/s}$  is yield coefficient of biomass from glucose substrate ( $\text{kg/kg}$ ),  $Y_{SA/s}$ ,  $Y_{AA/s}$ ,  $Y_{LA/s}$ ,  $Y_{FA/s}$  are yield coefficients for succinic acid, acetic acid, lactic acid, and

formic acid, respectively, from glucose substrate (kg/kg). The steady-state cell biomass balance by substitution became:

$$\mu = \frac{F}{V_L} = D \quad (4.13)$$

where  $D$  is dilution rate ( $s^{-1}$ ). Substituting this dilution rate into steady-state mass balances resulted in the following:

$$S_{ss} = \frac{DK_s}{\mu_m - D} \quad (4.14)$$

$$X_{ss} = \frac{D(S_0 - S_{ss})}{\left( D \left( \left( \frac{1}{Y_{x/s}} \right) + \left( \frac{\alpha_{SA}}{Y_{SA/s}} \right) + \left( \frac{\alpha_{AA}}{Y_{AA/s}} \right) + \left( \frac{\alpha_{LA}}{Y_{LA/s}} \right) + \left( \frac{\alpha_{FA}}{Y_{FA/s}} \right) \right) + \left( \frac{\beta_{SA}}{Y_{SA/s}} \right) + \left( \frac{\beta_{AA}}{Y_{AA/s}} \right) + \left( \frac{\beta_{LA}}{Y_{LA/s}} \right) + \left( \frac{\beta_{FA}}{Y_{FA/s}} \right) + m_s \right)} \quad (4.15)$$

$$P_{SA,ss} = \alpha_{SA} X_{ss} + \frac{\beta_{SA} X_{ss}}{D} \quad (4.16)$$

$$P_{AA,ss} = \alpha_{AA} X_{ss} + \frac{\beta_{AA} X_{ss}}{D} \quad (4.17)$$

$$P_{LA,ss} = \alpha_{LA} X_{ss} + \frac{\beta_{LA} X_{ss}}{D} \quad (4.18)$$

$$P_{FA,ss} = \alpha_{FA} X_{ss} + \frac{\beta_{FA} X_{ss}}{D} \quad (4.19)$$

An additional steady-state equation for volumetric succinic acid productivity was included:

$$DP_{SA,ss} = \alpha_{SA} DX_{ss} + \frac{\beta_{SA} X_{ss}}{D} \quad (4.20)$$

The steady-states of Eq. 4.20 were then plotted against dilution rate. Graphically determined

optimal dilution rate corresponding to maximum steady-state volumetric productivity was used to obtain the steady-state outlet liquid-phase biomass, glucose, and carboxylic acid product concentrations. Optimal dilution rate was also obtainable by setting the derivative of steady-state volumetric productivity with respect to dilution rate to 0. The fermentor liquid volume specifying dimensions for the baseline process as well as the CFD simulation was the ratio of F to optimal dilution rate. A 3:1 liquid fermentor height to diameter ratio was then assumed:

$$D_T = \left( \frac{4V_L}{3\pi} \right)^{1/3} \quad (4.21)$$

Where  $D_T$  is fermentor diameter (m). Single-phase flow for Newtonian fluid, a three-impeller, 6-blade Rushton-turbine agitator, and a uniform inter-impeller axial spacing and distance from the bottom [46] equal to impeller diameter which itself was a third of fermentor diameter were assumed for both the baseline process and CFD simulation. For the baseline process, 40°C inlet temperature and 200 rpm agitation speed was assumed. CFD was used to simulate the effect of inlet temperature at 40°C and 42°C and impeller speeds at a minimal value, 100 rpm, and 200 rpm on cooling jacket area. Minimal impeller speed was estimated as follows [34]:

$$N_0 = \left( 1.22 + 1.25 \left( \frac{D_T}{D_{impeller}} \right) \right) \left( \frac{\sigma g}{\rho_f} \right)^{1/4} \quad (4.22)$$

where  $N_0$  is minimum impeller speed (rps),  $\sigma$  is surface tension of fermentation broth (dyne/m) and  $\rho_f$  is fermentation broth density (kg/m<sup>3</sup>).

In addition to this simulation, the CFD flow fields resulting from a smaller fermentor liquid

volume and alternate impeller spacing [47] were visualized. For this the bottom, middle, and top impeller distance from the fermentor bottom were instead multiples of 0.166, 1.2, and 1.967 times the fermentor diameter. The multiple reference frame (MRF) model was applied until the flow fields in the stirred-tank fermentor converged to steady-state values. MRF involved a steady-state approach in which individual cell zones moved at different rotational speeds. The flow fields for zones with impellers were solved with MRF equations, whereas those with no moving parts were solved using stationary-frame equations. The CFD governing equations were provided in the FLUENT (v.6.3.26) documentation [36]. Among these were the continuity equations, momentum equations, and turbulence model equations used to calculate the fluctuations involving momentum. To predict the effects of inlet temperature and impeller speed, non-aerated agitator power consumption was calculated by CFD as follows:

$$P_{impeller_0} = 2\pi N_{impeller} M \quad (4.23)$$

where  $P_{impeller_0}$  is non-aerated impeller power consumption (W), and  $M$  is torque (moment) on the axis due to the impeller (N•m). Alternatively, a dimensionless power number  $N_p$  could be determined graphically from a Reynold's Number to estimate non-aerated power consumption as follows [44]:

$$Re_p = \frac{N_{impeller} D_{impeller}^2 \rho_f}{\mu_f} \quad (4.24)$$

where  $\mu_f$  is fermentation broth dynamic viscosity and [44]:

$$P_{impeller_0} = N_p \rho_f N_{impeller}^3 D_{impeller}^5 \quad (4.25)$$

The Finite Volume Method (FVM) was the CFD numerical solution technique used since it accommodated unstructured meshes and was based on fundamental laws of conservation [48]. The continuity and momentum equations were discretized into algebraic equations and then solved numerically. The SIMPLE algorithm was used to solve velocity-pressure coupled differential equations. No-slip boundary conditions were applied on all walls. The wall temperature was set at the fermentation broth temperature 39°C [6]. The convergence criteria required that the scaled residuals decrease to 10<sup>-5</sup> for each conservative equation. For gas-liquid two-phase flow where  $Re > 10,000$ , mixing time (s) was estimated as follows [44]:

$$t_m = \frac{6 \left( \frac{D_T}{D_{impeller}} \right)^3}{N_{impeller} N_p^{0.33}} \quad (4.26)$$

Aerated power consumption  $P_{impeller_g}$  was then calculated [44]:

$$\frac{P_{impeller_g}}{P_{impeller_0}} = 0.10 \left( \frac{F_g}{N_{impeller} V_L} \right)^{-0.25} \left( \frac{N_{impeller}^2 D_{impeller}^4}{g H_{impeller} V_L^{2/3}} \right)^{-0.20} \quad (4.27)$$

where  $F_g$  is volumetric CO<sub>2</sub> gas flow rate (m<sup>3</sup>/s),  $g$  is gravitational constant (m<sup>2</sup>/s), and  $H_{impeller}$  is height of impeller blade (m). The rate  $F_g$  was obtained from  $V_L$  and the 0.25 vvm of pure CO<sub>2</sub> reportedly sparged in *M. succiniciproducens MBEL55E* fermentation [6]. A superficial CO<sub>2</sub> gas velocity  $v_g$  (m/s) was obtained from  $F_g$  and  $D_T$ , and a volumetric gas-liquid mass transfer coefficient  $k_L a$  (s<sup>-1</sup>) was calculated from an empirical correlation for non-coalescing (dirty) dispersions as follows [34]:

$$k_L a = 0.002 \left( \frac{P_{impeller\ g}}{V_L} \right)^{0.7} v_g^{0.2} \quad (4.28)$$

Using the CFD-derived  $k_L a$ , the steady-state  $CO_2$  liquid-phase concentration exiting the fermentor  $[CO_{2L}]_{ss}$  ( $kg/m^3$ ) was then solved from the following steady-state mass balance:

$CO_2$  Liquid-Phase Mass Balance:

$$\frac{dV_L [CO_{2L}]_{ss}}{dt} = 0 = F_L ([CO_{2L}]_0 - [CO_{2L}]_{ss}) + K_g a V_L P \left( y - \frac{H [CO_{2L}]_{ss}}{P} \right) - r_{co_2} V_L \quad (4.29)$$

where  $[CO_2]_0$  is inlet  $CO_2$  concentration ( $kg/m^3$ ),  $y$  is  $CO_2$  mass fraction in inlet gas sparging stream,  $H$  is Henry's Law constant ( $Pa\ kg\ CO_2\ m^{-3}$ ),  $P$  is total pressure ( $Pa$ ),  $r_{co_2}$  is volumetric rate of consumption of  $CO_2$  by reaction in the liquid phase ( $kg/s$ ), and  $K_g a$  is overall gas phase mass transfer coefficient ( $kg\ Pa^{-1}\ s^{-1}$ ). The  $K_g a$  was approximated with  $k_g a$  assumed negligible:

$$\frac{1}{K_g a} = \frac{1}{k_g a} + \frac{H}{k_L a} \quad (4.30)$$

It was assumed that there was no axial or time-dependence on the gas phase composition of the bubble since pure  $CO_2$  was assumed sparged and  $y = 1$ . Total pressure accounted for atmospheric and fermentor height-dependent hydrostatic pressure.  $CO_2$  is incorporated in the PEP carboxylation pathway [32], and a reported 1:1 ratio of moles of  $CO_2$  fixed to moles of succinic acid produced [6] was used for calculation of  $r_{co_2}$ . Metabolic production of  $CO_2$  by *M. succiniciproducens* was not modeled [6]. The Henry's Law constant was adjusted for ionic strength of fermentation broth using Bunsen coefficients [32]. The inlet liquid-phase concentration  $[CO_2]_0$  was  $0\ kg/m^3$ .

Flow rates and solved  $[CO_{2L}]_{ss}$  concentration and inlet gas-phase concentration  $[CO_{2G}]_0$  were then used to calculate steady-state gas-phase  $CO_2$  concentration  $[CO_{2G}]_{ss}$  exiting the fermentor at the top ( $kg/m^3$ ) from a total  $CO_2$  fermentor mass balance. The mass fraction of water vapor also exiting the top was estimated from ratio of water vapor pressure estimated with the Antoine equation [49] at atmospheric pressure and  $39^\circ C$  to total atmospheric pressure. This and the exiting  $CO_2$  gas mass flow rate  $F_{CO_{2g-out}}$  ( $kg/s$ ) were then used to obtain a mass flow rate of exiting water vapor  $F_{waternvapor-out}$  ( $kg/s$ ). With gas and liquid-phase mass flow rates now specified, a fermentor energy balance provided the heat removed term using the agitator power consumption and exiting  $CO_2$  and water vapor enthalpy terms obtained from CFD simulation:

$$Q_{removed} = \eta_{impeller} P_{impeller_g} + \sum_{i=1}^n F_{i_{in}} H_{i_{in}} - \sum_{i=1}^n F_{i_{out}} H_{i_{out}} \quad (4.31)$$

Where  $Q_{removed}$  removed is rate of heat to be removed ( $J/s$ ),  $\eta_{impeller}$  is gearbox efficiency,  $F_{i_{in}}$  and  $F_{i_{out}}$  are inlet and outlet mass flow rates of components  $i$ , respectively ( $kg/s$ ),  $H_{i_{in}}$  and  $H_{i_{out}}$  are inlet and outlet mass enthalpy of components  $i$ , respectively ( $J/kg$ ). With exception of terms for water vapor involving a phase change and *M. succiniciproducens* cells, component enthalpy terms were calculated as follows:

$$H_i = H_i^\circ(T_R) + \int_{T_R}^{T_2} C_{p_i} dT \quad (4.32)$$

where  $H_i^\circ(T_R)$  is heat of combustion for component  $i$  ( $J/kg$ ) at reference temperature  $T_R = 25^\circ C$ ,  $T_2$  is fermentation broth temperature of  $39^\circ C$  for outlet streams and either the baseline  $40^\circ C$  or

simulated 42°C for inlet liquid streams, and  $C_{p_i}$  is heat capacity of component i (J/kg-C). Water vapor mass enthalpy was similarly calculated but by also adding an enthalpic enthalpy of vaporization for water vapor (J/kg). Heat of combustion mass enthalpy for *M. succiniciproducens* cell biomass on dry-weight, 8% ash-basis was calculated by the Dulong equation [34]:

$$H_{cell}^{\circ} = 8.076C + 34.462\left(H - \frac{O}{8}\right) \quad (4.33)$$

where C, H, and O represent the experimentally-determined weight fractions of carbon, hydrogen, and oxygen, respectively, for *M. succiniciproducens* from its cell elemental composition  $CH_{1.736}O_{0.367}N_{0.240}$  [6]. Assuming cooling water with inlet and outlet temperatures of 25°C and 35°C flowing through an external jacket having a small equivalent width of 0.0254 m, a high cooling water mass flow rate was obtained from  $Q_{removed}$ , temperature difference, and water heat capacity. Fermentor cooling jacket heat transfer area requirement was therefore calculated:

$$A_{heat} = \frac{Q_{removed}}{U(T_C - T_F)} \quad (4.34)$$

where U is overall heat transfer coefficient (W/m<sup>2</sup>-C), T<sub>C</sub> is average cooling water temperature of 30°C, and T<sub>F</sub> is fermentation broth temperature of 39°C. Like the previous overall mass transfer coefficient K<sub>g</sub>a, overall heat transfer coefficient was approximated as a sum of resistances in series as follows:

$$\frac{1}{U} = \frac{1}{h_F} + \frac{1}{h_{FD}} + \frac{\Delta x}{k_W} + \frac{1}{h_C} + \frac{1}{h_{CD}} \quad (4.35)$$

where  $h_F$  is heat transfer coefficient for the fermentation broth (W/m<sup>2</sup>-C),  $h_{FD}$  is heat transfer

coefficient (a.k.a. dirt factor) from fermentation broth fouling deposits ( $\text{W/m}^2\text{-C}$ ),  $k_w$  is thermal conductivity of the fermentor wall stainless steel ( $\text{J/m}^2$ ),  $\Delta x$  is fermentor wall thickness (m),  $h_c$  is cooling water heat transfer coefficient ( $\text{W/m}^2\text{-C}$ ), and  $h_{CD}$  is cooling water fouling deposits heat transfer coefficient ( $\text{W/m}^2\text{-C}$ ). The fermentation broth heat transfer coefficient  $h_F$  depended directly on impeller speed and diameter specified for CFD simulation as follows [34]:

$$\frac{h_F D_T}{k_F} = 0.42 \left( \frac{D_{impeller}^2 N_{impeller} \rho_F}{\mu_F} \right)^{0.66} \left( \frac{C_{pF} \mu_F}{k_F} \right)^{0.33} \left( \frac{\mu_F}{\mu_w} \right)^{0.14} \quad (4.36)$$

where  $\mu_w$  is wall viscosity ( $\text{kg/s-m}$ ) and  $k_F$  is fermentation broth thermal conductivity ( $\text{W/m-C}$ ). Effect of impeller speed and inlet temperature on heat transfer area was therefore simulated.

#### 4.3.4 Cell Microfiltration

A two-stage cross-flow tubular microfiltration unit, whereby the retentate of the first stage became the feed of the second stage, then removed and recovered all cells from the broth exiting the fermentor containing succinate, acetate, formate, lactate, and unconsumed glucose. The intended recycle of cells back to the fermentor for simplicity was not simulated. Final cell retentate concentration was limited to  $100 \text{ kg/m}^3$  because this corresponded to an exponential increase in viscosity and a non-Newtonian transition of a lactic acid fermentation broth increasing pump energy consumption [50]. For the mass balance, the permeate volumetric flow rate of the first stage was equal to that of the second stage, and inter-stage recycle ratio was equal to 1. All non-cell components in the feed transferred to the permeate because they were below the molecular weight

cutoff of the microfiltration membrane. Recirculation rate was 6m/s. Steady-state permeate flux was estimated using a gel polarization model [51, 52]:

$$J_{micro-2} = 1.31 \left( \frac{D_{cell}^2 \gamma}{L_{micro-2}} \right)^{1/3} \left( \frac{C_{gcell}}{C_{ocell}} - 1 \right)^{1/3} \quad (4.37)$$

where  $D_{cell}$  is particle diffusion coefficient of *M. succiniciproducens* cells in succinic acid fermentation broth ( $m^2/s$ ),  $L_{micro-2}$  is tube length (m),  $\gamma$  is shear rate ( $s^{-1}$ ),  $C_{gcell}$  is gel polarization volume fraction, and  $C_{ocell}$  is bulk cell volume fraction. Effect of single-stage on area and power requirements, calculated as before, was simulated and compared to two-stage baseline process.

#### 4.3.5 Absorption and Desorption

A granulated activated carbon (GAC) counter-current moving-bed adsorber then removed 98% of glucose from microfiltration permeate to further purify the products. Intended recycle of glucose back to the fermentor for simplicity was not simulated. Only 2.5% lactate and 1% succinate was lost in the sorption process. GAC sorbent was selected for its low cost and future derivation from biochar via pyrolysis of recovered lignin. Column height was estimated from the product of NTU (Number of Transfer Units) and HTU (Height of Transfer Units). NTU was calculated by integrating area from a plot of the single-component glucose equilibrium curve and of the mass balance-derived operating line [53]. The adsorption equilibrium curve was generated from Langmuir single-component glucose-GAC equilibria isotherm data [54]:

$$q_{glu} = \frac{q_{m_{glu}} b C_{glu}}{1 + b C_{glu}} \quad (4.38)$$

where  $q_{\text{glu}}$  is glucose concentration in GAC sorbent phase (mol glucose/kg GAC sorbent),  $q_m$  is maximum sorbent capacity (mol glucose/kg GAC sorbent),  $C_{\text{glu}}$  is glucose concentration in liquid phase (mol glucose/m<sup>3</sup> feed solution). HTU was estimated as follows [53]:

$$HTU = \frac{v_{\text{adsorber}}}{K_{\text{adsorber}} a_i} \quad (4.39)$$

where  $K_{\text{adsorber}}$  is overall mass transfer coefficient (m/s),  $v_{\text{adsorber}}$  is industry-acceptable adsorber hydraulic loading rate based on selected column diameter (m/s), and  $a_i$  is particle interfacial area/volume ratio (m<sup>-1</sup>) calculated as follows:

$$a_i = \frac{6(1 - \varepsilon)}{d_p} \quad (4.40)$$

where  $\varepsilon$  is bed porosity or void fraction (dimensionless) and  $d_p$  is GAC particle diameter (m), which for the baseline process was 800  $\mu\text{m}$  but was also simulated at 600  $\mu\text{m}$ . Overall mass transfer coefficient  $K_{\text{adsorber}}$  was estimated as follows [55]:

$$\frac{1}{K_{\text{adsorber}}} = \frac{1}{k_{\text{film}}} + \frac{1}{q_m k_s} \quad (4.41)$$

where  $k_{\text{film}}$  is film-mass transfer coefficient (m/s) and  $k_s$  is intra-particle mass transfer coefficient (m/s). The  $k_{\text{film}}$  and  $k_s$  and associated effective and Knudsen diffusivities were estimated from empirical correlations [55]. Adsorber column pressure drop for pump power consumption was estimated with the Ergun equation [56]. For a desorber column, it was assumed that regenerant had 0% glucose entering. A 96% regeneration yield in the desorber was assumed using 90°C hot water with 4% NaOH, 0.3% oxidant, and 0.1% surfactant [57]. Regeneration flow rate was assumed 25%

greater than adsorber feed flow rate.

#### 4.3.6 Nanofiltration

A single-stage cross-flow hollow-fiber nanofiltration unit then separated the succinate from all formate, acetate, and most lactate by exploiting both the unique divalent ( $2^-$ ) charge of succinate and its molecular weight and size [17]. Succinate rejection in quaternary solutions containing monovalent formate, lactate, and acetate anions was shown to be much higher than that in single-salt solution because of their facilitated transport due to Donnan effect in the presence of divalent succinate anion [17]. For the mass balance, at maximum permeate flux, the rejection coefficients were 95%, 38%, 0.01%, and -60% for succinate, lactate, acetate, and formate, respectively [17]. The quaternary mixture of 0.3 M succinate, 0.1 M acetate, 0.1 M lactate, and 0.1 M formate salts that corresponded to these rejection coefficients using an NF45 membrane was formulated to simulate an actual fermentation medium [17]. These published values were deemed applicable for our model because the feed mixture's 0.3 M succinate concentration [17] was similar to the 0.284 M succinate concentration from our process mass balance. Similarly high succinate rejection coefficients of 97%, 95%, and 84% at 400, 300, and 200 psig trans-membrane pressures, respectively, were also previously obtained in another work and suggested that succinate rejection became increasingly less dependent on transmembrane pressure as transmembrane pressure increased. [26]. Hollow-fiber modules were selected over plate-frame module because particulate plugging was a low risk. Operating conditions for recirculation flow

rate, trans-membrane pressure, number and length of hollow fibers were from literature [17, 58]. Retentate bulk and gel polarization concentrations depended on succinate having highest molecular weight and concentration of all salts. Steady-state permeate flux was estimated via a gel polarization model for dissolved solutes [58]:

$$J_{nano} = k_{nano} \ln \frac{C_{gsuc}}{C_{0suc}} \quad (4.42)$$

where  $k_{nano}$  is succinate mass transfer coefficient (m/s),  $C_{g-suc}$  is gel polarization concentration ( $\text{kg/m}^3$ ), and  $C_{o-suc}$  is bulk feed concentration of succinate ( $\text{kg/m}^3$ ). The  $C_{g-suc}$  was obtained by first plotting steady-state permeate flux as a function of trans-membrane pressure for reported succinate concentrations [17]. Natural logarithm of sodium succinate concentration was then plotted against these fluxes to yield a straight line equation where the x-intercept corresponding to  $J_{nano} = 0$  at  $C_g/C_o = 1$  represented the  $C_{g-suc}$  of interest. The  $k_{mt}$  was determined from a  $j_D$ -factor correlation for hollow fibers and turbulent flow regime [58]. Area and power requirement were calculated as before.

#### 4.3.7 Ion-Exchange Chromatography

Nanofiltration retentate then entered one of two fixed-bed ion exchanger columns containing weak anion exchange Dowex resin to both acidify and purify the undisassociated (protonated) succinic acid from lactic acid via its greater hydrophobicity and unique divalent charge [31]. Column loading of the binary lactate and succinate mixture occurred at  $\text{pH}=4$  above the  $\text{pK}_a$  of lactic acid and below the  $\text{pK}_{a1}$  of succinic acid [31]. While one column was loaded, a second was regenerated

with three bed volumes of 90°C water [59]. Loading and regeneration times were equal for steady-state operation. Sorption temperature exceeded 55°C to prevent crystallization of the highly concentrated succinic acid, although its adsorption efficiency on Amberlite resin is reportedly reduced at higher temperatures [60]. Ion exchange column height was the sum of SBH (Stoichiometric Bed Height) [61] and LUB (Length of Unused Bed) [40]:

$$LUB = \left(1 - \frac{t_b}{t^*}\right)L_1 \quad (4.43)$$

where  $L_1$  is length of small-scale column (m),  $t_b$  is breakthrough time for succinic acid (s),  $t^*$  is midpoint time for succinic acid (s).  $t_b$  and  $t^*$  were estimated from the breakthrough curves of lactic and succinic acids on Dowex resin column [31], and:

$$SBH = \frac{v_{ion} t_s}{(1 - \varepsilon) \left( \frac{q_0}{c_0} \right)} \quad (4.44)$$

where  $v_{ion}$  is industry-acceptable ion-exchanger hydraulic loading rate based on selected column diameter (m/s),  $q_0/c_0$  is ratio of feed succinate liquid-phase concentration to Dowex sorbent succinate solid phase-concentration in equilibrium, and  $t_s$  is service time (s). A service time of 3600 seconds corresponded to 15 column-bed loading volumes when column regeneration initiated [31]. To derive  $q_0/c_0$ , a multi-component equilibria Langmuir model and constants accounting for 1-1 and 1-2 binding were used to generate equilibrium curves [31].

#### 4.3.8 Crystallization

Ion exchanger eluant then entered an idealized continuous, circulating magma, stirred-tank,

cooling-type MSMPR (Mixed Solution Mixed Product Removal) crystallizer to supersaturate only anhydrous 2- succinic acid from solution at pH = 2 and 4°C [16]. Yield was obtained [62]:

$$Y_{cry} = S_{ow} R_h [C_{0suc-cry} - C_{Fsuc-cry} (1 + V_d - V_e)] \quad (4.45)$$

where  $Y_{cry}$  is maximum yield rate of crystal produced (kg/s),  $S_{ow}$  is weight of original free solvent water (kg/s),  $V_d$  is added diluent (kg/kg original free solvent water),  $V_e$  is solvent loss from evaporation (kg/kg original free solvent water),  $C_{0suc-cry}$  is initial concentration of succinic acid crystal in feed (kg anhydrous succinic acid/kg free solvent water),  $C_{Fsuc-cry}$  is final concentration assumed to be solubility at 4°C and pH = 2 of succinic acid crystal in saturated mother liquor (kg anhydrous succinic acid/kg free solvent water), and  $R_h$  is ratio of molecular weights of hydrate and anhydrous salts. About 2% of the water in the feed was assumed evaporated. Crystal growth was size-dependent, and nucleation was mediated by both primary and secondary mechanisms from crystal-crystallizer impeller or wall collisions [63]. To estimate crystallizer volume, experimentally-derived batch kinetic expressions for succinic acid nucleation and growth rates as functions of supersaturations were available in literature [30]:

$$B = k_B \Delta c^b M_T^v N_{cry-impeller}^z \quad (4.46)$$

$$G = k_g \Delta c^s N_{cry-impeller}^p \quad (4.47)$$

However, we combined these into a more useful relative-kinetic expression:

$$B = k_n N_{cry-impeller}^h G^g M_T^j \quad (4.48)$$

where B is crystal nucleation rate ( $s^{-1}$ ), G is crystal growth rate ( $s^{-1}$ ), N is impeller speed (rps),  $M_T$

is magma density (kg succinic acid crystal/m<sup>3</sup> mother liquor), and  $k_n$ ,  $k_g$ ,  $k_B$ ,  $h$ ,  $s$ ,  $j$ ,  $b$ ,  $v$ ,  $z$  are dimensionless coefficients and exponents. Assuming a power-volume ratio  $\varepsilon$  proportional to impeller speed as  $\varepsilon = P/V \sim N^3$ , by substitution crystallizer residence time was then estimated [63]:

$$L_m = 3.67 \left[ \frac{\varepsilon^{-3h} M_T^{1-j} \tau^{g-1}}{6k_v \rho_c k_n} \right]^{\frac{1}{g+3}} \quad (4.49)$$

where  $\tau$  is residence time (s),  $L_m$  is median crystal size (m),  $\varepsilon$  is power-volume ratio,  $k_v$  is succinic acid crystal rhombic shape factor [30, 64],  $\rho_c$  is succinic acid crystal density (kg/m<sup>3</sup>). Because  $j = 1$ , crystal size and residence time were not functions of magma density. Also, because the growth to nucleation ratio  $>1$  and  $g > j$ , crystal size was a function of residence time. The crystallizer did not include fines removal or crystal size classification. However, a 550  $\mu\text{m}$  median crystal size was assumed and corresponded to a low 17.8% by weight adherence of residual mother liquor [63] to later affect filter cake porosity and reduce downstream rotary drum filter liquid washing costs. As for fermentor, crystallizer magma volume was estimated from volumetric flow rate and residence time.

#### 4.3.8 Economic Analysis

The biorefinery was considered an attractive investment only if recovery of investment period was less than 5 years. All costs were indexed for year 2010. No financial costs were included. Operating costs, investments and their adjustments by capital costs estimated from the materials of construction, etc. for sized units of operation from an ethanol biorefinery were used from literature [37]. Fixed costs were adjusted to include shift operators, shift supervisors, and yard employees for

the operation of the downstream processes. The current variable cost of \$60 U.S./t of corn stover included harvesting, storage, transportation, and handling costs. A 10% per year depreciation rate for fixed-capital equipment with no salvage value was assumed. Sensitivity analysis was done to determine production costs when corn stover prices were \$60/t and increased to \$80 and \$100/t, assuming a succinic acid yield of 1) that obtained in our baseline simulated process (Scenario A), 2) 15% (Scenario B), and 3) 19% (Scenario C). Current and future product market selling prices of \$1/kg, \$1/kg, \$0.20/kg, \$0.30/kg, and \$40MW/h for succinic acid, acetic acid, formic acid, ethanol, and generated electricity, respectively, were used to determine annual revenues[65]. Because the targeted product was succinic acid, contributions to total production cost were assumed 60%, 5%, 5%, and 30% for succinic acid, acetic acid, formic acid, and ethanol, respectively.

#### **4.4. Results and Discussion**

An overall yield of 12.9% succinic acid, 10% ethanol, 5.4% acetic acid, 5.3% formic acid, and 0.5% lactic acid from corn stover feedstock was estimated after crystallization for the baseline process (Figure 4.3)

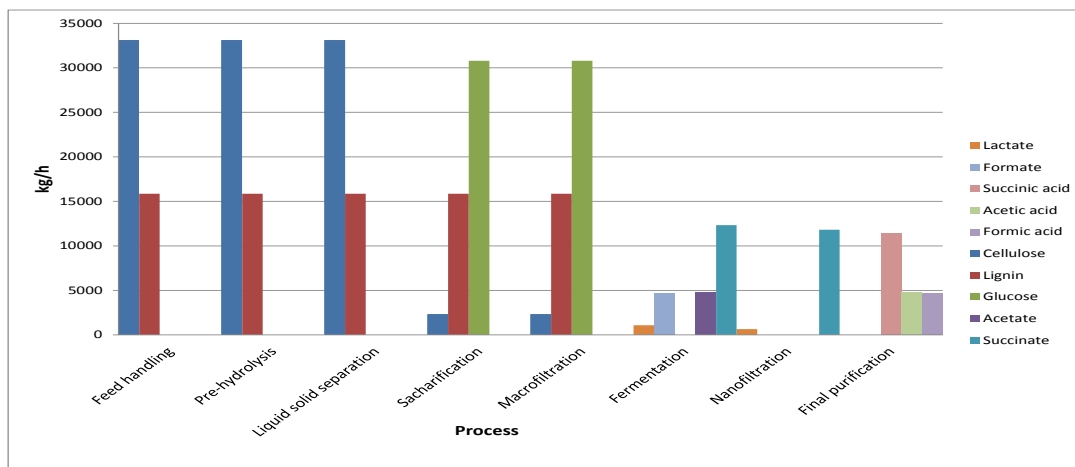


Figure 4.3. Changes in major stream flow rates throughout process

The major process mass flow rates, temperatures, and pressures are depicted (Table 4.3). For 88542 kg/hr of corn stover feedstock, 11453 kg/hr succinic acid crystal was produced. Estimated area or volume requirements for the downstream units of operation are shown (Table 4.4). Simulation of microfiltration of insoluble lignin showed that area requirement decreased and pump power consumption increased with increasing recirculation rate (Figure 4.4). The baseline 6 m/s recirculation rate consumed 123.325 kW and resulted in a permeate flux of 0.0048 m/s.

Table 4.3. Major processes and associated flow rates, temperatures, and pressures

Corn Stover Feed Handling	Values	Pre-Hydrolysis	Values	Blow-Down Tank	Values	Liquid-Solid Separation	Values
Temperature (°C)	40	Temperature (°C)	245	Temperature (°C)	101	Temperature (°C)	70
Pressure (atm)	1	Pressure (atm)	13.6	Pressure (atm)	1	Pressure (atm)	1
Stream ID	Flow rate (kg/hr)	Stream ID	Flow rate (kg/hr)	Stream ID	Flow rate (kg/hr)	Stream ID	Flow rate (kg/hr)
1	88542	5	137565	8	295139	10	256479
2	15625	6	3250	9	38660	11	148758
3	12042	7	154324			12	312095
4	45440						
Slurring Tank	Values	Sacharification	Values	Lignin Microfiltration	Values	Centrifugation	Values
Temperature (°C)	65	Temperature (°C)	65	Temperature (°C)	65	Temperature (°C)	65
Pressure (atm)	1	Pressure (atm)	1	Pressure (atm)	1.48	Pressure (atm)	1
Stream ID	Flow rate (kg/hr)	Stream ID	Flow rate (kg/hr)	Stream ID	Flow rate (kg/hr)	Stream ID	Flow rate (kg/hr)
13	93142	16	262335	17	262335	18	78004
14	564					19	37694
15	168628						
Fermentation	Values	Cell Microfiltration Stage#1	Values	Cell Microfiltration Stage#2	Values	Adsorption and Desorption	Values
Temperature (°C)	39	Temperature (°C)	39	Temperature (°C)	39	Temperature (°C)	68
Pressure (atm)	1	Pressure (atm)	1.97	Pressure (atm)	1.97	Pressure (atm)	1
Stream ID	Flow rate (kg/hr)	Stream ID	Flow rate (kg/hr)	Stream ID	Flow rate (kg/hr)	Stream ID	Flow rate (kg/hr)

20	40310	23	224641	25	144952.5	28	159377
21	184331	24	79688.5	26	79688.5	29	199287
22	224641			27	65264	30	199221
Nanofiltration	Values	2-Column Ion Exchange	Values	Crystallization	Values		
Temperature (°C)	25	Temperature (°C)	73	Temperature (°C)	4		
Pressure (atm)	20.41	Pressure (atm)	1	Pressure (atm)	1		
Stream ID	Flow rate (kg/hr)	Stream ID	Flow rate (kg/hr)	Stream ID	Flow rate (kg/hr)		
31	159310	34	51424.2	37	795		
32	99569	35	59741.3	38	39168		
33	59741	36	51424.2	39	11461		

Using the available baseline kinetic terms of *M. succiniciproducens* for fermentation resulted in an overall succinic acid 12.9% yield that was less than the 18.65% yield from dried biomass from *C. glutamicum* [5] having unreported kinetic model parameters. However, replacing the *M. succiniciproducens* succinic acid productivity term  $\alpha_{SA} = 1.169$  (kg/kg) with the  $\alpha_{SA} = 3.60$  (kg/kg) reported for *A. succinogenes*, overall succinic yield nearly doubled to 25%, exceeding even the *C. glutamicum* yield. Such 25% yield using a term not of *C. glutamicum* but of the less productive *A. succinogenes* suggests improvements in both fermentation and our novel downstream recovery and purification are responsible. An optimal dilution rate of  $1.20 \text{ hr}^{-1}$  corresponding to maximum *M. succiniciproducens* volumetric succinic acid productivity of  $69.23 \text{ kg m}^{-3} \text{ hr}^{-1}$  was predicted graphically (Figure 4.5) and compared well with the reported maximum *M. succiniciproducens*

specific growth rate of  $1.12 \text{ hr}^{-1}$  at a dissolved  $\text{CO}_2$  concentration of  $23.3 \text{ mM}$  [32]. This optimal dilution rate then provided a baseline fermentor liquid volume of  $178.29 \text{ m}^3$ , liquid height of  $12.69 \text{ m}$ , and diameter of  $4.23 \text{ m}$  as CFD inputs.

Table 4.4. Dimensional Requirements of Units of Operation for Simulated Baseline Process

Unit of Operation	Area ( $\text{m}^2$ )	Volume ( $\text{m}^3$ )
Lignin Microfiltration	6.82	-
Centrifuge	106.48	
Fermentor	-	178.40
Fermentor Cooling Jacket	46.83	-
Cell Microfiltration	765	-
Adsorber	-	25.91
Nanofiltration	6220	-
Ion Exchanger	-	17.14
Crystallizer	-	16.60

The extent that cooling jacket heat transfer area was linearly reduced by increasing  $N_{impeller}$  from 10 rpm to 200 rpm at both  $40^\circ\text{C}$  and  $42^\circ\text{C}$  inlet temperatures were simulated (Figure 4.6). At inlet  $T_2$  of  $40^\circ\text{C}$ , at 200 rpm, CFD predicted the average liquid speed of  $3.01 \text{ m/s}$ ,  $P_{impeller_0}$  of  $433391 \text{ Watts}$ ,  $k_{La}$  of  $0.230 \text{ s}^{-1}$ ,  $[CO_{2L}]_{ss}$  of  $34.9 \text{ mM}$ , and  $A_{heat}$  of  $19.4 \text{ m}^2$ , while at 100 rpm, CFD predicted an average liquid speed of  $1.50 \text{ m/s}$ ,  $P_{impeller_0}$  of  $54575.3 \text{ Watts}$ ,  $k_{La}$  of  $0.052 \text{ s}^{-1}$ ,  $[CO_{2L}]_{ss}$  of  $33.32 \text{ mM}$ , and  $A_{heat}$  of  $55.4 \text{ m}^2$ . The  $A_{heat}$  appears to linearly decrease with a regression coefficient of  $r^2=0.9896$  as follows:

$$A_{heat} = -0.4291N_{impeller} + 103.47 \quad (4.50)$$

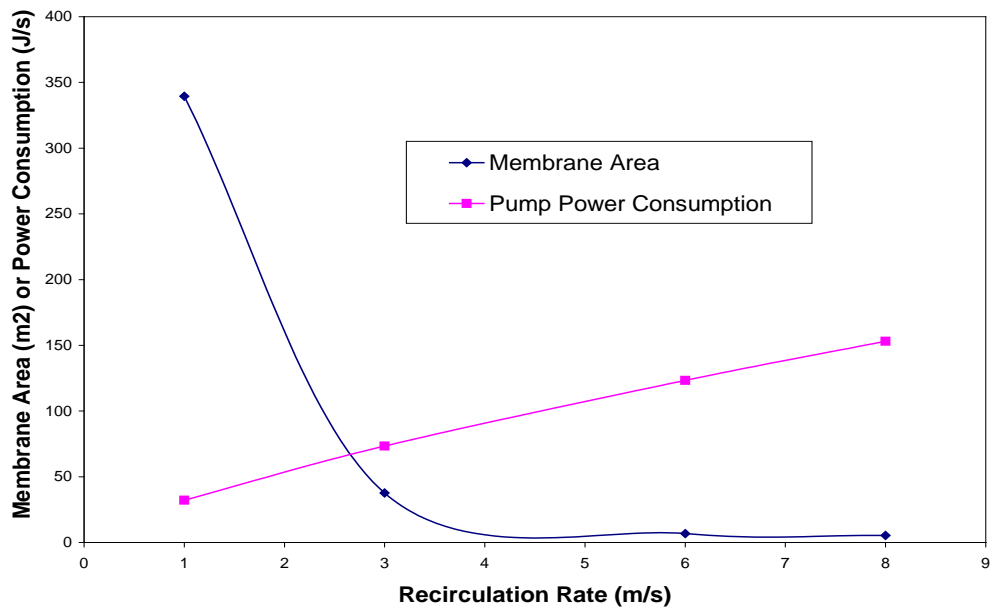


Figure 4.4. Lignin microfiltration membrane area and power consumption vs. recirculation rate

The predicted  $[CO_{2L}]_{ss}$  values at these conditions are within the same order of magnitude as the reported 23.3 mM when sparging with pure  $CO_2$  at partial pressure of 101.4 kPa ( $y = 1$ ) in a 2.2 L liquid volume fermentor at 39°C agitated at 200 rpm [32]. Assuming instead an inlet  $T_2$  of 42°C and minimal  $N_0$  of 10 rpm, a higher heat term  $Q_{removed}$  of 869993 W resulted, and CFD predicted an  $A_{heat}$  of 211.7 m<sup>2</sup> exceeding the available fermentor surface area of 168.6 m<sup>2</sup>. Another external heat exchanger or more efficient spiral-wound cooling coils are therefore necessary for cooling at these impeller and inlet temperature conditions.

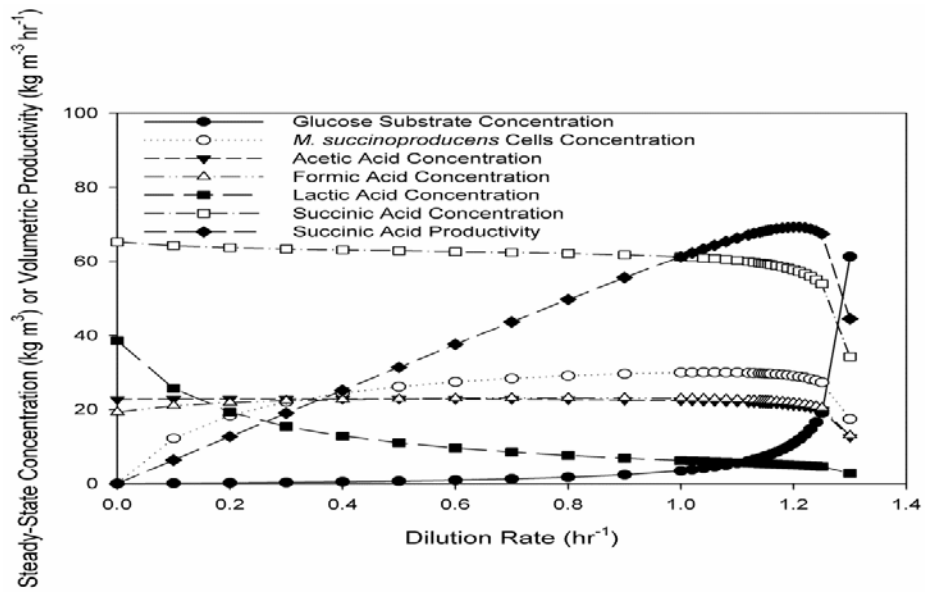


Figure 4.5. Graphical estimation of optimal steady-states and dilution rate for *M.*

*succinoproducens* fermentor

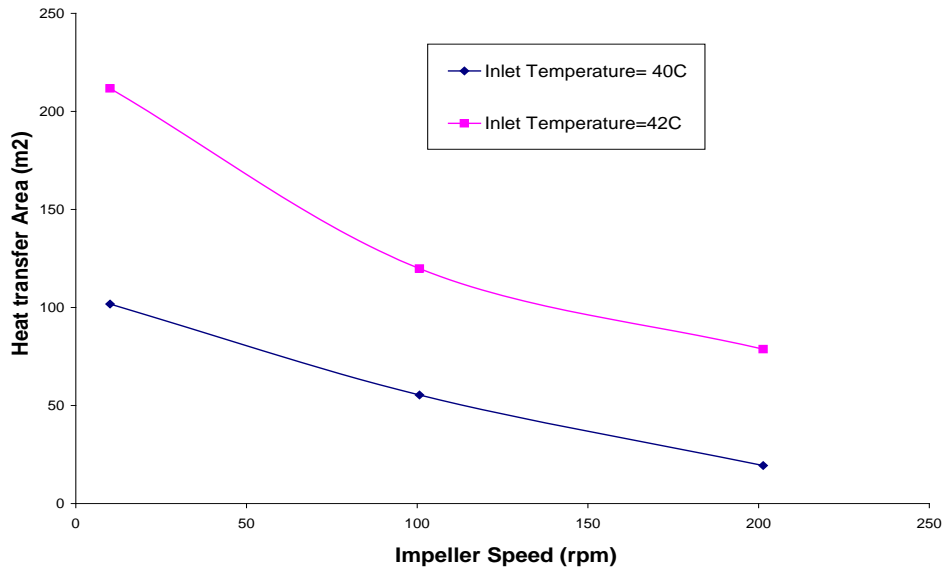


Figure 4.6. CFD Simulation of Cooling Heat Transfer Area vs. Impeller Speed for 178 m<sup>3</sup> fermentor

The CFD fermentor flow fields simulated at 10 rpm, 100 rpm, and 200 rpm are visually presented (Figure 4.7). There is a more pronounced increase in average velocity from 10-100 rpm than from 100-200 rpm. At 200 rpm, using instead a graphical power number correlation for power consumption, heat transfer area increases with impeller diameter up to an asymptotic value of 48 m<sup>2</sup> corresponding to the impeller diameter of 2 m (Figure 4.8). The CFD fermentor flow field simulated at 200 rpm for both baseline 178 m<sup>3</sup> and a 78 m<sup>3</sup> fermentor are visually presented (Figure 4.9). Maximum velocity of 16.9 m/s and 10.4 m/s is predicted for the large and small fermentor, respectively. A 3:1 height to diameter ratio was specified for our process, but future CFD simulations can instead predict hydrodynamic changes from varying fermentor height. At

minimum, additional hydrostatic head from increased liquid height would impact the gas-liquid  $\text{CO}_2$  mass transfer of rising bubble flow.

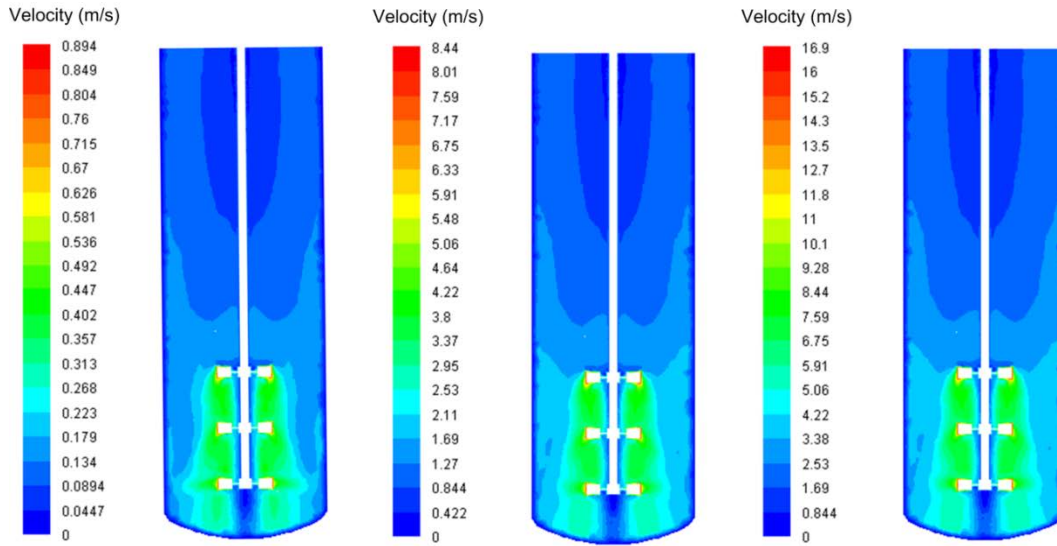


Figure 4.7. CFD average liquid velocity flow fields at 10, 100, and 200 rpm in 178 m<sup>3</sup> fermentor

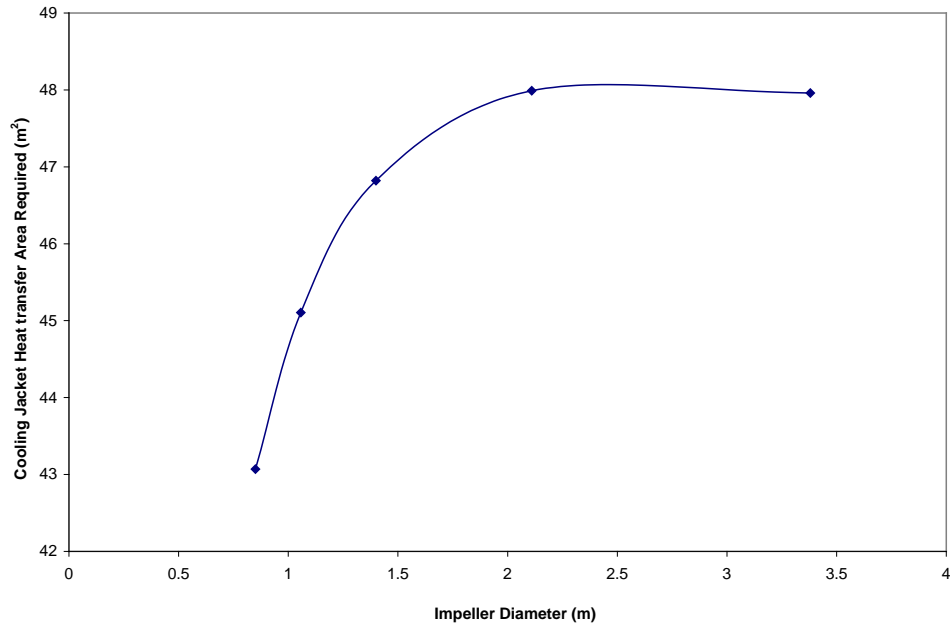


Figure 4.8. Cooling heat transfer area requirement vs. impeller diameter for 178 m<sup>3</sup> fermentor

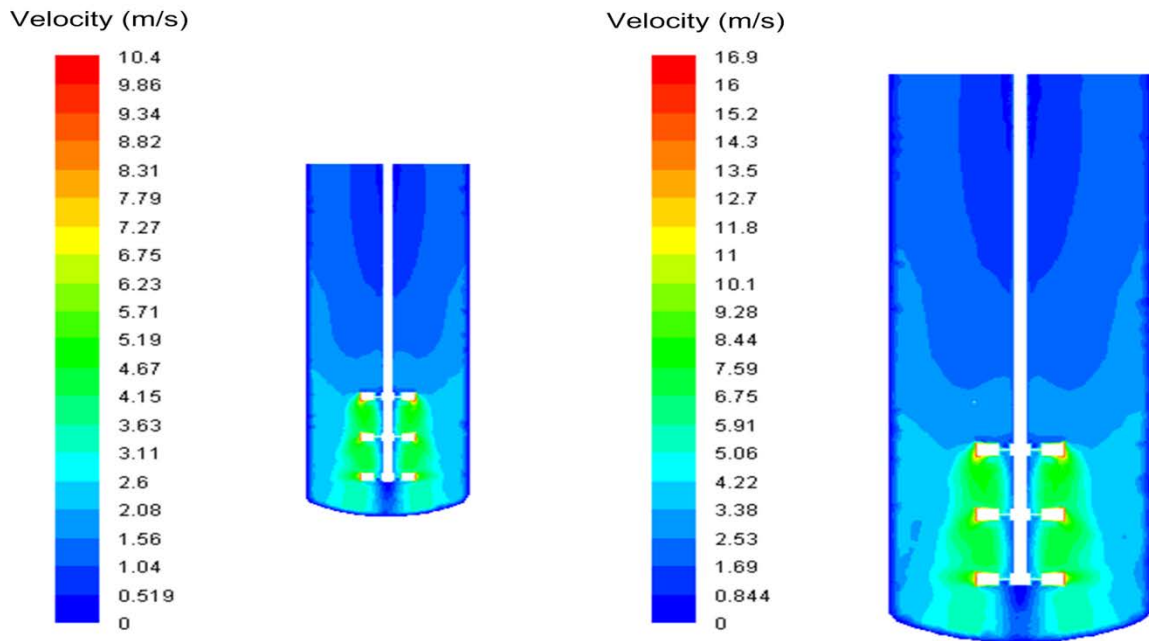


Figure 4.9. CFD Liquid velocity flow patterns at 78 m<sup>3</sup> and 178 m<sup>3</sup> fermentor volumes

The CFD fermentor flow fields simulated at 200 rpm for the smaller 78 m<sup>3</sup> fermentor employing either the uniform impeller spacing [46] for the baseline process or a previously described alternate spacing [47] are visually presented (Figure 4.10). Evidently, the alternate spacing resulted in a higher maximum liquid velocity of 7.92 m/s and homogeneity and much less localized mixing, approaching more the assumed CSTR of the baseline process. Using the baseline 200 rpm and uniform impeller spacing, mixing time  $t_m$  was estimated to be 60.67 s for the 178 m<sup>3</sup> fermentor. With greater computational power and resources available, multi-phase CFD fermentor simulations involving sparged CO<sub>2</sub> gas and liquid can help process engineers optimize flow conditions and scale-up. In addition, mixing time can be used to schedule feeding of MgCO<sub>3</sub> solution to both neutralize inhibitory carboxylic acid products and provide a more soluble and storable carbon source than CO<sub>2</sub> gas in the fermentor [32].

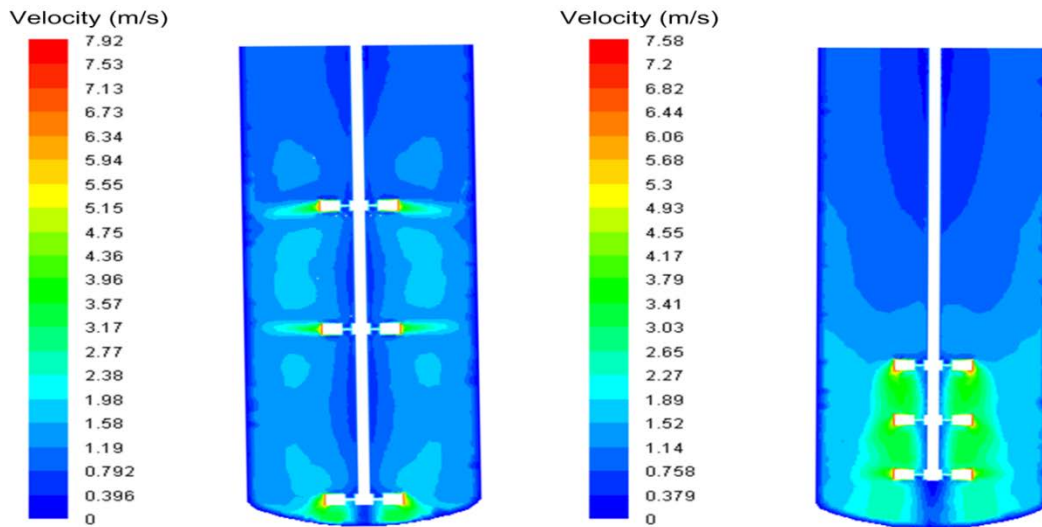


Figure 4.10. CFD Liquid velocity flow patterns at alternating (left) and fixed axial impeller spacing (right) for 78 m<sup>3</sup> fermentor

Although the recycle of cells back to the fermentor after downstream microfiltration recovery was for simplicity not simulated, it is essential to note the potential outcomes if it were. The fermentation industry has long recognized the benefits of cell recycle using membranes or even expanded-bed adsorbers for increasing cell density and volumetric productivity in fermentations, and its mathematical depiction can include such things as a recycle ratio in the mass balances [66, 67]. In one study, a cell-recycled *A. succiniciproducens* fermentation achieved a high cell concentration of 6.5 g DCW/L and a three-times higher succinic acid productivity compared to batch culture, without (1) morphologically changing to an inactive spherical state at the stressful high shear rates of 800 rpm that were used to limit membrane fouling, and (2) without becoming CO<sub>2</sub>-limited even at the highly-consuming recycled high cell densities by virtue of the concurrent supply of both pH neutralizer and inorganic carbon in the form of NaHCO<sub>3</sub> and

Na<sub>2</sub>CO<sub>3</sub> [68].

In another recent instance, succinic acid was produced by *Actinobacillus succinogenes* sp. 130Z in an external membrane continuous cell-recycle fermentor [67]. Compared to batch reactor, cell concentration increased three-fold to 16.4 g/L at a dilution rate 0.2 h<sup>-1</sup>, and succinic acid volumetric productivity increased five-fold to 6.63 g L<sup>-1</sup> h<sup>-1</sup> at a dilution rate of 0.5 h<sup>-1</sup>. [67]. At high dilution rate, contamination by a lactic acid producer and severe membrane fouling were observed [67]. *M. succiniciproducens* MBEL55E in this cell-recycle fermentor also achieved a cell concentration and succinic acid productivity at the dilution rate of 0.3 h<sup>-1</sup> that were at least 3 and 2.3 times higher, respectively, compared with those at 0.1 h<sup>-1</sup> dilution rate [67]. Cell concentration increased with dilution rate, even though it often oscillated before settling to a constant value [67]. Future studies to simulate the effect of such cell recycle, in addition to glucose recycle, and compare productivity gains obtained by either acid neutralization or electrodialysis removal of inhibitory acid levels, should be further done to augment the scope of this current work, as these are expected to positively impact biosuccinic acid production.

Simulation of cell microfiltration with tubes of 0.75 m length and 0.007 m inner diameter resulted in a total area requirement and power consumption of 876 m<sup>2</sup> and 78.80 kW for single-stage and a lower 765 m<sup>2</sup> and 68.80 kW for the two-stages of our baseline process. Because permeate flux was predicted using gel polarization theory and was a function of the ratio C<sub>g</sub>/C<sub>o</sub>, it was possible to have an intermediary bulk feed cell concentration C<sub>o</sub> from the first stage that

differed from that of the second stage and resulted in different permeate fluxes for each stage [53].

A primary aim of this work was to simulate a large-scale, continuous succinic acid biorefinery process. Advantages of membrane separation like microfiltration include the ability to operate without phase change, at near ambient temperatures, with relatively low energy consumption. Cross-flow microfiltration for macromolecular insoluble lignin and cells where feed flows parallel to the membrane surface was assumed more suitable for a continuous process than the relatively simpler dead-end filtration configuration requiring lower capital and maintenance costs [69], where the feed contacts the membrane surface at a perpendicular angle. This was primarily due to the intended high retentate concentrations or particle loading of insoluble lignin and cells that may otherwise rapidly compact on the filter surface as a cake layer and increase transmembrane pressure and pumping energy consumption. Also, cross-flow filtration with suitably selected membrane geometry was assumed to be less cumbersome and offer relatively more stable filtration rates and flexibility to periodically backwash or backpulse and reversibly remove some fouling, increasing long-term membrane performance and limiting membrane replacement and labor costs [69].

The *M. succiniciproducens* MBEL55E being fermented in the baseline simulated process is a rod-shaped bacteria [1]. It is again interesting to note that the morphology of this and other fermented succinic acid-producing anaerobes like *A. succinogenes* can also become more spherical and less productive for succinic acid due to high inhibitory glucose substrate

concentrations above 80 g/L [70], which exceeded the calculated 10.89 g/L steady-state glucose concentration of this work. Rod-like bacterial morphology, unlike that of yeast cell layers, has in turn also influenced cake resistance differently in both dead-end and cross-flow filtration [71]. Activated carbon adsorption was previously used in downstream succinic acid recovery and purification processes [8, 26]. Simulation of the GAC adsorption column (Figure 4.11) resulted in an overall mass transfer coefficient of  $5.29 \times 10^{-7}$  m/s and pressure drop of 59 Pa/m for the baseline 841 $\mu$ m GAC particle diameter and a coefficient of  $7.33 \times 10^{-7}$  m/s and pressure drop of 90 Pa/m for a 600  $\mu$ m particle diameter. Evidently, greater mass transfer efficiency must be balanced with higher pump power consumption costs.

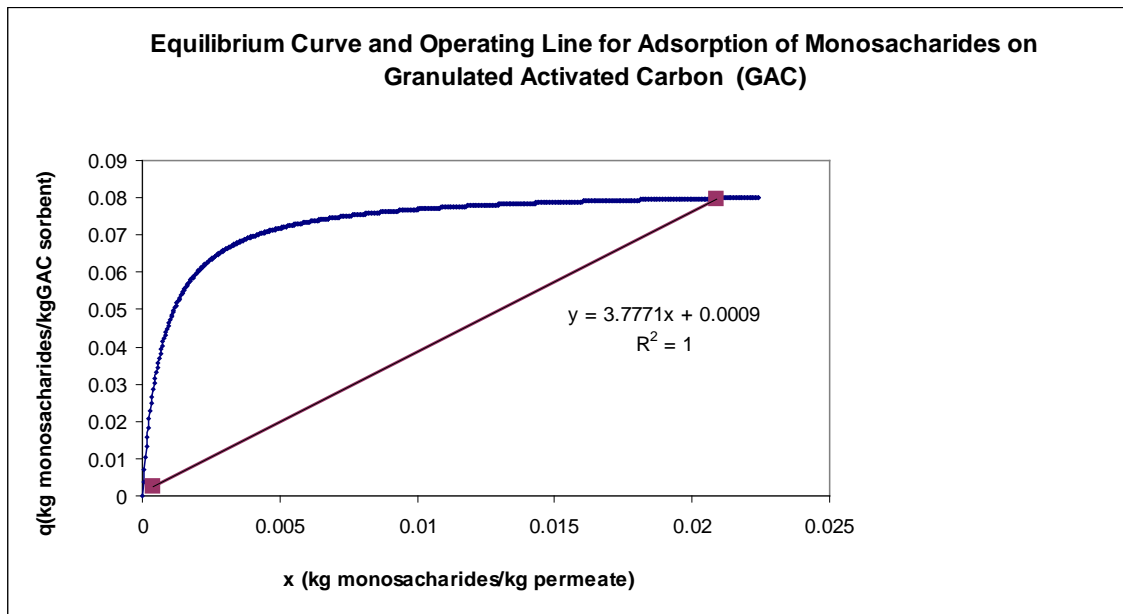


Figure 4.11. Adsorption equilibrium curve and operating line for glucose removal

The resulting nanofiltration retentate concentrations for succinate and lactate were 197.77 and 10.85 g/L, respectively, while their permeate concentrations were 3.83 and 4.12 g/L, respectively. A graphical method was used to predict gel-polarization concentration for the nanofiltration unit of the baseline process (Figure 4.12). For this, only three data points corresponding to succinate concentrations of 0.1, 0.2, and 0.3M were available from the literature to relate permeate flux with trans-membrane pressure [17] but a reasonably high  $R^2$  value of 0.9397 was still obtained from these. A gel-polarization concentration value of 303.2 kg/m<sup>3</sup> succinate using the relatively simple gel-polarization model that assumes a steady-state permeate flux to be both independent of transmembrane pressure but dependent on solute concentration was calculated and then used to predict a steady-state flux of  $1.42 \times 10^{-6}$  m/s which was the same order magnitude but lower than the experimentally observed  $4.44 \times 10^{-6}$  m/s corresponding to 95% succinate rejection [17] that resulted in a very high area requirement.

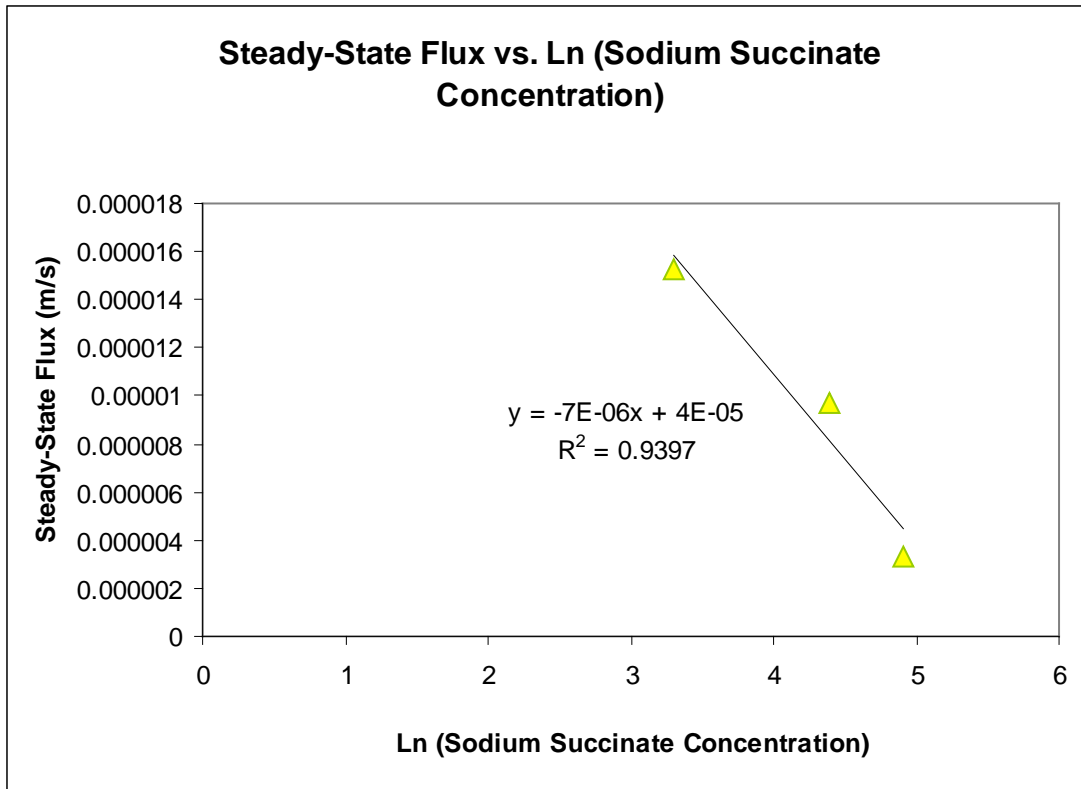


Figure 4.12. Estimation of gel polarization concentration for nanofiltration

Membrane nanofiltration performance depends on the complex interaction of many factors, and various models have been developed to try to predict actual phenomena but do not always perfectly succeed, as the results in this study also indicate [40, 42, 72, 73]. For instance, molecular weight, molecular size (length and width), acid disassociation constant, hydrophobicity and hydrophilicity, and diffusion coefficient were identified as key solute parameters primarily affecting solute rejection [73]. Also, molecular weight cut-off, pore size, surface charge (measured as zeta potential), hydrophobicity and hydrophilicity (measured as contact angle), and surface morphology (measured as roughness) were identified as key membrane properties primarily

affecting rejection [73]. Furthermore, solute rejection was affected by feed composition, like ionic strength, pH, hardness, and organic matter [73]. Another study evaluated the effects of pH, salt concentration, and temperature on the lactate flux and rejection when using a FILMTECTM NF-200B membrane nanofiltration of concentrated organic/inorganic mixtures of salt (up to 17% (w/v)) and lactic acid (2% (w/v)). Salt rejection was low, and lactate rejection was highest at neutral pH, decreasing with temperature and salt concentration for all evaluated solutions [27]. The measured flux and rejection values indicated that skin shrinkage in concentrated salt solutions and membrane sorption of lactate influences nanofiltration beyond the typical effects of charge, solute size and osmotic difference between the retentate and permeate streams [27].

According to the literature from which the high 95% succinate rejection values for simulation were derived, divalent anions of succinate in monovalent anion solutions could also dramatically decrease the rejection of the monovalent anions of formate, lactate, and acetate in the transport through nanofiltration membranes [17]. In this previous work, flux changed with concentration even at identical pressure, and rejection of succinate by NF45 membrane for different concentrations was plotted versus transmembrane pressures and permeate [17]. The succinate rejection increased from 23 to 94% with flux and mainly depended on the flux independent of the concentration [17]. The typically observed decrease of a solute's rejection with its concentration likely due to the increased screening of membrane surface charge by counter-ions like sodium was not observed in the cited study because even the lowest 0.1 M concentration of Na<sup>+</sup> tested was

probably already high enough to fully screen the membrane surface charge [17]. Clearly, this current biorefinery simulation work can be improved with more comprehensive and intensive evaluation of all significant factors affecting succinate rejection in nanofiltration. Operating conditions should as a result be further optimized to exploit this technology enabling non-destructive separation of succinate from other co-products in real-life industrial processes.

Capacity, low-cost regenerability, and specificity for succinate when acidifying and purifying it were factored into the selection of Dowex MWA-1 ion exchange resin and will also be considered in more comprehensive future economic studies. Nonetheless, it was before noted that a final concentration exceeding 100 g of succinic acid/L was likely economically feasible if achieved with resins that included XUS-40285 and XFS-40422 that were similarly manufactured by Dow® [59], and, in this work, a concentration of 222.87 g of succinic acid /L was predicted. As previously mentioned, an ion exchange resin like Amberlite IR-120 that was similarly used to acidify organic salts but that, in contrast, required HCl or H<sub>2</sub>SO<sub>4</sub> regeneration, was also viewed as economically favorable to electrodialysis in some instances [18]. As for the fermentor, future multi-phase CFD simulation of crystallizer involving solid succinic acid crystal and liquid mother liquor can be done to assess the effect of impeller speeds on complex crystal nucleation and growth phenomena. The general biorefinery energy balance is shown (Table 4.5).

Table 4.5. General energy balance for succinic acid biorefinery process

Feedstock/Product	Energy Content (MJ/h)	% of Total
Dry corn-stover biomass	1416667	100
Electricity	15120	1.1
Ethanol	141667	10
Lactic Acid	13161	0.9
Acetic Acid	153021	10.8
Formic Acid	149147	10.6
Succinic Acid	367641	26
Steam+ Hot Water	511142	36
Losses	65173	4.6

Approximately 15938 kg/h of lignin was recovered via microfiltration to fuel a boiler to generate steam and electricity, and 47.9% of the corn-stover feedstock (42412 kg/hr) was not converted into products. Lignin-generated steam  $m_{\text{steam}}$  was estimated at 69410 kg/hr. However, to meet the biorefinery requirement of 154324 kg/hr of steam [37], first the steam pressure and temperature were increased by assuming instead that a commercial bubbling fluidized-bed boiler produced up to 160000 kg/h of steam at 15 MPa and  $T = 450^{\circ}\text{C}$  with  $h_{\text{steam}} = 3157$  kJ/kg. Second, 42% of the biomass lost in the process was assumed recovered to provide the 17863 kg/h needed to fuel this new boiler. Since the new assumed steam conditions exceeded pre-hydrolysis requirements, the steam energy content was used to produce extra electricity in a steam turbine-generator system. Assuming a total efficiency of 52%, corresponding to 65% efficiency of turbine and 80% efficiency for generator when steam pressure and temperature drop to 1.36 MPa and  $245^{\circ}\text{C}$ , respectively, the generated power capacity was 4.2 MW, and electricity production was

36847 MWh/year. Total biorefinery power consumption, including that estimated from CFD for the fermentor, was estimated as 8561 MWh/year. The difference between energy generated and consumed (27847 MWh/year) was therefore exported to the grid for \$1131420/year of revenues.

By integrating costs and capital investments literature data for ethanol biorefineries [37] with feedstock costs, product pricing, and the predicted product yields and steam generation of the baseline simulated succinic acid biorefinery process, the rough estimates of costs, revenues, and income for the baseline succinic acid bioprocess were obtained and are shown (Table 4.6).

Table 4.6. Summary of Biorefinery Economic Analysis

Description of Analyzed Economic Parameter	USD \$
Total Project Investment(installed equipment and indirect costs)	2.93E+08
Annual Fixed Operating Costs (i.e. labor, overhead)	11504720
Annual Variable Operating Costs (i.e. feedstock, cooling water, etc)	55756068
Annual Depreciation costs	34367862
Annual Revenues (Assumes product and lignin-electricity selling prices and yields)	1.75E+08
Annual Income	73207273
Return on Investment Period	4.00

Corn stover raw material represented the highest variable operating cost. Assuming a \$1 U.S./kg succinic acid selling price for scenarios involving our 12.9% baseline yield, 15%, and 19%, the effect of increasing corn stover costs on ROI period is summarized (Figure 4.13). The succinic biorefinery was therefore profitable and attractive with an ROI period of 5 years or less only if

succinic acid selling exceeded \$1.6/kg.

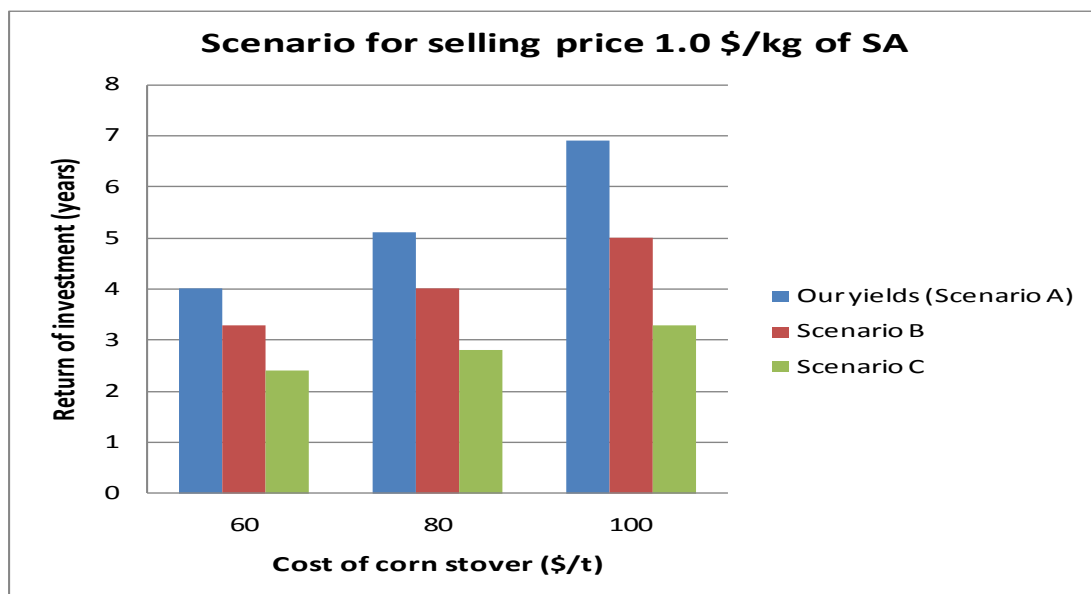


Figure 4.13. Periods of return of investment for succinic acid selling price of \$1 U.S./kg

#### 4.5. Conclusions

A novel industrial-scale biorefinery succinic acid process was described and integrated pre-treatment and hydrolysis with lignin removal and recovery to provide on-site steam and electricity generation, glucose removal and recovery, and non-destructive nanofiltration succinate separation. A multi-unit process model was developed for important units of operation to enable future optimization. For the fermentor, Computational Fluid Dynamics (CFD) through its coupling to the kinetics, mass and energy balances was demonstrated to be a valuable and useful tool for scale-up. The succinic acid biorefinery was considered profitable and attractive only if the selling price of the succinic acid exceeded \$1.6/kg. This work represents the first reported industrial-scale process design model for biochemically-derived succinic acid.

#### 4.6. References

- [1] H. Song, S.Y. Lee. Production of succinic acid by bacterial fermentation. *Enzyme Microb and Technol* 39 (2006) 352-61.
- [2] J.G. Zeikus, M.K. Jain, P. Elankovan. Biotechnology of succinic acid production and markets for derived industrial products. *Applied Microb and Biotechnol* 51 (1999) 545-52.
- [3] J.J. Beauprez, M. De Mey, W.K. Soetaert. Microbial succinic acid production: Natural versus metabolic engineered producers. *Process Biochem* 45 (2010) 1103-14.
- [4] L.R. Lynd, C. Wyman, M. Laser, D. Johnson, R. Landucci. *Strategic Biorefinery Analysis: Analysis of Biorefineries*. 2005.
- [5] L. Luo, E. van der Voet, G. Huppes. Biorefining of lignocellulosic feedstock - Technical, economic and environmental considerations. *Bioresource Technology* 101 (2010) 5023-32.
- [6] H. Song, S.H. Jang, J.M. Park, S.Y. Lee. Modeling of batch fermentation kinetics for succinic acid production by *Mannheimia succiniciproducens*. *Biochemical Engineering J* 40 (2008) 107-15.
- [7] T. Werpy, G. Petersen, A. Aden, J. Bozell, J. Holladay, J. White, et al. *Top Value Added Chemicals From Biomass. Volume I: Results of Screening for Potential Candidates from Sugars and Synthesis Gas*. NREL, 2004.
- [8] S.K.C. Lin, C.Y. Du, A.C. Blaga, M. Camarut, C. Webb, C.V. Stevens, et al. Novel resin-based vacuum distillation-crystallisation method for recovery of succinic acid crystals from

fermentation broths. *Green Chem* 12 (2010) 666-71.

[9] M. Mccoy. Big Plans For Succinic Acid. *Chemical & Engineering News* 87 (2009) 23-5.

[10] J. Elbert. The quest to commercialize biobased succinic-acid. *Biomass Magazine. Power and Thermal*. 2008.

[11] J. Yu, Z.M. Li, Q. Ye, Y. Yang, S.L. Chen. Development of succinic acid production from corn cob hydrolysate by *Actinobacillus succinogenes*. *J Ind Microbiol Biotechnol* 37 (2010) 1033-40.

[12] R. Luque, C.S.K. Lin, C.Y. Du, D.J. Macquarrie, A. Koutinas, R.H. Wang, et al. Chemical transformations of succinic acid recovered from fermentation broths by a novel direct vacuum distillation-crystallisation method. *Green Chem* 11 (2009) 193-200.

[13] H. Song, Y.S. Huh, S.Y. Lee, W.H. Hong, Y.K. Hong. Recovery of succinic acid produced by fermentation of a metabolically engineered *Mannheimia succiniciproducens* strain. *J Biotechnol* 132 (2007) 445-52.

[14] J. Li, X.Y. Zheng, X.J. Fang, S.W. Liu, K.Q. Chen, M. Jiang, et al. A complete industrial system for economical succinic acid production by *Actinobacillus succinogenes*. *Bioresour Technol* 102 (2011) 6147-52.

[15] Y.S. Huh, Y.S. Jun, Y.K. Hong, H. Song, S.Y. Lee, W.H. Hong. Effective purification of succinic acid from fermentation broth produced by *Mannheimia succiniciproducens*. *Process Biochem* 41 (2006) 1461-5.

- [16] Q. Li, D. Wang, Y. Wu, W.L. Li, Y.J. Zhang, J.M. Xing, et al. One step recovery of succinic acid from fermentation broths by crystallization. *Sep Purif Technol* 72 (2010) 294-300.
- [17] S.H. Kang, Y.K. Chang. Removal of organic acid salts from simulated fermentation broth containing succinate by nanofiltration. *J Membr Sci* 246 (2005) 49-57.
- [18] Y.M. Wang, C.H. Huang, T.W. Xu. Which is more competitive for production of organic acids, ion-exchange or electrodialysis with bipolar membranes? *J Membr Sci* 374 (2011) 150-6.
- [19] I. Meynial-Salles, S. Dorotyn, P. Soucaille. A new process for the continuous production of succinic acid from glucose at high yield, titer, and productivity. *Biotechnol Bioeng* 99 (2008) 129-35.
- [20] C.H. Huang, T.W. Xu, Y.P. Zhang, Y.H. Xue, G.W. Chen. Application of electrodialysis to the production of organic acids: State-of-the-art and recent developments. *J Membr Sci* 288 (2007) 1-12.
- [21] E.G. Lee, S.H. Kang, H.H. Kim, Y.K. Chang. Recovery of lactic acid from fermentation broth by the two-stage process of nanofiltration and water-splitting electrodialysis. *Biotechnol Bioprocess Eng* 11 (2006) 313-8.
- [22] D.A. Glassner, P. Elankovan, D.R. Beacom, K.A. Berglund. Purification Process For Succinic Acid Produced By Fermentation. *Appl Biochem Biotechnol* 51-2 (1995) 73-82.
- [23] F. Alvarez, R. Alvarez, J. Coca, J. Sandeaux, R. Sandeaux, C. Gavach. Salicylic acid production by electrodialysis with bipolar membranes. *J Membr Sci* 123 (1997) 61-9.

- [24] D. Glassner. Process for the Production and Purification of Succinic Acid. U.S.P.T.O., 1992.
- [25] Y.M. Wang, X. Zhang, T.W. Xu. Integration of conventional electro dialysis and electro dialysis with bipolar membranes for production of organic acids. *J Membr Sci* 365 (2010) 294-301.
- [26] N. Nghiem, H. Davison Brian, I. Donnelly Mark, S.-P. Tsai, G. Frye John. An Integrated Process for the Production of Chemicals from Biologically Derived Succinic Acid. *Chemicals and Materials from Renewable Resources. American Chemical Society* 784 (2001) 160-73.
- [27] V. Freger, T.C. Arnot, J.A. Howell. Separation of concentrated organic/inorganic salt mixtures by nanofiltration. *J Membr Sci* 178 (2000) 185-93.
- [28] J.L. Gineste, G. Pourcelly, Y. Lorrain, F. Persin, C. Gavach. Analysis of factors limiting the use of bipolar membranes: A simplified model to determine trends. *J Membr Sci* 112 (1996) 199-208.
- [29] E. Zondervan, M. Nawaz, A.B. de Haan, J.M. Woodley, R. Gani. Optimal design of a multi-product biorefinery system. *Comput Chem Eng* 35 (2011) 1752-66.
- [30] Y.F. Qiu, A.C. Rasmuson. Nucleation And Growth Of Succinic Acid In A Batch Cooling Crystallizer. *Aiche J* 37 (1991) 1293-304.
- [31] S.M. Husson, C.J. King. Multiple-acid equilibria in adsorption of carboxylic acids from dilute aqueous solution. *Ind Eng Chem Res* 38 (1999) 502-11.
- [32] H.H. Song, J.W. Lee, S. Choi, J.K. You, W.H. Hong, S.Y. Lee. Effects of dissolved CO<sub>2</sub>

levels on the growth of *Mannheimia succiniciproducens* and succinic acid production. *Biotechnol Bioeng* 98 (2007) 1296-304.

[33] S.K.C. Lin, C.Y. Du, A. Koutinas, R.H. Wang, C. Webb. Substrate and product inhibition kinetics in succinic acid production by *Actinobacillus succinogenes*. *Biochem Eng J* 41 (2008) 128-35.

[34] H.W. Blanch, D.S. Clark. *Biochemical Engineering*. New York Marcel Dekker, Inc., 1997.

[35] C.K. Harris, D. Roekaerts, F.J.J. Rosendal, F.G.J. Buitendijk, P. Daskopoulos, A.J.N. Vreenegoor, et al. Computational fluid dynamics for chemical reactor engineering. *Chem Eng Sci* 51 (1996) 1569-94.

[36] FLUENT 6.3 User's Guide. FLUENT, Inc., Lebanon, NH, 2006.

[37] A. Aden, M. Ruth, K. Ibsen, J. Jechura, K. Neeves, J. Sheehan, et al. Lignocellulosic Biomass to Ethanol Process Design and Economics Utilizing Co-Current Dilute Acid Prehydrolysis and Enzymatic Hydrolysis for Corn Stover. Technical Report, NREL. National Renewable Energy Laboratory, Golden, Colorado, 2002.

[38] S.M. Sadrameli, W. Seames, M. Mann. Prediction of higher heating values for saturated fatty acids from their physical properties. *Fuel* 87 (2008) 1776-80.

[39] O. Wallberg. Design of Ultrafiltration Process for Extraction of Lignin from Kraft black liquor, Internal Report. Lund, Sweden, 2005. p. 1-9.

[40] R.G. Harrison, P. Todd, S.T. Rudge, D. Petrides. *Bioseparations Science And Engineering*.

Oxford, Oxford University Press, 2003.

[41] R.W. Field, G.K. Pearce. Critical, sustainable and threshold fluxes for membrane filtration with water industry applications. *Adv Colloid Interface Sci* 164 (2011) 38-44.

[42] M. Mulder. *Handbook Basic Principles of Membrane Technology*. Second ed, Klumer Academic Publishers, 1996.

[43] P. Zheng, L. Fang, Y. Xu, J.J. Dong, Y. Ni, Z.H. Sun. Succinic acid production from corn stover by simultaneous saccharification and fermentation using *Actinobacillus succinogenes*. *Bioresour Technol* 101 (2010) 7889-94.

[44] K. van't Riet, J. Tramper. *Basic Bioreactor Design*. New York, Marcel Dekker, Inc., 1991.

[45] H. Lange, P. Taillandier, J.P. Riba. Effect of high sheer stress on microbial viability. *J Chem Technol Biotechnol* 76 (2001) 501-5.

[46] J.M. Lee. *Biochemical Engineering*, Prentice-Hall, Inc, 1992.

[47] E.L. Paul, V.A. Atiemo-Obeng, S.M. Kresta. *Handbook of industrial mixing-Science and Practice*, 2004.

[48] H.K. Versteeg, W. Malalasekera. *An Introduction to Computational Fluid Dynamics* Harlow, England, Addison Wesley Longman Limited, 1995.

[49] C. Antoine. Tensions des vapeurs; nouvelle relation entre les tensions et les températures. *Comptes Rendus des Séances de l'Académie des Sciences* 107 (1888) 681-4, 778-80, 836-7

[50] L.L. Diosady, T. Puzanov. Membrane Fermentation of Lactic Acid. *International Journal of*

Applied Science and Engineering 3 (2005) 19-25.

[51] L.F. Song. Flux decline in crossflow microfiltration and ultrafiltration: mechanisms and modeling of membrane fouling. *J Membr Sci* 139 (1998) 183-200.

[52] L.F. Song. A new model for the calculation of the limiting flux in ultrafiltration. *J Membr Sci* 144 (1998) 173-85.

[53] J.M. Coulson, J.F. Richardson. *Chemical Engineering* 4ed, Butterworth Heinemann, 1991.

[54] J.W. Lee, T.O. Kwon, I.S. Moon. Adsorption of mono saccharides, disaccharides, and maltooligosaccharides on activated carbon for separation of maltopentaose. *Carbon* 42 (2004) 371-80.

[55] H. Uchida, Y. Iwai, M. Amiya, Y. Arai. Adsorption behaviors of 2,6- and 2,7-dimethylnaphthalenes in supercritical carbon dioxide using NaY-type zeolite. *Ind Eng Chem Res* 36 (1997) 424-9.

[56] K. Knaebel. A "How-To" Guide for Adsorber Design. Adsorption Research, Inc., Dublin, Ohio, 1990.

[57] K. Sun, J.C. Jiang, J.M. Xu. Decolorization And Chemical Regeneration Of Granular Activated Carbon Used In Citric Acid Refining. *Bull Chem Soc Ethiop* 23 (2009) 29-36.

[58] M.R. Ladisch. *Bioseparations Engineering. Principles, Practice, and Economics.*, John Wiley & Sons, Inc., 2001.

[59] B.H. Davison, N.P. Nghiem, G.L. Richardson. Succinic acid adsorption from fermentation

broth and regeneration. *Appl Biochem Biotechnol* 113 (2004) 653-69.

[60] H.G. Nam, K.M. Park, S.S. Lim, S. Mun. Adsorption Equilibria of Succinic Acid and Lactic Acid on Amberchrom CG300C Resin. *J Chem Eng Data* 56 (2011) 464-71.

[61] D.O. Cooney. Adsorption design for wastewater treatment , CRC Press, LLC, 1999.

[62] N.S. Tavare. Industrial Crystallization. Process Simulation Analysis and Design, Plenum Press, 1995.

[63] S.J. Jancik, P.A.M. Grootcholten Industrial Crystallization, Delft University Press, 1984.

[64] J.W. Mullin, M.J.L. Whiting. Succinic Acid Crystal-Growth Rates In Aqueous-Solution. *Industrial & Engineering Chemistry Fundamentals* 19 (1980) 117-21.

[65] J. Chang. Indicative Chemical Prices A-Z In: J. Chang, (Ed.) ICIS Chemical Business. Reed Business Information Limited, 2011.

[66] T.H. Park, H. Juan, H.C. Lim. Theoretical-Analysis Of The Effect Of Cell Recycling On Recombinant Cell Fermentation Processes. *Biotechnol Prog* 7 (1991) 77-84.

[67] M.I. Kim, N.J. Kim, L. Shang, Y.K. Chang, S.Y. Lee, H.N. Chang. Continuous Production of Succinic Acid Using an External Membrane Cell Recycle System. *J Microbiol Biotechnol* 19 (2009) 1369-73.

[68] P.C. Lee, S.Y. Lee, H.N. Chang. Cell recycled culture of succinic acid-producing *Anaerobiospirillum succiniciproducens* using an internal membrane filtration system. *J Microbiol Biotechnol* 18 (2008) 1252-6.

- [69] J.N. Mhurchú. Dead-end and crossflow microfiltration of yeast and bentonite suspensions: experimental and modelling studies incorporating the use of artificial neural networks. Dublin Dublin City University, 2008.
- [70] R.I. Corona-Gonzalez, A. Bories, V. Gonzalez-Alvarez, C. Pelayo-Ortiz. Kinetic study of succinic acid production by *Actinobacillus succinogenes* ZT-130. *Process Biochem* 43 (2008) 1047-53.
- [71] M. Mota, J.A. Teixeira, A. Yelshin. Influence of cell-shape on the cake resistance in dead-end and cross-flow filtrations. *Sep Purif Technol* 27 (2002) 137-44.
- [72] I. Koyuncu, D. Topacik. Effect of organic ion on the separation of salts by nanofiltration membranes. *J Membr Sci* 195 (2002) 247-63.
- [73] C. Bellona, J.E. Drewes, P. Xu, G. Amy. Factors affecting the rejection of organic solutes during NF/RO treatment - a literature review. *Water Res* 38 (2004) 2795-809.

## CHAPTER 5 : GENERAL CONCLUSIONS

This study addressed microalgal cultivation and harvesting limitations to photosynthetic biorefinery commercialization. Appropriate microalgal strain selection and identification of preferable operating culture conditions were considered critical to overcome these challenges for improved and optimal production of biomass and target-products in a biorefinery. Two new oleaginous, multi-trophic, halo-alkaline tolerant microalgae, ALP2 and SLP2, were isolated from soda lakes in Washington State, U.S.A. and screened as candidates for a two-stage cultivation process designed to address issues regarding contamination, land acreage for inoculum, cold winters, inorganic carbon supply, nutrient supply, low lipid accumulation, and inefficient harvesting. The two-stage process involved culturing microalgae in a fermentor heterotrophically or photobioreactor mixotrophically as first-stage to rapidly obtain high cell densities for inoculating a phototrophic open-pond culture featuring high levels of  $\text{NaHCO}_3$ , pH, and salinity as second-stage.

As an oleaginous *Chlorella sp.* ALP2 was able to grow on multiple carbon sources (i.e. glycerol, acetate, glucose, bicarbonate), as well as at high pH (i.e. 9-10) and high  $\text{NaHCO}_3$  levels (i.e. 17-28 g/L). ALP2 grew rapidly at a high rate of  $1.7 \times 10^8$  cells  $\text{ml}^{-1}\text{day}^{-1}$  cell in the first stage under optimized heterotrophic conditions comprising the use of BG-11<sub>0</sub> medium supplemented with 10.0 g/L glucose and 0.529 g/L urea at 28°C. pH-control (optimally at pH 9) with aqueous HCl acid, as well as use of urea and anaerobically-digested food waste nitrogen sources in place of

NaNO<sub>3</sub>, were found to further promote ALP2 phototrophic growth. ALP2 that was inoculated from a heterotrophic first-stage grew to a final DCW of 2.528 g/L and achieved a neutral lipid content and productivity of 39.92% of DCW and 0.078 g L<sup>-1</sup> day<sup>-1</sup>, respectively, in the second-stage under optimized phototrophic conditions. These conditions involved the use of BG-11<sub>0</sub> medium supplemented with 17.0 g/L NaHCO<sub>3</sub> and 0.133 g/L urea, and maintenance of a pH 9 using aqueous HCl.

Relatively high levels of supplemental inorganic bicarbonate promoted ALP2 growth. High alkalinity, buffered by high concentration of bicarbonate ion, contributed to increased ALP2 cell size, granularity, optical density, and neutral lipid accumulation. ALP2 was found to be photosynthetically well-adapted to extreme haloalkaline culture conditions, based on observed state transition and the ability to maintain constant and high values for the photosynthetic parameters  $F_v/F_m$ , O<sub>2</sub>-evolution and respiration, NPQ, and  $\Psi_{II}$  at high pH and NaHCO<sub>3</sub> levels. ALP2 carotenoid/chlorophyll ratio decreased with increasing NaHCO<sub>3</sub> levels. Proving the ability of ALP2 to replicate at high NaHCO<sub>3</sub> concentrations and high pH, and to use bicarbonate ion as a major carbon source in both growth and lipid accumulation phases of second-stage is a significant development for the two-stage cultivation strategy. The additional ability of ALP2 to grow rapidly heterotrophically or mixotrophically to high cell densities makes it a good candidate for further optimization and scale-up of a productive two-stage cultivation process for commercial algal bio-oil production.

A multi-unit process model that coupled 2-D single-phase CFD hydrodynamics with microbial kinetics, energy and mass conservation, and heat and mass transfer was developed and applied to simulate a continuous, industrial-scale fermentor for the production of high-value succinic acid and co-products by *M. succiniciproducens* within a novel, commercial-scale, multi-unit, integrated biorefinery process that used corn-stover biomass feedstock. The coupling of microbial kinetics, mass and energy balances, with velocity flow fields described using Computational Fluid Dynamics was demonstrated to be predictive with regards to dissolved CO<sub>2</sub> concentration and a valuable scale-up tool to enable future optimization. The succinic acid biorefinery was considered profitable and attractive only if the selling price of the succinic acid exceeded \$1.6/kg. This represented an industrial-scale process design model for biochemically-derived succinic acid.